INFORMATION TO USERS

The most advanced technology has been used to photograph and reproduce this manuscript from the microfilm master. UMI films the original text directly from the copy submitted. Thus, some dissertation copies are in typewriter face, while others may be from a computer printer.

In the unlikely event that the author did not send UMI a complete manuscript and there are missing pages, these will be noted. Also, if unauthorized copyrighted material had to be removed, a note will indicate the deletion.

Oversize materials (e.g., maps, drawings, charts) are reproduced by sectioning the original, beginning at the upper left-hand corner and continuing from left to right in equal sections with small overlaps. Each oversize page is available as one exposure on a standard 35 mm slide or as a 17″ × 23″ black and white photographic print for an additional charge.

Photographs included in the original manuscript have been reproduced xerographically in this copy. 35 mm slides or 6″ × 9″ black and white photographic prints are available for any photographs or illustrations appearing in this copy for an additional charge. Contact UMI directly to order.

Accessing the World's Information since 1938

300 North Zeeb Road, Ann Arbor, MI 48106-1346 USA

GEOMETRICALLY NONLINEAR ANALYSIS OF THIN ARBITRARY SHELLS USING DISCRETE-KIRCHHOFF CURVED TRIANGULAR ELEMENTS

Subramanian, Balakrishnan, Ph.D.
The University of Arizona, 1985

U·M·I
300 N. Zeeb Rd.
Ann Arbor, MI 48106

PLEASE NOTE:

In all cases this material has been filmed in the best possible way from the available copy. Problems encountered with this document have been identified here with a check mark __√__.

1. Glossy photographs or pages _____
2. Colored illustrations, paper or print _____
3. Photographs with dark background _____
4. Illustrations are poor copy _____
5. Pages with black marks, not original copy _____
6. Print shows through as there is text on both sides of page _____
7. Indistinct, broken or small print on several pages _____
8. Print exceeds margin requirements _____
9. Tightly bound copy with print lost in spine _____
10. Computer printout pages with indistinct print _____
11. Page(s) 169 lacking when material received, and not available from school or author.
12. Page(s) _____ seem to be missing in numbering only as text follows.
13. Two pages numbered _____. Text follows.
14. Curling and wrinkled pages _____
15. Dissertation contains pages with print at a slant, filmed as received _____
16. Other _____

_____

_____

GEOMETRICALLY NONLINEAR ANALYSIS OF THIN ARBITRARY SHELLS USING DISCRETE-KIRCHHOFF CURVED TRIANGULAR ELEMENTS

by

Subramanian Balakrishnan

A Dissertation Submitted to the Faculty of the

DEPARTMENT OF CIVIL ENGINEERING AND ENGINEERING MECHANICS

In Partial Fulfillment of the Requirements
For the Degree of

DOCTOR OF PHILOSOPHY
WITH A MAJOR IN ENGINEERING MECHANICS

In the Graduate College

THE UNIVERSITY OF ARIZONA

1 9 8 5

THE UNIVERSITY OF ARIZONA
GRADUATE COLLEGE

As members of the Final Examination Committee, we certify that we have read the dissertation prepared by Subramanian Balakrishnan

entitled GEOMETRICALLY NONLINEAR ANALYSIS OF THIN ARBITRARY SHELLS USING DISCRETE-KIRCHHOFF CURVED TRIANGULAR ELEMENTS

and recommend that it be accepted as fulfilling the dissertation requirement for the Degree of Doctor of Philosophy.

(Dr. Richard H. Gallagher)	Date 11/11/85
(Dr. Chandrakant S. Desai)	Date 11/8/85
(Dr. Hussein A. Kamel)	Date 11/20/85
(Dr. Ralph M. Richard)	Date 11/8/85
(Dr. Bruce R. Simon)	Date 10/21/85

Final approval and acceptance of this dissertation is contingent upon the candidate's submission of the final copy of the dissertation to the Graduate College.

I hereby certify that I have read this dissertation prepared under my direction and recommend that it be accepted as fulfilling the dissertation requirement.

Dissertation Director	Date 11/11/85

STATEMENT BY AUTHOR

This dissertation has been submitted in partial fulfillment of requirements for an advanced degree at The University of Arizona and is deposited in the University Library to be made available to borrowers under rules of the Library.

Brief quotations from this dissertation are allowable without special permission, provided that accurate acknowledgment of source is made. Requests for permission for extended quotation from or reproduction of this manuscript in whole or in part may be granted by the head of the major department or the Dean of the Graduate College when in his or her judgment the proposed use of the material is in the interests of scholarship. In all other instances, however, permission must be obtained from the author.

SIGNED: 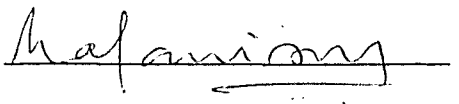

DEDICATION

To my dear father, N. Subramanian.

ACKNOWLEDGMENTS

It is a great privilege to be a student of Dr. Richard H. Gallagher, Vice-President and Dean of the Faculty, Worcester Polytechnic Institute, Massachusetts and formerly the Dean of Engineering, University of Arizona, Tucson. It is a great pleasure to be guided and supervised for this dissertation by Dr. R.H. Gallagher, a pioneer in the field of Finite Element Techniques. His profound knowledge and valuable guidance were immensely useful in the successful completion of this dissertation. His kind help and constant encouragement will be remembered with unfathomable gratitude.

The author records with a deep sense of gratitude to Dr. T. Triffet, Associate Dean of Engineering and Dr. Paul H. King, Head, Department of Civil Engineering and Engineering Mechanics, for their kind help on many occasions. Thanks are also due to Professors C.S. Desai, R.M. Richard, of the Department of Civil Engineering and Engineering Mechanics, and Dr. H.A. Kamel and Dr. B.R. Simon of the Department of Aerospace and Mechanical Engineering, for their encouragement and helpful criticism as members of the Doctoral Committee.

Grateful thanks are due to Dr. T. Triffet, Associate Dean and Dr. R.M. Richard, Professor, for providing computer time generously. The author is short of words to express his profound gratitude to Mrs. Blanche A. Seferlis, Coordinator, Engineering Administration, for her invaluable help and kindness.

Many thanks are also due to all the members of the staff of the Dean's office and the office of the Civil Engineering Department for their kind help and cooperation. Special thanks are due to Ms. Rose Guoyat for her help on the IBM personal computer. Thanks are also due to Mr. Peter Mather, Director, Engineering Experiment Station, and his staff for their kind help many times.

No amount of thanks would adequately express the author's gratitude to Dr. Kenneth J. Saczalski, Professor, Mechanical Engineering, Northern Arizona University, Flagstaff, for his invaluable help, encouragement and discussions.

Words are not sufficient to adequately express the gratitude to the consultants, University Computer Center, for their enthusiastic help and cooperation. Special thanks are due to Ms. Linda and Ms. Brenda, but for whom the complex computer programming could not have been successful.

Grateful thanks are due to Ms. Linda Harper for typing this dissertation and for other assistance. The author also thanks all his friends for their invaluable help.

Last, but not least, the author remembers with profound gratitude, his mother, brothers and sisters for their prayers and blessings that provided great moral strength during the whole period of study. Special rememberance is due to my wife, Dr. K.K.M. Lakshmi and my children Vijai and Kumar, for their patience and support in the difficult days.

TABLE OF CONTENTS

TABLE OF CONTENTS--continued

LIST OF ILLUSTRATIONS

LIST OF ILLUSTRATIONS--continued

LIST OF ILLUSTRATIONS--continued

LIST OF ILLUSTRATIONS--continued

LIST OF TABLES

LIST OF TABLES--continued

ABSTRACT

The research work presented here deals with the problems of geometrically nonlinear analysis of thin shell structures. The specific objective was to develop geometrically nonlinear formulations, using Discrete-Kirchhoff Curved Triangular (DKCT) thin shell elements. The DKCT elements, formulated in the natural curvilinear coordinates, based on arbitrary deep shell theory and representing explicit rigid body modes, were successfully applied to linear elastic analysis of composite shells in an earlier research work.

A detailed discussion on the developments of classical linear and nonlinear shell theories and the Finite Element applications to linear and nonlinear analysis of shells has been presented. The difficulties of developing converging shell elements due to Kirchhoff's hypothesis have been discussed. The importance of formulating shell elements based on deep shell theory has also been pointed out. The development of shell elements based on Discrete-Kirchhoff's theory has been discussed. The development of a simple 3-noded curved triangular thin shell element with 27 degrees-of-freedom in the tangent and normal displacements and their first-order derivatives, formulated in the natural curvilinear coordinates and based on arbitrary deep shell theory, has been described. This DKCT element has been used to develop geometrically nonlinear formulation for the nonlinear analysis of thin shells.

A detailed derivation of the geometrically nonlinear (GNL) formulation, using the DKCT element based on the Total Lagrangian approach and the principles of virtual work has been presented. The techniques of solving the nonlinear equilibrium equations, using the incremental methods has been described. This includes the derivation of the Tangent Stiffness matrix. Various Newton-Raphson solution algorithms and the associated convergence criteria have been discussed in detail. Difficulties of tracing the post buckling behavior using these algorithms and hence the necessity of using alternative techniques have been mentioned.

A detailed numerical evaluation of the GNL formulation has been carried out by solving a number of standard problems in the linear buckling and GNL analysis. The results compare well with the standard solutions in linear buckling cases and are in general satisfactory for the GNL analysis in the region of large displacements and small rotations.

It is concluded that this simple and economical element will be an ideal choice for the expensive nonlinear analysis of shells. However, it is suggested that the element formulation should include large rotations for the element to perform accurately in the region of large rotations.

CHAPTER 1

INTRODUCTION

Curves are naturally attractive and so are shells. Shells can be seen everywhere in nature. Shells derive great strength from their intrinsic shape and are hence widely used in every branch of engineering and industry. Cooling towers and containments in civil engineering, pipes and pressure vessels in mechanical and nuclear engineering, automobiles, aircrafts and spacecrafts are some of the examples of shell applications.. While the awesome beauty of shell roofs, covering large unobstructed areas have always fascinated architects, their mathematical complexities have frustrated engineers However, the efficiency with which shells carry the loads and their ever increasing use in industries, has drawn engineers into more and more sophisticated study of the behavior of shells.

Although theoretical and experimental studies of thin shells began in the 1820s, intensive research works began only after 1930. Kirchhoff's[1] plate theory was instrumental in Love's[2] development of the earliest bending theory of linear elastic thin shells. Pioneering works on thin shell theories were done later by numerous researchers like Meissner[3], Vlasov[4], Naghdi[5], Sanders[6], Koiter[7], Goldenveizer[8], Novozhilov[9], and Budiansky[10]. Reissner[11] is one of the principal architects of modern theory of shells. An excellent review of the historical development of shell research has been given by Sechler[12].

The earliest theories of shells were developed on the assumption that the shell is thin and shallow. The former assumption enabled to neglect the normal stress and the displacements and stresses parallel to the middle surface to be assumed to vary linearly across the thickness. Thus, a three-dimensional theory of elasticity was reduced to a two-dimensional theory. The latter assumption neglects the surface slopes and tangential displacements, resulting in simplified governing equations.

Due to simplicity, the earliest theories were developed on the assumption of linear behavior. However, nature exhibits, in general, nonlinear behavior. Shells, in particular, are generally thin and can undergo large deformations. Also, shells carry loads by membrane compression and are, therefore, susceptible to buckling. When the deformations can no longer be assumed infinitesimal, as in the linear theory, the strain-displacement relations become nonlinear and the effects of geometry changes cannot be neglected. It is, therefore, often desirable to seek nonlinear solutions in order to understand the true behavior of structures and thereby achieve economical and efficient design.

The earliest nonlinear theory of shallow shells was due to Marguerre[13]. Donnell[14] developed an appropriate theory for cylinders. Mushtari and Galimov[15] developed a theory for quasi-shallow shells. Novozhilov[16] has presented nonlinear strain displacement equations from general three-dimensional elasticity. A completely generalized theory of thin shells is found in a paper by Synge and Chien[17] and Chien[18,19]. Erickson and Trusdell[20] have given an elegant and

general formulation of the problem. An exact theory for large deflections of thin arbitrary shells has been presented by Sanders[21] and independently by Leonard[22] and Koiter[23]. Exact equilibrium equations for nonlinear membrane shell theory have been derived by Budiansky[24]. Reissner[25] has developed a nonlinear theory allowing arbitrary large deformations and strains.

A new approach to the derivation of geometrically nonlinear small strain shell theories, which provides a better understanding of their range of applicability and gives a deeper insight into questions of consistency, is given in the works of Pietraszkiewicz[26-29]. It is shown[29] how a consistent, entirely Lagrangian description of geometric and static boundary conditions can be achieved in the frame work of a geometrically nonlinear first approximation of Kirchhoff-Love type shell theory for small strains and unrestricted rotations. In the ref. 26-28, the polar decomposition theorem is applied to shell structures according to which the deformation in each point of the shell may be decomposed exactly, apart from a rigid body translation, into a pure stretch along the principal directions of strain and a rigid body rotation. This makes it possible to impose restrictions on strains and rotations independently.

Shell theories may be classified according to the magnitude of the rotation as (i) small rotation, (ii) moderate rotation, (iii) large rotation and (iv) finite or unrestricted rotation. In literature consistent with this classification scheme, several entirely Lagrangian geometrically nonlinear first approximation shell

theories, associated variational principles, stability and post buckling equations and numerical studies have been given in the range of unrestricted, large and moderate rotations. Detailed derivation of the above theories in an entirely Lagrangian description can be found in reference 30.

1.1 Finite Elements in Linear and Nonlinear Analysis

In spite of the development of several shell theories, the analysis and design of shell structures were restricted to certain well defined geometries, loading and boundary conditions. This is due to the fact that in practice, unusual conditions of the above type arise and formulation and solution of the governing equations are extremely difficult. Thanks to the development of a powerful numerical technique- the Finite Element Method- details of which are now well documented, and can be found in numerous text books - e.g., references 31-35.

The history of finite element procedures for shells spans over 20 years. Starting from the earliest work of Adini[36] there have been scores of publications on the finite element linear analysis of shells employing various types of shell elements and the associated variational principles. Extensive critical surveys of developments have been given by Gallagher [37-40]. The success of the finite element method in the analysis of shell structures encouraged its application to nonlinear problems which hitherto was inaccessible to the engineering analysts.

When one undertakes the development of a general procedure for the nonlinear analysis of shells, the difficulties encountered increase considerably. Although finite element analysis of thin shells has been developed to a high degree of sophistication, basic questions relating to the geometrical form of the elements and definition of interpolation functions for displacements and/or stresses are far from being settled. The main problem of finite element representation of thin shells is the lack of elements which can show good accuracy and efficiency. This is due to the fact that in the case of displacement models, the displacements as well as their first and second order derivatives with respect to Gaussian shell parameters are required as nodal degrees-of-freedom and the restrictions related to satisfaction of interelement continuity conditions, adequate representations of rigid body and constant strain modes lead to difficulties of developing converging elements.

The earliest attempt to employ finite element technique to the nonlinear analysis of shells date back to the late 1960s. Most of these efforts were limited to studies of shells of particular geometric shape, such as axisymmetric[41,42] or cylindrical shells[43] Since then there have been numerous publications in the nonlinear analysis of shells by the assumed displacement method. Owing to the difficulties of compatibility requirements in the displacement models, which increase in the case of arbitrary shells, nonlinear shell analysis using alternate formulations such as Mixed[44-47] and Hybrid[48-51] have been reported. However, in these models other

difficulties in the formulations of the model itself and solution remain[52]. A comprehensive treatment of various finite element formulations for nonlinear shell problems has been presented by Gallagher [53-57].

A significant portion of the available literature on geometrically nonlinear analysis of shells by the finite element method has been directed to the study of shallow shells. Although shallow shell theory is an interesting simplification of the general thin shell theory, significant errors can be introduced when shallow shell elements in curvilinear components are used for the analysis of deep shell structures[58]. One of the difficulties associated with deep shell elements is the selection of appropriate nonlinear shell theory. An alternative approach starts with three dimensional isoparametric elements and introduces shell assumptions, thereby developing a simple curved shell element without using any difficult shell theory. This so-called degeneration technique was first presented by Ahmad et al[59] for linear analysis. Although these elements originated as a tool for the analysis of thick shells, they have been successfully applied to thin shells as well. Application of degenerated shell elements have been reported by Wood[60-62], Ramm[63], Bathe[64,65] and Krakeland[66]. These elements have the drawback of producing stiffer results for thin shells. While reduced integration[67] or selective integration[66] circumvents this problem, spurious zero energy modes are introduced, resulting in rank deficiency of the element.

1.2 The Discrete-Kirchhoff (D-K) Element

Most of the elements mentioned so far fall into the categories of C^0 (Timoshenko-Mindlin-Reissner) or C^1 (Euler-Bernoulli-Kirchhoff) formulations. As discussed earlier, the requirements of interelement continuity, rigid body motions and uniform strain states complicate the analysis of Kirchhoff plates and shells. Interelement boundaries of a plate or shell have the requisite continuity only if the normal defining such boundaries remains continuous. Since the Kirchhoff hypothesis constrains the normal to remain straight and normal to the middle surface, the continuity can be achieved only if the deformed surface is smooth.

The complexity involved in using higher order polynomials to satisfy the continuity requirements has hampered the development of finite element models using C^1 elements for the analysis of shells. It is apparent that the source of difficulty is the Kirchhoff hypothesis. With this in mind, Wempner et al[69] developed a quadrilateral shell element with displacements and rotations of the normal as unknowns, enforcing Kirchhoff's constrains at discrete points and successfully applied it to the linear analysis of arbitrary shells. This is the earliest known Discrete-Kirchhoff (D-K) shell element.

Later, Dhatt[70] developed a curved triangular shallow shell element and Stricklin[71] et al. developed a triangular plate bending element. The popularity of this rapidly converging element should go to Batoz[72-74]. The earliest D-K formulations for small strain and finite rotation of flexible shells have been given by Wempner[75].

However, early application of the D-K element to nonlinear shallow shell problems seems to be by Dhatt[76]. Later, Batoz et al.[77] employed curved D-K-T (Discrete-Kirchhoff-Triangular) element for the nonlinear analysis of shallow shells and Bathe[78] used a flat D-K-T element for nonlinear arbitrary shell problems. The only curved triangular thin shell element formulated in curvilinear coordinates for deep shell problems seems to be due to Batoz[79]. However, Sridhara Murthy[80] recently developed a simple three noded curved triangular thin shell D-K element in curvilinear coordinates, including, explicitly, rigid body modes. This element has 27 degrees-of-freedom in the displacements and their derivatives with respect to local curvilinear coordinates. The formulation is based on linear shear deformation theory. The Kirchhoff constraints of zero transverse shear strains have been imposed at the three corner nodes and at the midpoints of the sides of the curved triangle. Explicit rigid body modes have been incorporated by isoparametric mapping. The element converges rapidly and has proved to be successful for isotropic as well as anisotropic shell problems.

In view of the simplicity and superiority of this element as an alternative to the degenerated element, it is desirable to add nonlinear capabilities to the element for the more relevant nonlinear shell analysis. The research work presented herein is the result of this objective.

1.3 Scope of the Study

The scope of this study is restricted to (i) large displacements but small rotations, (ii) isotropic material behavior, (iii) conservative loadings and (iv) tracing the nonlinear load-displacement paths up to the limit point or bifurcation point as the case may be. The developments are presented in the subsequent chapters as follows:

In the second chapter, tensor equations of kinematic deformations of an arbitrary thin shell, using a linear shear deformation theory, are presented. Nonlinear strain displacement relations for large displacements but small rotations are derived for membrane and bending strains. For transverse shear strains, linear variation has been assumed. The linear portions of these equations are adopted from reference 80.

In the third chapter, the linear formulation of the Discrete-Kirchhoff Curved Triangular (D-K-C-T) Element for the isotropic case, is presented. Herein the nodal degrees-of-freedom, the displacement interpolation, the strain energy of the element and the linear strain-displacement relations are presented in matrix form. The derivation of the linear element stiffness, after imposing the Kirchhoff constraints at the discrete points of the element thereby eliminating the midside nodes, is briefly presented. The transformation of the stiffness matrix and the consistent nodal load vector between the global cartesian and local curvilinear frames and the

condensation of the central node is also described briefly, details being found in reference 80.

In the fourth chapter, nonlinear formulations of the element are presented in detail. First, the continuum mechanics formulation with incremental equations of motion is described. This is followed by the Total Lagrangian description of the continuum equations. In Section 4.3, the finite element discretization of the continuum equations is presented. In Section 4.4 and 4.5, the use and derivation of the Tangent Stiffness matrix is described.

In the fifth chapter, various nonlinear solution techniques e.g.; the Newton-Raphson (N-R) method and its variations, are described. Difficulties of using the N-R techniques and alternate algorithms are briefly mentioned. In Section 5.1 various convergence criteria are described. In Section 5.2, the computer program developed for the nonlinear analysis is described briefly and a flowchart is presented.

In the sixth chapter, numerical examples, testifying the accuracy of the nonlinear formulation and the behavior of the element are presented. The examples start with linear buckling cases and proceed to full nonlinear analysis. Since shell is a general structural component, examples include, columns, plates, arches, and arbitrary shells. Finally, a summar, conclusions and suggestions for further study are presented in chapter seven.

CHAPTER 2

KINEMATICS OF DEFORMATION

The kinematics of deformation of a shell surface requires an understanding of the differential geometry of a curved surface. Exhaustive details of this in tensor formulation has been given in chapter 2.1 of reference 80. In order to have a continuity as well as to include the nonlinear part, most of the information and equations are reproduced here from chapters 2.2 through 2.3.3 of reference 80.

Figure 1. shows the motion of the shell element before and after deformation.

Let

θ^{α} = Arbitrary curvilinear coordinates of the middle surface

θ^{3} = Distance along the normal to the middle surface

$\hat{e}_i$ = Cartesian unit base vectors (i = 1,2,3)

$\hat{a}_3$ = Unit normal vector to the undeformed middle surface

$\bar{g}_{\alpha}$ = Base vectors of the spatial system (α = 1,2)

$\bar{a}_{\alpha}$ = Tangent vectors at the middle surface

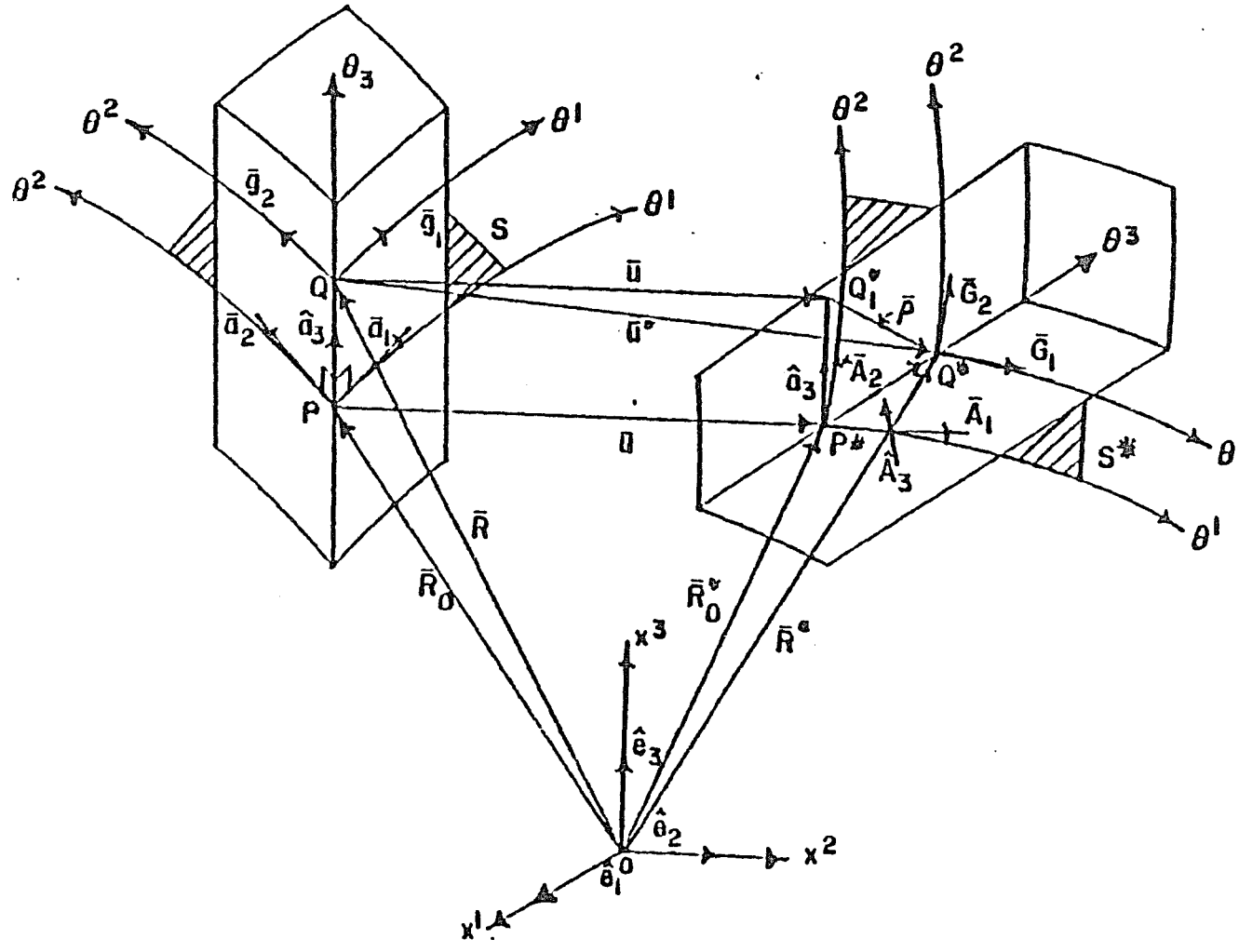

Figure 1. Motion of a shell element.

$\bar{R}_o(\theta^1,\theta^2)$ is the position vector of a point P on the middle surface of the undeformed shell and $\bar{R}(\theta^1,\theta^2)$ is that of an arbitrary point Q on the normal through P.

$$\bar{R}(\theta^1\theta^2) = \bar{R}_o(\theta^1\theta^2) + \theta^3\,\hat{a}_3 \tag{2.1}$$

After deformation, the point P moves to P* and Q moves to Q*. The position vector of P* is denoted as $\bar{R}^*_o(\theta^1,\theta^2)$ and that of Q* as $\bar{R}^*(\theta^1,\theta^2)$. It is to be noted that θ^3 line is assumed to be straight and normal to the middle surface before deformation and straight but not necessarily normal to the middle surface after deformation. Let $\hat{A}_3$ be a unit vector along the deformed θ^3 line.

$$\bar{R}^* = \bar{R}^*_o + \theta^3\hat{A}_3 \tag{2.2}$$

Let $\bar{u}$ and $\bar{u}^*$ be the displacement vectors of the points P and Q respectively. From figure 1, it follows that,

$$\bar{R}^*_o = \bar{R}_o + \bar{u} \tag{2.3}$$

$$\bar{R}^* = \bar{R} + \bar{u}^* \tag{2.4}$$

The vectors $\bar{u}$ and $\bar{u}^*$ differ by a vector $\bar{\rho}$ which represents the displacement caused by the rotation of $\hat{a}_3$ into $\hat{A}_3$. If the rotation of the normal are sufficiently small, they can be represented by a rotation vector $\bar{\phi}$. Then,

$$\bar{\rho} = \bar{\phi} \times (\Theta^3 \hat{a}_3) \qquad \text{(Cross product)} \tag{2.5}$$

$$\hat{A}_3 = \hat{a}_3 + \bar{\Phi} \times \hat{a}_3 \tag{2.6}$$

$$\bar{u}^* = \bar{u} + \bar{\rho} \tag{2.7}$$

$$= \bar{u} + \bar{\phi} \times (\Theta^3 \hat{a}_3) \tag{2.8}$$

From Eq. (2.4)

$$\bar{R}^* = \bar{R} + \bar{u} + \Phi^3 \bar{\lambda} \tag{2.9}$$

where

$$\bar{\lambda} = \bar{\phi} \times \hat{a}_3 \tag{2.10}$$

Let $\bar{G}_\alpha$ denote tangent base vectors of the deformed spatial coordinates

$$\bar{G}_\alpha = \bar{R}^*_{,\alpha} \quad (\text{Note: } R^*_{,\alpha} = \frac{\partial R^*}{\partial \alpha}) \tag{2.11}$$

$$= \bar{R}_{,\alpha} + \bar{u}_{,\alpha} + \Theta^3 \bar{\lambda}_{,\alpha} \tag{2.12}$$

$$\bar{G}_3 = \bar{R}^*_{,3} = \bar{R}_{,3} + \bar{\lambda} \tag{2.13}$$

From the differential geometry of a curved surface,

$$\bar{g}_\alpha = \bar{R}_{,\alpha} \tag{2.14}$$

$$= \bar{R}_{o,\alpha} + \theta^3 \hat{a}_{3,\alpha} \tag{2.15}$$

and

$$\bar{g}_3 = \bar{R}_{,3} = \hat{a}_3 \tag{2.16}$$

Hence equation 2.12 becomes

$$\bar{G}_\alpha = \bar{g}_\alpha + \bar{u}_{,\alpha} + \theta^3 \bar{\lambda}_{,\alpha} \tag{2.17}$$

and

$$\bar{G}_3 = \hat{a}_3 + \bar{\lambda} \tag{2.18}$$

The covariant components of the metric tensor $G_{\alpha\beta}$ of the spatial coordinates of the deformed shell are given by

$$G_{\alpha\beta} = \bar{G}_\alpha \cdot \bar{G}_\beta \qquad \text{(Dot product)} \tag{2.19}$$

and

$$G_{\alpha 3} = \bar{G}_\alpha \cdot \bar{G}_3 \tag{2.20}$$

Substituting Eq. (2.17) into Eq. (2.19),

$$G_{\alpha\beta} = (\bar{g}_\alpha + \bar{u}_{,\alpha} + \theta^3 \bar{\lambda}_{,\alpha}) \cdot (\bar{g}_\beta + \bar{u}_{,\beta} + \theta^3 \bar{\lambda}_{,\beta}) \tag{2.21}$$

$$G_{\alpha\beta} = g_{\alpha\beta} + \bar{g}_\alpha \cdot \bar{u}_{,\beta} + \bar{g}_\beta \cdot \bar{u}_{,\alpha} + \Theta^3 (\bar{g}_\alpha \cdot \bar{\lambda}_{,\beta}$$

$$+ \bar{g}_\beta \cdot \bar{\lambda}_{,\alpha}) + \bar{u}_{,\alpha} \cdot \bar{u}_{,\beta} + \Theta^3 (\bar{u}_{,\alpha} \cdot \bar{\lambda}_{,\beta}$$

$$+ \bar{u}_{,\beta} \cdot \bar{\lambda}_{,\alpha}) + (\Theta^3)^2 \bar{\lambda}_{,\alpha} \cdot \bar{\lambda}_{,\beta} \qquad (2.22)$$

The base vectors $\bar{g}_\alpha$ of the spatial system can be expressed as

$$\bar{g}_\alpha = \bar{a}_\alpha - \Theta^3 b_\alpha^\beta \bar{a}_\beta \qquad (2.23)$$

where b_α^β are the mixed variant components of the curvature tensor.

Substituting Eq. (2.23) into Eq. (2.22) and neglecting terms of $(\Theta^3)^2$ and higher order terms in $\bar{\lambda}$

$$G_{\alpha\beta} - g_{\alpha\beta} = \bar{a}_\alpha \cdot \bar{u}_{,\beta} + \bar{a}_\beta \cdot \bar{u}_{,\alpha} + \bar{u}_{,\alpha} \cdot \bar{u}_{,\beta}$$

$$+ [\bar{a}_\alpha \cdot \bar{\lambda}_{,\beta} + a_\beta \cdot \bar{\lambda}_{,\alpha} - b_\alpha^\gamma \bar{a}_\gamma \cdot \bar{u}_{,\beta}$$

$$- b_\beta^\gamma \bar{a}_\gamma \cdot \bar{u}_{,\alpha}]\Theta^3 \qquad (2.24)$$

Let

$$^m\varepsilon^o_{\alpha\beta} = 1/2[\bar{a}_\alpha \cdot \bar{u}_{,\beta} + \bar{a}_\beta \cdot \bar{u}_{,\alpha}] \qquad (2.24a)$$

$$ {}^{b}\varepsilon_{\alpha\beta} = 1/2[\bar{a}_{\alpha} \cdot \bar{\lambda}_{,\beta} + \bar{a}_{\beta} \cdot \bar{\lambda}_{,\alpha} - b_{\alpha}^{\gamma}\bar{a}_{\gamma} \cdot \bar{u}_{,\beta} $$

$$ - b_{\beta}^{\gamma}\bar{a}_{\gamma} \cdot \bar{u}_{,\alpha}] \qquad (2.24b) $$

$$ {}^{mL}\varepsilon_{\alpha\beta} = 1/2[\bar{u}_{,\alpha} \cdot \bar{u}_{,\beta}] \qquad (2.24c) $$

Eq. (2.24) then can be written as

$$ 1/2[G_{\alpha\beta} - g_{\alpha\beta}] = {}^{mo}\varepsilon_{\alpha\beta} + {}^{mL}\varepsilon_{\alpha\beta} + \Theta^3 \, b_{\varepsilon_{\alpha\beta}} \qquad (2.25) $$

Similarly, the components $G_{\alpha 3}$ are given from Eqs. (2.17, 2.18, 2.20) as

$$ G_{\alpha 3} = (\bar{g}_{\alpha} + \bar{u}_{,\alpha} + \Theta^3 \, \bar{\lambda}_{,\alpha}) \cdot (\hat{a}_3 + \bar{\lambda}) \qquad (2.26) $$

After carrying out the dot product and neglecting higher order terms, it can be shown that

$$ G_{\alpha 3} = \bar{a}_{\alpha} \cdot \bar{\lambda} + \hat{a}_3 \cdot \bar{u}_{,\alpha} \qquad (2.27) $$

2.1 Strain Tensor

The strain tensor is defined as

$$ \bar{\varepsilon}_{ij} = 1/2[G_{ij} - g_{ij}] \qquad (2.28) $$

from Eq. (2.25)

$$ \bar{\varepsilon}_{\alpha\beta} = {}^{mo}\varepsilon_{\alpha\beta} + {}^{mL}\varepsilon_{\alpha\beta} + \Theta^3 \, b_{\varepsilon_{\alpha\beta}} \qquad (2.29) $$

$$\bar{\varepsilon}_{\alpha 3} = 1/2[\bar{a}_{\alpha} \cdot \bar{\lambda} + \hat{a}_3 \cdot \bar{u}_{,\alpha}] \tag{2.30}$$

where

${}^{m}\varepsilon^{o}_{\alpha\beta}$ = Linear part of membrane strain

${}^{m}\varepsilon^{L}_{\alpha\beta}$ = Nonlinear part of the membrane strain

${}^{b}\varepsilon_{\alpha\beta}$ = Bending strain component

$\bar{\varepsilon}_{\alpha 3}$ = Transverse shear strain

2.2 Strain Tensor in Cartesian Coordinates

The position vector of the undeformed middle surface $\bar{R}_o$ is given by

$$\bar{R}_o(\theta^1,\theta^2) = x^i \hat{e}_i \qquad (i = 1,2,3) \tag{2.31}$$

The tangent base vectors at the middle surface are

$$\bar{a}_{\alpha} = \bar{R}_{o,\alpha} = x^i_{,\alpha} \hat{e}_i \tag{2.32}$$

The unit normal vector to the middle surface is given by

$$\hat{a}_3 = \frac{\hat{a}_1 \times \hat{a}_2}{|\hat{a}_1 \times \hat{a}_2|} = n^i \hat{e}_i \tag{2.33}$$

It can be shown that,

$$|\hat{a}_1 \times \hat{a}_2| = \sqrt{a} \tag{2.34}$$

where a is the determinant of the covariant metric tensor.

The displacement and rotation vectors are expressed in cartesian components as

$$\bar{u} = u^i \hat{e}_i \tag{2.35}$$

and

$$\bar{\phi} = \phi^i \hat{e}_i \tag{2.36}$$

similarly,

$$\bar{u}_{,\alpha} = u^i_{,\alpha} \hat{e}_i \tag{2.37}$$

and

$$\bar{\phi}_{,\alpha} = \phi^i_{,\alpha} \hat{e}_i \tag{2.38}$$

2.2.1 Linear Membrane Strain Tensor

Substituting Eqs. (2.32), (2.37) and (2.38) in Eq. (2.24), the linear part of the membrane strain tensors can be written as

$$2^m\varepsilon^o_{\alpha\beta} = x^i_{,\alpha} u^i_{,\beta} + x^i_{,\beta} u^i_{,\alpha} \tag{2.39}$$

2.2.2 Bending Strain Tensor

The bending strain tensor can be written from Eq. (2.24b) as

$$2^{b}\varepsilon_{\alpha\beta} = a_{\alpha} \cdot \bar{\lambda}_{\beta} + \bar{a}_{\beta} \cdot \bar{\lambda}_{,\alpha} - b_{\alpha}^{\mu}\bar{a}_{\mu} \cdot \bar{u}_{,\beta} - b_{\beta}^{\mu}\bar{a}_{\mu} \cdot \bar{u}_{,\alpha} \tag{2.40}$$

From Eq. (2.10),

$$\bar{\lambda}_{,\alpha} = (\bar{\phi} \times \hat{a}_3),\alpha \tag{2.41}$$

$$= \bar{\phi}_{,\alpha} \times \hat{a}_3 + \bar{\phi} \times \hat{a}_{3,\alpha} \tag{2.42}$$

From Eqs. (2.33) and (2.38)

$$\bar{\phi}_{,\alpha} \times \hat{a}_3 = e_{ijk}\, \phi^{,i}\, n^j\, \hat{e}_k \tag{2.43}$$

$\hat{a}_{3,\alpha}$ can be expressed as

$$\hat{a}_{3,\alpha} = - b_{\alpha}^{\beta}\bar{a}_{\beta} \tag{2.44}$$

so that

$$\bar{\phi} \times \hat{a}_{3,\alpha} = (\phi^{i}\, \hat{e}_i) \times (-b_{\alpha}^{\beta}\, x^{j}_{,\beta}\, \hat{e}_j) \tag{2.45}$$

$$= -b_{\alpha}^{\beta} e_{ijk}\, \phi^{i}\, x^{j}_{,\beta}\, \hat{e}_k \tag{2.46}$$

Eq. (2.42) can now be written as

$$\bar{\lambda}_{,\alpha} = (e_{ijk}\,\phi^{i}_{,\alpha}\,n^{j} - b^{\mu}_{\alpha}\,e_{ijk}\,\phi^{i}\,x^{j}_{,\mu})\hat{e}_{k} \tag{2.47}$$

$$\bar{a}_{\alpha} \cdot \bar{\lambda}_{,\beta} = x^{m}_{,\alpha}\,\hat{e}_{m} \cdot \bar{\lambda}_{,\beta} \tag{2.48}$$

$$= (e_{ijk}\,\phi^{i}_{,\beta}\,n^{j} - b^{\mu}_{\beta}\,e_{ijk}\,\phi^{i}\,x^{j}_{,\mu})x^{k}_{,\alpha} \tag{2.49}$$

Similarly,

$$\bar{a}_{\beta} \cdot \bar{\lambda}_{,\alpha} = (e_{ijk}\,\phi^{i}_{,\alpha}n^{j} - b^{\mu}_{\alpha}e_{ijk}\,\phi^{i}\,x^{j}_{,\mu})x^{k}_{,\beta} \tag{2.50}$$

and

$$(b^{\mu}_{\alpha}\,\bar{a}_{\mu} \cdot \bar{u}_{,\beta} + b^{\mu}_{\beta}\bar{a}_{\mu} \cdot \bar{u}_{,\alpha}) = (b^{\mu}_{\alpha}\,x^{i}_{,\mu}\,u^{i}_{,\beta}$$

$$+ b^{\mu}_{\beta}\,x^{i}_{,\mu}\,u^{i}_{,\alpha}) \tag{2.51}$$

Using Eqs. (2.49-2.51)

$$2^{b}\varepsilon_{\alpha\beta} = [e_{ijk}\,\phi^{i}_{,\alpha}\,n^{j}\,x^{k}_{,\beta} + e_{ijk}\,\phi^{i}_{,\beta}\,n^{j}\,x^{k}_{,\alpha}]$$

$$- [b^{\mu}_{\alpha}\,e_{ijk}\,\phi^{i}\,x^{j}_{,\mu}\,x^{k}_{,\beta} + b^{\mu}_{\beta}\,e_{ijk}\,\phi^{i}\,x^{j}_{,\mu}\,x^{k}_{,\alpha}]$$

$$- [b^{\mu}_{\alpha}\,x^{i}_{,\mu}\,u^{i}_{,\beta} + b^{\mu}_{\beta}\,x^{i}_{,\mu}\,u^{i}_{,\alpha}] \tag{2.52}$$

2.2.3 Transverse Shear Strain Tensor

According to Eq. (2.30) the transverse shear strain is given by

$$2\bar{\varepsilon}_{\alpha 3} = [\bar{a}_{\alpha} \cdot \bar{\lambda} + \hat{a}_3 \cdot \bar{u}_{,\alpha}] \tag{2.53}$$

From Eq. (2.10)

$$\bar{\lambda} = \bar{\phi} \times \hat{a}_3 = e_{ijk}\, \phi^i\, n^j\, \hat{a}_k \tag{2.54}$$

Hence equation 2.53 can be written as

$$2\bar{\varepsilon}_{\alpha 3} = e_{ijk}\, \phi^i\, n^j\, x^k_{,\alpha} + n^i\, u^i_{,\alpha} \tag{2.55}$$

CHAPTER 3

THE DISCRETE-KIRCHHOFF CURVED TRIANGULAR (D-K-C-T) ELEMENT - A BRIEF REVIEW

The D-K-C-T element formulation for the case of a general anisotropic material are given in detail in reference 80. To give a better understanding of the later chapters, a portion of that work is reproduced here with particular reference to the isotropic case. There are some changes in the notations as well as representation of some of the equations from reference 80.

Figure 2 shows various coordinate systems used for the element. The curvilinear coordinates are denoted by α, β. Figure 2b shows the element definition in the α-β parametric plane. The element nodes are specified by their α, β coordinates and the element sides are specified as straight lines in the α, β parametric plane. This plane triangle is mapped onto the curvilinear element in the Euclidean space, as shown in Figure 2a, by the parametric equation of the middle surface. Figure 2c shows the natural coordinate system (ξ, η), where the triangle in the parametric plane is mapped onto the unit right angled triangle. The equation of the middle surface is described by the components of the position vector, $\overline{R}_0$ (α, β) as

$$\overline{R}_0(\alpha,\beta) = X(\alpha,\beta)\ \hat{e}_1 + Y(\alpha,\beta)\ \hat{e}_2 + Z(\alpha,\beta)\ \hat{e}_3 \qquad (3.1)$$

The mapping between the α-β and ξ-η planes is defined by the relations

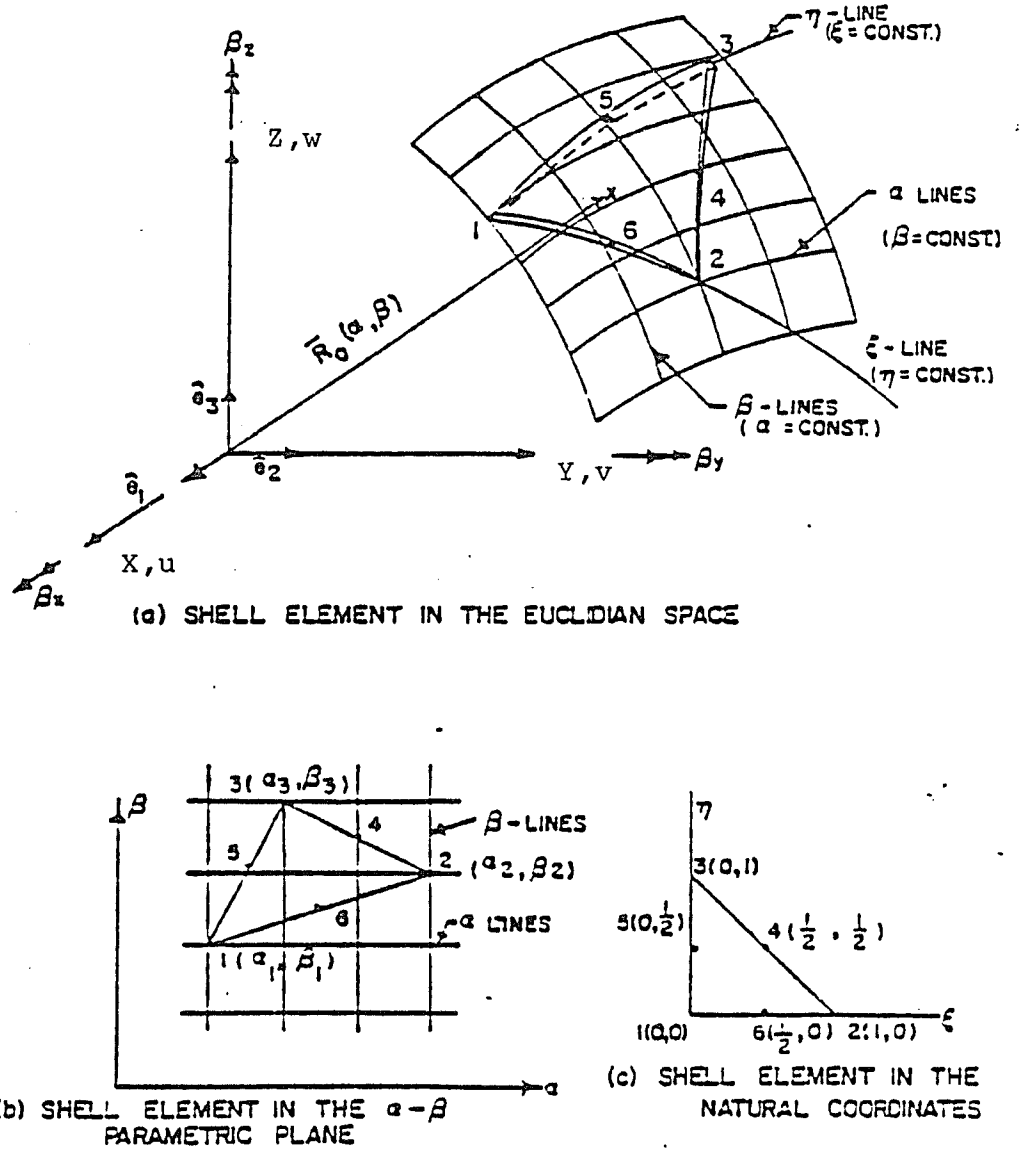

(a) SHELL ELEMENT IN THE EUCLIDIAN SPACE

(b) SHELL ELEMENT IN THE α−β PARAMETRIC PLANE

(c) SHELL ELEMENT IN THE NATURAL COORDINATES

Figure 2. Coordinate systems.

$$\alpha = \alpha_1 + (\alpha_2 - \alpha_1)\,\xi + (\alpha_3 - \alpha_1)\,\eta \tag{3.2a}$$

$$\beta = \beta_1 + (\beta_2 - \beta_1)\,\xi + (\beta_3 - \beta_1)\,\eta \tag{3.2b}$$

3.1 Interpolation of Displacements and Rotations

Each of the cartesian components of displacements, u, v or w is assumed as a complete cubic polynomial in ξ, η coordinates. For example,

$$u = a_1 + a_2\xi + a_3\eta + a_4\xi^2 + a_5\xi\eta + a_6\eta^2 + a_7\xi^3 + a_8\xi^2\eta + a_9\xi\eta^2 + a_{10}\eta^3 \tag{3.3}$$

$$= \lfloor p(\xi,\eta) \rfloor \{a\} \tag{3.4a}$$

where

$$\lfloor p(\xi,\eta) \rfloor = \lfloor 1 \;\; \xi \;\; \eta \;\; \xi^2 \;\; \xi\eta \;\; \eta^2 \;\; \xi^3 \;\; \xi^2\eta \;\; \xi\eta^2 \;\; \eta^3 \rfloor \tag{3.4b}$$

$$\{a\} = \lfloor a_1 \;\; a_2 \;\; a_3 \;\; a_4 \;\; a_5 \;\; a_6 \;\; a_7 \;\; a_8 \;\; a_9 \;\; a_{10} \rfloor^T \tag{3.4c}$$

After manipulation and transformation, the variation of u, v or w can be obtained in terms of the nodal values at the three corner nodes and the central node as

$$u = \lfloor N \rfloor \{u\} \tag{3.5a}$$

similarly,

$$v = \lfloor N \rfloor \{v\} \tag{3.5b}$$

and

$$w = \lfloor N \rfloor \{w\} \tag{3.5c}$$

where,

$\lfloor N \rfloor$ is a shape function vector

$$\{u\} = \lfloor u_1 \; u_{1,\alpha} \; u_{1,\beta} \; u_2 \; u_{2,\alpha} \; u_{2,\beta} \; u_3 \; u_{3,\alpha} \; u_{3,\beta} \; u_g \rfloor^T \tag{3.6a}$$

$$\{v\} = \lfloor v_1 \; v_{1,\alpha} \; v_{1,\beta} \; v_2 \; v_{2,\alpha} \; v_{2,\beta} \; v_3 \; v_{3,\alpha} \; v_{3,\beta} \; v_g \rfloor^T \tag{3.6b}$$

$$\{w\} = \lfloor w_1 \; w_{1,\alpha} \; w_{1,\beta} \; w_2 \; w_{2,\alpha} \; w_{2,\beta} \; w_3 \; w_{3,\alpha} \; w_{3,\beta} \; w_g \rfloor^T \tag{3.6c}$$

Each of the cartesian components of the rotation vectors β_x, β_y, or β_z is assumed as a complete quadratic polynomial in ξ-η coordinates. For example,

$$\beta_1 = b_1 + b_2\xi + b_3\eta + b_4\xi^2 + b_5\xi\eta + b_6\eta^2 \tag{3.7}$$

Again, after manipulation, β_x, β_y or β_z can be interpolated in terms of their nodal values at the three corner and three mid-side nodes.

$$\beta_x = \lfloor N' \rfloor \{\beta_x\} \tag{3.8a}$$

$$\beta_y = \lfloor N' \rfloor \{\beta_y\} \tag{3.8b}$$

$$\beta_z = \lfloor N' \rfloor \{\beta_z\} \tag{3.8c}$$

$$\{\beta_x\} = \lfloor \beta_{x_1} \ \beta_{x_2} \ \beta_{x_3} \ \beta_{x_4} \ \beta_{x_5} \ \beta_{x_6} \rfloor^T \tag{3.9a}$$

$$\{\beta_y\} = \lfloor \beta_{y_1} \ \beta_{y_2} \ \beta_{y_3} \ \beta_{y_4} \ \beta_{y_5} \ \beta_{y_6} \rfloor^T \tag{3.9b}$$

$$\{\beta_z\} = \lfloor \beta_{z_1} \ \beta_{z_2} \ \beta_{z_3} \ \beta_{z_4} \ \beta_{z_5} \ \beta_{z_6} \rfloor^T \tag{3.9c}$$

and

$\lfloor N' \rfloor$ is a shape function vector

3.2 Element Strain Energy

The total strain energy in a shell can be computed as the sum of the strain energies of the finite elements of the shell. The strain energy can be expressed as the sum of the energies associated with the stretching and bending of the shell and that due to transverse shear deformation. In the case of thin shells, the transverse shear strain energy is negligible and in order to converge to the thin shell solution, the energy due to transverse shear strain is neglected. The strain energy density per unit volume is then given by

$$u_s = 1/2 \left[\lfloor {}^m\varepsilon \rfloor \, [A] \, \{{}^m\varepsilon\} + \lfloor {}^b\varepsilon \rfloor \, [C] \, \{{}^b\varepsilon\} \right] \tag{3.10}$$

where

$$\lfloor {}^m\varepsilon \rfloor = \lfloor {}^m\varepsilon_{11} \ {}^m\varepsilon_{12} \ {}^m\varepsilon_{22} \rfloor \tag{3.11a}$$

$$\lfloor {}^b\varepsilon \rfloor = \lfloor {}^b\varepsilon_{11} \ {}^b\varepsilon_{12} \ {}^b\varepsilon_{22} \rfloor \tag{3.11b}$$

The stretching and bending rigidity matrices [A] and [C] are given by

$$[A] = \frac{E\ h}{(1-\nu^2)} \begin{bmatrix} (a^{11})^2 & 2\ a^{11}\ a^{12} & (1-\nu)(a^{12})^2 + \nu\ a^{11}\ a^{22} \\ & 2(1-\nu)\ a^{11}\ a^{22} + 2(1+\nu)(a^{12})^2 & 2\ a^{12}\ a^{22} \\ \text{Symm.} & & (a^{22})^2 \end{bmatrix} \tag{3.12a}$$

where

E = Young's Modulus

h = Element thickness

ν = Poisson's ratio

and $a^{\alpha\beta}$ (α = 1,2; β = 1,2) are the contravariant components of the metric tensor

$$[C] = \frac{h^2}{12}\,[A] \tag{3.12b}$$

3.2.1 Linear Strains

The linear part of the membrane strain ${}^{m}\varepsilon^{o}$ is given by Eq. 2.24a. After expanding the indices, it can be shown that,

$${}^{m}\varepsilon^{o}_{11} = \frac{\partial x}{\partial \alpha}\frac{\partial u}{\partial \alpha} + \frac{\partial y}{\partial \alpha}\frac{\partial v}{\partial \alpha} + \frac{\partial z}{\partial \alpha}\frac{\partial w}{\partial \alpha} \tag{3.13a}$$

$${}^{m}\varepsilon^{o}_{12} = \frac{1}{2}\left[\frac{\partial x}{\partial \alpha}\frac{\partial u}{\partial \beta} + \frac{\partial y}{\partial \alpha}\frac{\partial v}{\partial \beta} + \frac{\partial z}{\partial \alpha}\frac{\partial w}{\partial \beta} + \frac{\partial x}{\partial \beta}\frac{\partial u}{\partial \alpha} + \frac{\partial y}{\partial \beta}\frac{\partial v}{\partial \alpha} + \frac{\partial z}{\partial \beta}\frac{\partial w}{\partial \alpha}\right] \tag{3.13b}$$

$$ {}^{m}\varepsilon^{o}_{22} = \frac{\partial x}{\partial \beta}\frac{\partial u}{\partial \beta} + \frac{\partial y}{\partial \beta}\frac{\partial v}{\partial \beta} + \frac{\partial z}{\partial \beta}\frac{\partial w}{\partial \beta} \tag{3.13c} $$

The linear part of the bending strain ${}^{b}\varepsilon$, after expanding Eq. 2.24b, is given as follows:

$$ \begin{aligned} \chi_{11} = &-(c_1 \frac{\partial z}{\partial \alpha} - c_2 \frac{\partial y}{\partial \alpha})\beta_x - (c_2 \frac{\partial x}{\partial \alpha} - c_3 \frac{\partial z}{\partial \alpha})\beta_y \\ &- (c_3 \frac{\partial y}{\partial \alpha} - c_1 \frac{\partial x}{\partial \alpha})\beta_z + a_1 \frac{\partial \beta_x}{\partial \alpha} + a_2 \frac{\partial \beta_y}{\partial \alpha} + a_3 \frac{\partial \beta_z}{\partial \alpha} \\ &- (c_3 \frac{\partial u}{\partial \alpha} + c_1 \frac{\partial v}{\partial \alpha} + c_2 \frac{\partial w}{\partial \alpha}) \end{aligned} \tag{3.14a} $$

$$ \begin{aligned} \chi_{12} = \frac{1}{2}[&-(c_1 \frac{\partial z}{\partial \beta} - c_2 \frac{\partial y}{\partial \beta})\beta_x - (c_2 \frac{\partial x}{\partial \beta} - c_3 \frac{\partial z}{\partial \beta})\beta_y \\ &- (c_3 \frac{\partial y}{\partial \beta} - c_1 \frac{\partial x}{\partial \beta})\beta_z - (d_1 \frac{\partial z}{\partial \alpha} - d_2 \frac{\partial y}{\partial \alpha})\beta_x \\ &- (d_2 \frac{\partial x}{\partial \alpha} - d_3 \frac{\partial z}{\partial \alpha})\beta_y - (d_3 \frac{\partial y}{\partial \alpha} - d_1 \frac{\partial x}{\partial \alpha})\beta_z \\ &+ a_1 \frac{\partial \beta_x}{\partial \beta} + a_2 \frac{\partial \beta_y}{\partial \beta} + a_3 \frac{\partial \beta_z}{\partial \beta} + b_1 \frac{\partial \beta_x}{\partial \alpha} + b_2 \frac{\partial \beta_y}{\partial \alpha} + b_3 \frac{\partial \beta_z}{\partial \alpha} \\ &- (c_3 \frac{\partial u}{\partial \beta} + c_1 \frac{\partial v}{\partial \beta} + c_2 \frac{\partial w}{\partial \beta} + d_3 \frac{\partial u}{\partial \alpha} + d_1 \frac{\partial v}{\partial \alpha} + d_2 \frac{\partial w}{\partial \alpha})] \end{aligned} \tag{3.14b} $$

$$ \begin{aligned} \chi_{22} = &-(d_1 \frac{\partial z}{\partial \beta} - d_2 \frac{\partial y}{\partial \beta})\beta_x - (d_2 \frac{\partial x}{\partial \beta} - d_3 \frac{\partial z}{\partial \beta})\beta_y \\ &- (d_3 \frac{\partial y}{\partial \beta} - d_1 \frac{\partial x}{\partial \beta})\beta_z + b_1 \frac{\partial \beta_x}{\partial \beta} + b_2 \frac{\partial \beta_y}{\partial \beta} + b_3 \frac{\partial \beta_z}{\partial \beta} \\ &- (d_3 \frac{\partial u}{\partial \beta} + d_1 \frac{\partial v}{\partial \beta} + d_2 \frac{\partial w}{\partial \beta}) \end{aligned} \tag{3.14c} $$

$$ a_1 = n_2 \frac{\partial z}{\partial \alpha} - n_3 \frac{\partial y}{\partial \alpha}, \quad a_2 = n_3 \frac{\partial x}{\partial \alpha} - n_1 \frac{\partial z}{\partial \alpha}, \quad a_3 = n_1 \frac{\partial y}{\partial \alpha} - n_2 \frac{\partial x}{\partial \alpha} \tag{3.15a} $$

$$b_1 = n_2 \frac{\partial z}{\partial \beta} - n_3 \frac{\partial y}{\partial \beta}, \quad b_2 = n_3 \frac{\partial x}{\partial \beta} - n_1 \frac{\partial z}{\partial \beta}, \quad b_3 = n_1 \frac{\partial y}{\partial \beta} - n_2 \frac{\partial x}{\partial \beta} \tag{3.15b}$$

$$c_1 = b_1^1 \frac{\partial y}{\partial \alpha} + b_1^2 \frac{\partial y}{\partial \beta}, \quad c_2 = b_1^1 \frac{\partial z}{\partial \alpha} + b_1^2 \frac{\partial z}{\partial \beta}, \quad c_3 = b_1^1 \frac{\partial x}{\partial \alpha} + b_1^2 \frac{\partial x}{\partial \beta} \tag{3.15c}$$

$$d_1 = b_2^1 \frac{\partial y}{\partial \alpha} + b_2^2 \frac{\partial y}{\partial \beta}, \quad d_2 = b_2^1 \frac{\partial z}{\partial \alpha} + b_2^2 \frac{\partial z}{\partial \beta}, \quad d_3 = b_2^1 \frac{\partial x}{\partial \alpha} + b_2^2 \frac{\partial x}{\partial \beta} \tag{3.15d}$$

In the above equations, $n_i (i = 1, 3)$ are the components of the surface unit normal vector, and b_α^β $(\alpha,\beta = 1,2)$ are the mixed variant components of the curvature tensor.

It can be seen that the bending strains are functions of the rotations and their derivatives with respect to α and β. These rotations can be expressed in terms of the displacement degrees-of-freedom by solving the equations arising from the following constraints:

(i) The Discrete-Kirchoff (D-K) Constraints:

The D-K constraints are imposed at the six nodes of the element. The six D-K constraints at the three corner nodes are given by

$$(\varepsilon_{i3})_j = 0 \quad i = 1,2 \quad j = 1,2,3 \tag{3.16}$$

The three constraints at the three mid-side nodes are

$$(\bar{\varepsilon}_{s3})_k = 0 \quad k = 4,5,6 \tag{3.17}$$

where $\bar{\varepsilon}_{s3}$ is the transverse shear strain with the curvilinear direction s.

(ii) Surface Normal Rotation Constraints (SNRC)

The SNRC express the condition that the rotations of the shell about the surface normal be the same.

The rotation of the shell about the surface normal can be expressed in two ways. First, it is expressed in terms of the displacement gradients as

$$\Omega = \frac{1}{2\sqrt{a}} [(x_{,\beta}u_{,\alpha} - x_{,\alpha}u_{,\beta}) + (y_{,\beta}v_{,\alpha} - y_{,\alpha}v_{,\beta}) + (z_{,\beta}w_{,\alpha} - z_{,\alpha}w_{,\beta})] \tag{3.18}$$

Secondly, it is expressed in terms of the independent rotations as

$$\Omega = n_1\beta_x + n_2\beta_y + n_3\beta_z \tag{3.19}$$

Thus, the condition that Eq. (3.18) and Eq. (3.19) be the same at the six nodes of the element leads to six more equations.

(iii) Linear Variation of Normal Rotation Constraints (LVNRC)

The LVNRC impose a linear variation of the normal rotation along the element sides. If β_s denotes the component of the rotation vector along the tangent to the curvilinear side of the element, the LVNRC are given by

$$\beta_{sk} = 1/2\ (\beta_{si} + \beta_{sj}) \tag{3.20}$$

where k is the mid-side node on the curvilinear side joining the corner nodes i and j. This constraint is imposed at the three

mid-side nodes resulting in three more equations that also eliminates the three mid-side nodes.

These eighteen constraint equations (from Eqs. (3.16 - 3.20)) are used to eliminate the rotation degrees-of-freedom in terms of the displacement degrees-of-freedom. Thus, the element is reduced to three corner nodes and a centroidal node and the nodal degrees-of-freedom are reduced to thirty degrees-of-freedom (twenty-seven displacements and their gradients at the three corner nodes and three displacements at the centroidal node).

The linear strains in Eqs. (3.13) and (3.14) can, therefore, be expressed in terms of the thirty degrees-of-freedom as

$$\{\varepsilon^o\}_{6x1} = \left\{ \begin{matrix} m_{\varepsilon o} \\ \hline b_\varepsilon \end{matrix} \right\} = \left[\begin{matrix} {}^mB_o \\ \hline {}^bB \end{matrix} \right] \{U\}_{30x1} \tag{3.21}$$

where $\{U\}^T = \lfloor u_1\ u_{1,\alpha}\ u_{1,\beta}\ u_2\ u_{2,\alpha}\ u_{2,\beta}\ u_3\ u_{3,\alpha}\ u_{3,\beta}\ u_g$

$$v_1\ v_{1,\alpha}\ v_{1,\beta}\ v_2\ v_{2,\alpha}\ v_{2,\beta}\ v_3\ v_{3,\alpha}\ v_{3,\beta}\ v_g$$

$$w_1\ w_{1,\alpha}\ w_{1,\beta}\ w_2\ w_{2,\alpha}\ w_{2,\beta}\ w_3\ w_{3,\alpha}\ w_{3,\beta}\ w_g \rfloor \tag{3.22}$$

The coefficients of $[{}^mB_o]$ and $[{}^bB]$ cannot be expressed explicitly and are computed inside the program.

3.3 Linear Element Stiffness

The total potential energy of an element is given by

$$\Pi^{(e)} = U^{(e)} + V^{(e)} \tag{3.23}$$

where $V^{(e)}$ is the potential of the applied loads.

$$V^{(e)} = -\int (R_1 u + R_2 v + R_3 w) \sqrt{a}\, d\alpha\, d\beta \tag{3.24}$$

where R_1, R_2 and R_3 are the components of the external loads along the cartesian directions X, Y and Z respectively. The element strain energy is given from Eq. (3.10) as

$$U^{(e)} = 1/2 \int \lfloor \varepsilon \rfloor\, [D]\, \{\varepsilon\}\, \sqrt{a}\, d\alpha\, d\beta \tag{3.25}$$

where

$$\lfloor \varepsilon \rfloor = \lfloor {}^{m}\varepsilon^{o} \mid {}^{b}\varepsilon \rfloor \tag{3.26}$$

and

$$[D] = \left[\begin{array}{c|c} [A] & 0 \\ \hline 0 & [C] \end{array}\right] \tag{3.27}$$

Taking the stationary value of Π in Eq. (3.23) leads to the element stiffness matrix and the consistent nodal loads. Thus,

$$K_{ij} = \frac{\partial^2 U^{(e)}}{\partial U_i\, \partial U_j} = \int \lfloor \varepsilon_i \rfloor\, [D]\, \{\varepsilon_j\}\, \sqrt{a}\, d\alpha\, d\beta \tag{3.28}$$

$$R_i^{(j)} = \frac{\partial V^{(e)}}{\partial U_i} = \int R_j (U_j)_i\, \sqrt{a}\, d\alpha\, d\beta \tag{3.29}$$

The integrations are carried out by a numerical integration scheme of Cowper[81].

$$K_{ij} = \sum_{o}^{1}\sum_{o}^{1} \lfloor \epsilon_i \rfloor [D] \{\epsilon_j\} \sqrt{a}\, |J|\, d\xi\, d\eta \qquad (3.30a)$$

$$R_i^{(j)} = \sum_{o}^{1}\sum_{o}^{1} R_j (U_j)_i \sqrt{a}\, |J|\, d\xi\, d\eta \qquad (3.30b)$$

where $|J|$ is the Jacobian determinant and is given by

$$|J| = (\alpha_2 - \alpha_1)(\beta_3 - \beta_1) - (\alpha_3 - \alpha_1)(\beta_2 - \beta_1) \qquad (3.31)$$

It is apparent that the element stiffness matrix and the consistent nodal loads are started with respect to the global cartesian system. As the element variables are more relevant in the local curvilinear system (α, β), and also to facilitate the application of symmetric and support conditions, it is desirable to transform the element stiffness matrix $[k_o]$ and the consistent nodal load vector $\{R\}$ to the α, β curvilinear system.

If $[T]$ is a transformation matrix relating the two systems, then

$$[K_o]_\alpha = [T]^T [K_o] [T] \qquad (3.32)$$

and

$$\{R\}_\alpha = [T]^T \{R\} \qquad (3.33)$$

where the subscript α denotes the curvilinear frame with respect to the nodal degrees-of-freedom $\{U\}_\alpha$

$$\{U\}_{\alpha}^{T} = \lfloor \bar{u}_1\ \bar{u}_{1,\alpha}\ \bar{u}_{1,\beta}\ \bar{v}_1\ \bar{v}_{1,\alpha}\ \bar{v}_{1,\beta}$$
$$\bar{w}_1\ \bar{w}_{1,\alpha}\ \bar{w}_{1,\beta}\ \bar{u}_2\ \bar{u}_{2,\alpha}\ \bar{u}_{2,\beta}$$
$$\bar{v}_2\ \bar{v}_{2,\alpha}\ \bar{v}_{2,\beta}\ \bar{w}_2\ \bar{w}_{2,\alpha}\ \bar{w}_{2,\beta}$$
$$\bar{u}_3\ \bar{u}_{3,\alpha}\ \bar{u}_{3,\beta}\ \bar{v}_3\ \bar{v}_{3,\alpha}\ \bar{v}_{3,\beta}$$
$$\bar{w}_3\ \bar{w}_{3,\alpha}\ \bar{w}_{3,\beta}\ \bar{u}_g\ \bar{v}_g\ \bar{w}_g \rfloor \qquad (3.34)$$

where, for example, $\bar{u}_1$ is the displacement at node 1 in the direction of α

$$\{R\}_{\alpha}^{T} = \lfloor R_1(\bar{u}_1)\ R_1(\bar{u}_1)_{,\alpha}\ R_1(\bar{u}_1)_{,\beta}$$
$$R_1(\bar{v}_1)\ R_1(\bar{v}_1)_{,\alpha}\ R_1(\bar{v}_1)_{,\beta}$$
$$R_1(\bar{w}_1)\ R_1(\bar{w}_1)_{,\alpha}\ R_1(\bar{w}_1)_{,\beta}$$
$$R_2(\bar{u}_2)\ R_2(\bar{u}_2)_{,\alpha}\ R_2(\bar{u}_2)_{,\beta}$$
$$R_2(\bar{v}_2)\ R_2(\bar{v}_2)_{,\alpha}\ R_2(\bar{v}_2)_{,\beta}$$
$$R_2(\bar{w}_2)\ R_2(\bar{w}_2)_{,\alpha}\ R_2(\bar{w}_2)_{,\beta}$$
$$R_3(\bar{u}_3)\ R_3(\bar{u}_3)_{,\alpha}\ R_3(\bar{u}_3)_{,\beta}$$
$$R_3(\bar{v}_3)\ R_3(\bar{v}_3)_{,\alpha}\ R_3(\bar{v}_3)_{,\beta}$$
$$R_3(\bar{w}_3)\ R_3(\bar{w}_3)_{,\alpha}\ R_3(\bar{w}_3)_{,\beta}$$
$$R_3(\bar{u}_g)\ R_3(\bar{v}_g)\quad R_3(\bar{w}_g)\ \rfloor \qquad (3.35)$$

in which, for example, $R_1(\bar{u}_1)$ is the consistent nodal load at node 1 corresponding to the tangential displacement $\bar{u}_1$.

CHAPTER 4

NONLINEAR FORMULATION

The finite element formulation of nonlinear problems consists of kinematic formulation of the problem using the principles of continuum mechanics, identification of the constitutive relations and discretization of the equations using finite element procedures.

4.1 Continuum Mechanics Formulation

The continuum mechanics formulation of nonlinear problems is in general done by two approaches; (i) Lagrangian (material) and (ii) Eulerian (spatial). The difference between these two approaches is that in the former attention is focused on the material itself as it moves, while in the latter attention is focused on what happens at a specific spatial location. Eulerian formulations are used almost exclusively in fluid flow analysis, while Lagrangian descriptions are widely employed in solid mechanics problems.[82] The application of the Lagrangian approach to the solid mechanics problems is due to the fact that the boundaries of the body change during the history of motion and it is natural to use the description that follows the material of the body.

4.1.1 Incremental Equations of Motion

Consider the motion of a body in a cartesian coordinate system as shown in Figure 3. The equilibrium positions of the body at

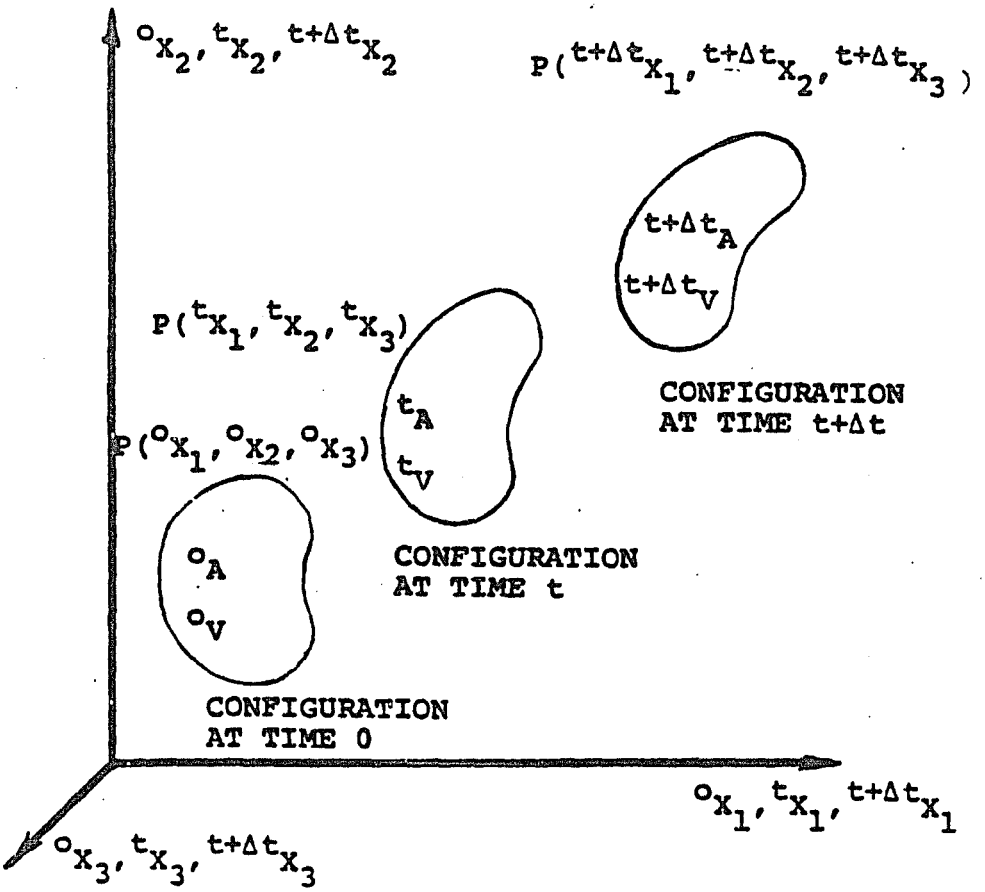

Figure 3. Motion of body in cartesian coordinate system.

various time increments Δt are to be evaluated. The equilibrium path at time $t + \Delta t$ requires the solution of all kinematic and static variables from the initial time 0 up to time t.

Let

$^{0}x_i$ = coordinates of a material point at time 0

$^{t}x_i$ = coordinates of the material point at time t

$^{t+\Delta t}x_i$ = coordinates of the material point at time $t + \Delta t$

$^{t}u_i$ = displacement of the material point at time t

$^{t+\Delta t}u_i$ = displacement of the material point at time $t + \Delta t$

Then,

$$^{t}x_i = {}^{0}x_i + {}^{t}u_i \tag{4.1a}$$

$$^{t+\Delta t}x_i = {}^{0}x_i + {}^{t+\Delta t}u_i \tag{4.1b}$$

The unknown increments in the displacements from time t to $t + \Delta t$ are

$$\Delta u_i = {}^{t+\Delta t}u_i - {}^{t}u_i \quad (i = 1,2,3) \tag{4.2}$$

During the motion of the body, its area, volume, mass density, stresses and strains are changing continuously.

Let dA and dV denote elemental area and volume of the body and A and V total area and volume of the body. Again, the superscripts 0, t and $t + \Delta t$ refer to these quantities at times 0, t and $t + \Delta t$ respectively.

Let

${}^{t+\Delta t}_{t}f_k$ = body force per unit mass at time $t + \Delta t$ but measured in configuration t

${}^{t+\Delta t}_{t}q_k$ = surface traction at time $t + \Delta t$ but measured in configuration t

${}^{t+\Delta t}\tau_{ij}$ = Cauchy stress tensor at time $t + \Delta t$

Assuming solutions have been obtained at all discrete times 0 to t with increments Δt, the virtual work equation at time $t + \Delta t$ can be written as

$$\int_{t+\Delta t_V} {}^{t+\Delta t}\tau_{ij}\ {}^{t+\Delta t}\delta e_{ij}\ {}^{t+\Delta t}dv = \int_{t+\Delta t_A} {}^{t+\Delta t}_{t}q_k\ \delta u_k\ {}^{t+\Delta t}dA$$

$$+ \int_{t+\Delta t_V} {}^{t+\Delta t}\rho\ {}^{t+\Delta t}_{t}f_k\ \delta u_k\ {}^{t+\Delta t}dV \qquad (4.3)$$

where

δe_{ij} = variation of Almansi strain tensor

δu_k = variation in current displacement component

${}^{t+\Delta t}\rho$ = mass density at time $t + \Delta t$

Eq. (4.3) cannot be solved directly since the configuration at time $t + \Delta t$ is not known. A solution can be obtained by referring to any one of the previously calculated equilibrium configurations. The choice is essentially either the initial configuration (time = 0) or the configuration at time t. The former is known as the Total

Lagrangian (T.L) and the latter the Updated Lagrangian (U.L). Details of the principles involved in the T.L and U.L formulations can be found in several textbooks and a few of them are given in references 83-86. Only the T.L formulation, which has been adopted in the present work, is described below.[87]

4.2 Total Lagrangian (T.L) Formulation

In this formulation, all variables are referred to the initial configuration. The applied traction and the body forces with respect to the initial configuration can be evaluated using

$$ {}^{t+\Delta t}_{t}q_k \; {}^{t+\Delta t}dA = {}^{t+\Delta t}_{o}q_k \; {}^{o}dA \tag{4.4a} $$

$$ {}^{t+\Delta t}_{t}f_k \; {}^{t+\Delta t}dV = {}^{t+\Delta t}_{o}f_k \; {}^{o}dV \qquad k = 1,2,3 \tag{4.4b} $$

The Cauchy stress tensor τ_{ij} at time $t + \Delta t$ can be related to the second Piola-Kirchoff (2nd. P-K) stress tensor S_{ij} at time $t + \Delta t$ but measured at time 0, by the principle of work conjugacy

$$ {}^{t+\Delta t}\tau_{ij} \; {}^{t+\Delta t}\delta e_{ij} \; {}^{t+\Delta t}dV = {}^{t+\Delta t}_{o}S_{ij} \; {}^{t+\Delta t}\delta_o E_{ij} \; {}^{o}dV \tag{4.5} $$

where

${}^{t+\Delta t}\delta_o E_{ij}$ = variation of the Green-Lagrange strain tensor at time $t + \Delta t$ but measured in configuration 0

Substituting Eqs. (4.4) and (4.5) into Eq. (4.3), the equilibrium equation for the body at time $t + \Delta t$, but referred to the configuration at time 0, is obtained as

$$\int_{{}_oV} {}_oS_{ij}\ {}^{t+\Delta t}_{o}\delta_o E_{ij}\ {}_odV = \int_{{}_oA} {}_oq_k\ \delta u_k\ {}_odA + \int_{{}_oV} {}_o\rho\ {}^{t+\Delta t}_{o}f_k\ \delta u_k\ {}_odV = {}^{t+\Delta t}R \tag{4.6}$$

Since the stresses ${}^{t+\Delta t}_{o}S_{ij}$ and strains ${}^{t+\Delta t}_{o}E_{ij}$ are unknown at time $t + \Delta t$, the following incremental decompositions are used.

$${}^{t+\Delta t}_{o}S_{ij} = {}^{t}_{o}S_{ij} + {}_oS_{ij} \tag{4.7a}$$

$${}^{t+\Delta t}_{o}E_{ij} = {}^{t}_{o}E_{ij} + {}_oE_{ij} \tag{4.7b}$$

The incremental second P-K stresses ${}_oS_{ij}$ and the incremental Green-Lagrange strains ${}_oE_{ij}$ are related by the constitutive relation

$${}_oS_{ij} = {}_oC_{ijk\ell}\ {}_oE_{k\ell} \tag{4.8}$$

Eq. (4.6) can now be written as

$$\int_{{}_oV} {}_oC_{ijk\ell}\ {}_oE_{k\ell}\ \delta_o E_{ij}\ {}_odV + \int_{{}_oV}^{t} {}_oS_{ij}\ \delta\,{}^{t}_{o}E_{ij}\ {}_odV = {}^{t+\Delta t}R \tag{4.9}$$

Eq. (4.9) represents a nonlinear equation for the displacement u_i. The nonlinear equation of equilibrium will be discretized using the standard finite element procedures into a set of incremental

equations and solved iteratively, until the equilibrium configuration is achieved.

4.3 Finite Element Discretization

A material particle p in the initial undeformed configuration (time = 0) is identified by the Lagrangian coordinates as

$$\{X\} = \lfloor X \quad Y \quad Z \rfloor^T \tag{4.10}$$

The same particle in the deformed configuration is identified by the Eulerian coordinates as

$$\{x\} = \lfloor x \quad y \quad z \rfloor^T \tag{4.11}$$

If the displacements $\{u\}$ of the particle can be given as functions of $\{X\}$ or $\{x\}$

$$\begin{Bmatrix} u \\ v \\ w \end{Bmatrix} = \begin{Bmatrix} u(\underset{\sim}{x}) \\ v(\underset{\sim}{x}) \\ w(\underset{\sim}{x}) \end{Bmatrix} = \begin{Bmatrix} u(\underset{\sim}{X}) \\ v(\underset{\sim}{X}) \\ w(\underset{\sim}{X}) \end{Bmatrix} \tag{4.12}$$

then the final coordinates of the particle are given by

$$\{x\} = \{X\} + \{u\} \tag{4.13}$$

Considering a single element, the cartesian component of the displacements within the element are given as a function of the nodal displacements, as in Eq. (3.5)

$$\begin{Bmatrix} u \\ v \\ w \end{Bmatrix} = \begin{bmatrix} \lfloor N \rfloor & \lfloor 0 \rfloor & \lfloor 0 \rfloor \\ \lfloor 0 \rfloor & \lfloor N \rfloor & \lfloor 0 \rfloor \\ \lfloor 0 \rfloor & \lfloor 0 \rfloor & \lfloor N \rfloor \end{bmatrix} \begin{Bmatrix} \underset{\sim}{u} \\ \underset{\sim}{v} \\ \underset{\sim}{w} \end{Bmatrix} \tag{4.14}$$

or

$$\underset{3x1}{\{u\}} = \underset{3x30}{[N]} \quad \underset{30x1}{\{U\}} \tag{4.15}$$

where

$$[N] = [N(\underset{\sim}{x})] \tag{4.16a}$$

and

$$\{U\} = \lfloor \underset{\sim}{u} \; \underset{\sim}{v} \; \underset{\sim}{w} \rfloor^T = \lfloor u_1 \ldots u_g \; v_1 \ldots v_g \; w_1 \ldots w_g \rfloor^T \tag{4.16b}$$

The variation in the displacements {du} are given by

$$\{du\} = [N] \{dU\} \tag{4.17}$$

Let $\{\varepsilon\}$ represent the Green-Lagrange strain vector

$$\{\varepsilon\} = \{\varepsilon^0\} + \{\varepsilon^L\} \tag{4.18}$$

where

$\{\varepsilon^0\}$ = linear part of the strain

and

$\{\varepsilon^L\}$ = nonlinear part of the strain.

From Eq. (3.21), the linear part of the strains can be expressed as,

$$\underset{6x1}{\{\varepsilon^0\}} = \underset{6x30}{[B_0]} \quad \underset{30x1}{\{U\}} \tag{4.19}$$

The nonlinear part of the Green-Lagrange strains $\{\varepsilon^L\}$ is given in Eq. (2.24c). Expanding the indices,

$$\varepsilon^L_{11} = \frac{1}{2}\left[u^2_{,\alpha} + v^2_{,\alpha} + w^2_{,\alpha}\right] \tag{4.20a}$$

$$\varepsilon^L_{12} = \frac{1}{2}\left[u_{,\alpha}\, u_{,\beta} + v_{,\alpha}\, v_{,\beta} + w_{,\alpha}\, w_{,\beta}\right] \tag{4.20b}$$

$$\varepsilon^L_{22} = \frac{1}{2}\left[u^2_{,\beta} + v^2_{,\beta} + w^2_{,\beta}\right] \tag{4.20c}$$

$$\begin{Bmatrix} \varepsilon^L_{11} \\ \varepsilon^L_{12} \\ \varepsilon^L_{22} \\ \hline 0 \end{Bmatrix} = \frac{1}{2} \left[\begin{array}{ccc:ccc} u_{,\alpha} & v_{,\alpha} & w_{,\alpha} & 0 & 0 & 0 \\ \frac{1}{2}u_{,\beta} & \frac{1}{2}v_{,\beta} & \frac{1}{2}w_{,\beta} & \frac{1}{2}u_{,\alpha} & \frac{1}{2}v_{,\alpha} & \frac{1}{2}w_{,\alpha} \\ 0 & 0 & 0 & u_{,\beta} & v_{,\beta} & w_{,\beta} \\ \hline \multicolumn{3}{c:}{0} & \multicolumn{3}{c}{0} \end{array}\right] \begin{Bmatrix} u_{,\alpha} \\ v_{,\alpha} \\ w_{,\alpha} \\ u_{,\beta} \\ v_{,\beta} \\ w_{,\beta} \end{Bmatrix}$$

$$\underset{6x1}{\{\varepsilon^L\}} = 1/2 \underset{6x6}{[A_\Theta]} \quad \underset{6x1}{\{\Theta\}} \tag{4.22}$$

where $[A_\Theta]$ and $\{\Theta\}$ are the displacement gradient matrix and vector respectively.

The displacement gradient vector $\{\Theta\}$ can be expressed as

$$\begin{Bmatrix} u_{,\alpha} \\ v_{,\alpha} \\ w_{,\alpha} \\ u_{,\beta} \\ v_{,\beta} \\ w_{,\beta} \end{Bmatrix} = \begin{bmatrix} \lfloor N_{,\alpha} \rfloor & \lfloor 0 \rfloor & \lfloor 0 \rfloor \\ \lfloor 0 \rfloor & \lfloor N_{,\alpha} \rfloor & \lfloor 0 \rfloor \\ \lfloor 0 \rfloor & \lfloor 0 \rfloor & \lfloor N_{,\alpha} \rfloor \\ \lfloor N_{,\beta} \rfloor & \lfloor 0 \rfloor & \lfloor 0 \rfloor \\ \lfloor 0 \rfloor & \lfloor N_{,\beta} \rfloor & \lfloor 0 \rfloor \\ \lfloor 0 \rfloor & \lfloor 0 \rfloor & \lfloor N_{,\beta} \rfloor \end{bmatrix} \{U\} \qquad (4.23)$$

or

$$\underset{6x1}{\{\Theta\}} = \underset{6x30}{[G]} \quad \underset{30x1}{\{U\}} \qquad (4.24)$$

Substituting Eq. (4.24) into Eq. (4.22)

$$\{\varepsilon^L\} = \frac{1}{2} [A_\Theta][G] \{U\} \qquad (4.25a)$$

$$= \frac{1}{2} [B_L] \{U\} \qquad (4.25b)$$

Eq. (4.18) can now be written as

$$\{\varepsilon\} = \{\varepsilon^0\} + \{\varepsilon^L\} = [B_0] + \frac{1}{2} [B_L] \{U\} \qquad (4.26)$$

The variation in the Green-Lagrange strain is given by

$$\{d\varepsilon\} = \{d\varepsilon^0\} + \{d\varepsilon^L\} \qquad (4.27)$$

where

$$\{d\varepsilon^0\} = [B_0] \{dU\} \qquad (4.28)$$

from Eq. (4.22),

$$\underset{6x1}{\{d\varepsilon^L\}} = \frac{1}{2}[A_\Theta]\{d\Theta\} + \frac{1}{2}[dA_\Theta]\{\Theta\} \tag{4.29}$$

$$= [A_\Theta]\{d\Theta\} \tag{4.30}$$

$$= [A_\Theta][G]\{dU\} \tag{4.31}$$

$$= \underset{6x30}{[B_L(\underset{\sim}{U})]}\ \underset{30x1}{\{dU\}} \tag{4.32}$$

where

$$\underset{6x30}{[B_L(\underset{\sim}{U})]} = \underset{6x6}{[A_\Theta]}\ \underset{6x30}{[G]} \tag{4.33}$$

Eq. (4.27), therefore, becomes

$$\{d\varepsilon\} = [B(\underset{\sim}{U})]\{dU\} \tag{4.34}$$

where

$$[B(\underset{\sim}{U})] = [B_o] + [B_L(\underset{\sim}{U})] \tag{4.35}$$

The second P-K stresses $\{\sigma\}$ are considered as linear functions of the Green-Lagrange strains $\{\varepsilon\}$ through the constitutive relation

$$\underset{6x1}{\{\sigma\}} = \underset{6x6}{[D]}\ \underset{6x1}{\{\varepsilon\}} \tag{4.36a}$$

and the variation of $\{\sigma\}$ is given by

$$\underset{6x1}{\{d\sigma\}} = \underset{6x6}{[D]}\ \underset{6x1}{\{d\varepsilon\}} \tag{4.36b}$$

The Total Lagrangian virtual work equation (4.6) can now be approximated by the finite element discretization by substituting Eqs. (4.15) to (4.36). Replacing d with δ,

$$\delta\{U\}^T \int_{{}^0V} [B]^T \{\sigma\}\, d^0V = \delta\{U\}^T \int_{{}^0V} [N]^T \{f\}\, \rho\, d^0V + \delta\{U\}^T \int_{{}^0A} [N]^T \{q\}\, d^0A \tag{4.37}$$

Since the virtual nodal displacements $\delta\{U\}$ are arbitrary, the element nonlinear equilibrium equations can be written as

$$\int_{{}^0V} [B]^T \{\sigma\}\, d^0V = \{R\} \tag{4.38}$$

where

$$\{R\} = \int_{{}^0V} [N]^T \{f\}\, \rho\, d^0V + \int_{{}^0A} [N]^T \{q\}\, d^0A \tag{4.39}$$

Eq. (4.39) represents a vector of consistent nodal forces due to body and traction forces and may also include other load terms that may be present on the body. It should be noted that the forces are assumed to be conservative.

The nonlinear equilibrium equation in (4.38) for an element or in the assembled form can be written as

$$\{\psi(\underset{\sim}{U})\} = \int_{{}^0V} [B]^T \{\sigma\}\, d^0V - \{R\} = \{0\} \tag{4.40}$$

4.4 Solution of Nonlinear Equilibrium Equations

The nonlinear equations (4.40) can be solved by the well-known Newton-Raphson (N-R) method, involving a series of solutions to the linear incremental equilibrium equations.

If an initial estimate $\{U\}_i$ for the total displacements is made, then $\{\psi(U)_i\} \neq 0$, which means that there will be some residual nodal forces. An improved value of $\{U\}_{i+1}$ can be obtained by expanding $\{\psi\}$ in Taylor's series up to linear term and equating it to zero.

$$\{\psi(\underset{\sim}{U})_{i+1}\} = \{\psi(\underset{\sim}{U})_i\} + \left[\frac{\partial\{\psi\}}{\partial\{U\}}\right]_{\underset{\sim}{U}=\underset{\sim}{U}_i} \{\Delta U\}_i + \ldots = \{0\} \qquad (4.41)$$

$$[K_T]\ \{\Delta U\}_i + \{\psi(U)\}_i = \{0\} \qquad (4.42)$$

where

$[K_T]$ = tangent stiffness matrix

$$= \left[\frac{\partial\{\psi\}}{\partial\{U\}}\right] \qquad (4.42a)$$

Eq. (4.42) represents the linear incremental equilibrium equations which gives the linearized approximation to the relation between the residual forces $\{\psi\}$ and the incremental displacements $\{\Delta U\}$ on the equilibrium path. The improved solution is then found as

$$\{U\}_{i+1} = \{U\}_i + \{\Delta U\}_i \qquad (4.43)$$

The solution process is repeated until the equilibrium equation (4.40) is nearly satisfied.

4.5 The Tangent Stiffness Matrix

From Eq. (4.40)

$$\{d\psi\} = \int_{{}^{o}V} [B]^T \{d\sigma\}\, d^{o}V + \int_{{}^{o}V} [dB]^T \{\sigma\}\, d^{o}V \qquad (4.44)$$

From Eq. (4.34) and (4.36),

$$\int_{{}^{o}V} [B]^T \{d\sigma\}\, d^{o}V = \int_{{}^{o}V} [B]^T [D]\, [B]\, d^{o}V \{dU\} \qquad (4.45)$$

Using Eqs. (4.33) and (4.35)

$$\int_{{}^{o}V} [dB]^T \{\sigma\}\, d^{o}V = \int_{{}^{o}V} [G^T]\, [dA_\Theta]^T \{\sigma\}\, d^{o}V \qquad (4.46)$$

The generalized second P-K stress resultants are

$$\{\sigma\} = \lfloor N_\alpha \; N_{\alpha\beta} \; N_\beta \; M_\alpha \; M_{\alpha\beta} \; M_\beta \rfloor^T \qquad (4.47)$$

where N_α $N_{\alpha\beta}$ and N_β are the membrane forces and M_α $M_{\alpha\beta}$ and M_β are the bending moments.

It can be shown that

$$[dA_\Theta]^T \{\sigma\} = [S] \{d\Theta\} \qquad (4.48)$$

$$= [S]\, [G] \{dU\} \qquad (4.49)$$

where the second P-K stress matrix [S] is given by

$$[S]_{6x6} = \begin{bmatrix} N_\alpha [I_3] & N_{\alpha\beta} [I_3] \\ N_{\alpha\beta} [I_3] & N_\beta [I_3] \end{bmatrix}_{6x6} \tag{4.50}$$

where $[I_3]$ is a unit matrix of order 3.

The incremental equilibrium equations can be written as

$$\{d\psi\} = \int_{{}^oV} [B]^T [D] [B] \, d^oV + \int_{{}^oV} [G]^T [S] [G] \, {}^odV \, \{dU\} \tag{4.51}$$

$$= [K_T] \{dU\} \tag{4.52}$$

where the tangent stiffness matrix $[K_T]$ can be expressed as

$$[K_T] = [K_o] + [K_L] + [K_{LL}] + [K_\sigma] \tag{4.53}$$

where

$$[K_o] = \int_{{}^oV} [B_o]^T [D] [B_o] \, d^oV \tag{4.54a}$$

$$[K_L] = \int_{{}^oV} [B_o]^T [D] [B_L] \, d^oV + \int_{{}^oV} [B_L]^T [D] [B_o] \, d^oV \tag{4.54b}$$

$$[K_{LL}] = \int_{{}^oV} [B_L]^T [D] [B_L] \, d^oV \tag{4.54c}$$

and

$$[K_\sigma] = \int_{{}^oV} [G]^T [S] [G] \, d^oV \tag{4.54d}$$

$[K_o]$ = initial stiffness or linear stiffness matrix

$[K_L]$ = first order initial displacement matrix

$[K_{LL}]$ = second order initial displacement matrix

$[K_\sigma]$ = initial stress matrix

Once again, $[K_T]$ and $[d\psi]$ can be transformed with respect to the nodal degrees-of-freedom of the curvilinear system giving

$$\underset{30x1}{\{d\psi\}_\alpha} = \underset{30x30}{[K_T]_\alpha} \underset{30x1}{\{dU\}_\alpha} \tag{4.55}$$

where

$$[K_T]_\alpha = [T]^T [K_T] [T] \tag{4.56}$$

and

$$\{d\psi\}_\alpha = [T]^T \{d\psi\} \tag{4.57}$$

and

$$\{dU\}_\alpha = \lfloor d\bar{u}_1 \; d\bar{u}_{1,\alpha} \; d\bar{u}_{1,\beta} \; d\bar{v}_1 \; d\bar{v}_{1,\alpha} \; d\bar{v}_{1,\beta} \; d\bar{w}_1 \; d\bar{w}_{1,\alpha} \; d\bar{w}_{1,\beta} \; d\bar{u}_2 \; \ldots\ldots \; d\bar{w}_{2,\beta} \; d\bar{u}_3 \; \ldots\ldots \; d\bar{w}_{3,\beta} \; d\bar{u}_g \; d\bar{v}_g \; d\bar{w}_g \rfloor^T_{30x1} \tag{4.58}$$

The centroidal degrees-of-freedom will be eliminated by static condensation so that

$$\underset{27x1}{\{d\psi\}_\alpha} = \underset{27x27}{[\bar{K}_T]_\alpha} \underset{27x1}{\{dU\}_\alpha} \tag{4.59}$$

where

$$\{d\psi\}_{\substack{\alpha \\ 27x1}} = \lfloor d\psi_1(\bar{u}_1)\ d\psi_{1,\alpha}(\bar{u}_1)\ d\psi_{1,\beta}(\bar{u}_1)$$

$$d\psi_1(\bar{v}_1)\ d\psi_{1,\alpha}(\bar{v}_1)\ d\psi_{1,\beta}(\bar{v}_1)\ d\psi_1(\bar{w}_1)\ d\psi_{1,\alpha}(\bar{w}_1)\ d\psi_{1,\beta}(\bar{w}_1)$$

$$d\psi_2(\bar{u}_2) \ \ldots\ldots\ldots\ldots\ldots\ldots\ldots\ldots\ d\psi_{2,\beta}(\bar{w}_2) \quad (4.60)$$

$$d\psi_3(\bar{u}_3) \ \ldots\ldots\ldots\ldots\ldots\ldots\ldots\ldots\ d\psi_{3,\beta}(\bar{w}_3)\rfloor^T$$

where, for example, $d\psi_1(\bar{u}_1)$ denotes the residual load at node 1 corresponding to the curvilinear $\bar{u}_1$ degree-of-freedom.

$$\{dU\}_{\substack{\alpha \\ 27x1}} = \lfloor d\bar{u}_1\ d\bar{u}_{1,\alpha}\ d\bar{u}_{1,\beta}\ d\bar{v}_1\ d\bar{v}_{1,\alpha}\ d\bar{v}_{1,\beta}\ d\bar{w}_1\ d\bar{w}_{1,\alpha}\ d\bar{w}_{1,\beta}$$

$$d\bar{u}_2 \ \ldots\ldots\ldots\ldots\ldots\ldots\ldots\ldots\ d\bar{w}_{2,\beta}$$

$$d\bar{u}_3 \ \ldots\ldots\ldots\ldots\ldots\ldots\ldots\ldots\ d\bar{w}_{3,\beta}\rfloor^T \quad (4.61)$$

The subscript α denotes the curvilinear reference frame.

CHAPTER 5

NONLINEAR SOLUTION TECHNIQUES

The solution of equilibrium equations, in the case of linear problems, can be accomplished without difficulty in a direct manner. However, in the case of nonlinear situations, more sophisticated solution strategies have to be employed. In fact, solution of the discretized system of equations represents the most expensive and troublesome computational step in any nonlinear finite element analysis. One of the difficulties that may be encountered in a nonlinear analysis is that numerical instabilities can occur if the chosen solution algorithm is not suitable for the type of problem under consideration.

Since the solution of the nonlinear equations has to be achieved in an incremental form, a reasonable number of increments must be used. This is also required to trace the nonlinear load-displacement path. The choice of the load step is, therefore, important. The solution of nonlinear equations is achieved using the standard Newton-Raphson (N-R) techniques. In employing a full N-R technique, one faces a dilemma, i.e., whether to use smaller load steps and hence more load increments and fewer iterations, or to use larger load steps and hence fewer load increments and more iterations. In either case, the computational cost will be high as the tangent stiffness of an element has to be computed and a new set of equations has to be solved each time. There are alternative methods, like the modified N-R methods, that

prove to be economical and efficient. These methods will be described below for a one degree-of-freedom case for simplicity.

5.1 The Standard Newton-Raphson Method

Most of the incremental nonlinear solution procedures are combined with equilibrium iterations in order to dissipate the out of balance (residual) forces $\{\psi\}$. The first step is to calculate an initial estimate of displacements $\{U\}$. The additional corrective displacements $\{\Delta U\}$ are obtained by equilibrium iterations. It is important that, within each increment, the constitutive equations and equilibrium are satisfied.

Let n = number of load increments and i = number of iterations within each load increment. The total load $\{R\}$ is applied to the structure in increments such that,

$$\{R\}^n = \lambda^n \{R\} \tag{5.1}$$

where λ^n is the load factor for 1 to n number of increments.

The algorithm is explained in the following steps:

(a) The initial tangent stiffness $[K_{T_o}^n]$ is computed

$$[K_{T_o}^n] = [K_{T_o}^n(\underset{\sim}{U})]_{\underset{\sim}{U}=\underset{\sim}{U}_o^n} \tag{5.2}$$

The initial estimate of displacements is then computed

(b) $$\{\Delta U\}_o^n = -[K_{T_o}^n]^{-1} \lambda^n \{R\} \tag{5.3}$$

Start iteration

Update

(c) $$\{U\}_i^n = \{U\}_{i-1}^n + \{\Delta U\}_{i-1}^n \tag{5.4}$$

(d) $$\{\sigma\}_i^n = \{\sigma\}_{i-1}^n + \{\Delta\sigma\}_{i-1}^n \tag{5.5}$$

(e) $$[K_{T_i}^n] = [K_{T_i}^n(\underset{\sim}{U})]_{\underset{\sim}{U}=\underset{\sim}{U}_i^n} \tag{5.6}$$

The out of balance force is computed from

(f) $$\{\psi\}_i^n = \int_{{}^0V} [B_i(\underset{\sim}{U})]^T \{\sigma\}_i \, d^0V - \lambda^n \{R\} \tag{5.7}$$

The improved approximation to the displacements are

(g) $$\{\Delta U\}_i^n = -[K_{T_i}^n]^{-1} \{\psi\}_i^n \tag{5.8}$$

Steps (c) to (g) are repeated until

$$\{\psi\}_i^n = \{0\} \tag{5.9}$$

The next load increment is then applied and steps (a) to (g) are repeated. This process of updating the tangent stiffness at each load increment and iteration and solving the equations is the well-known standard or full N-R method, which is shown in Figure 4a.

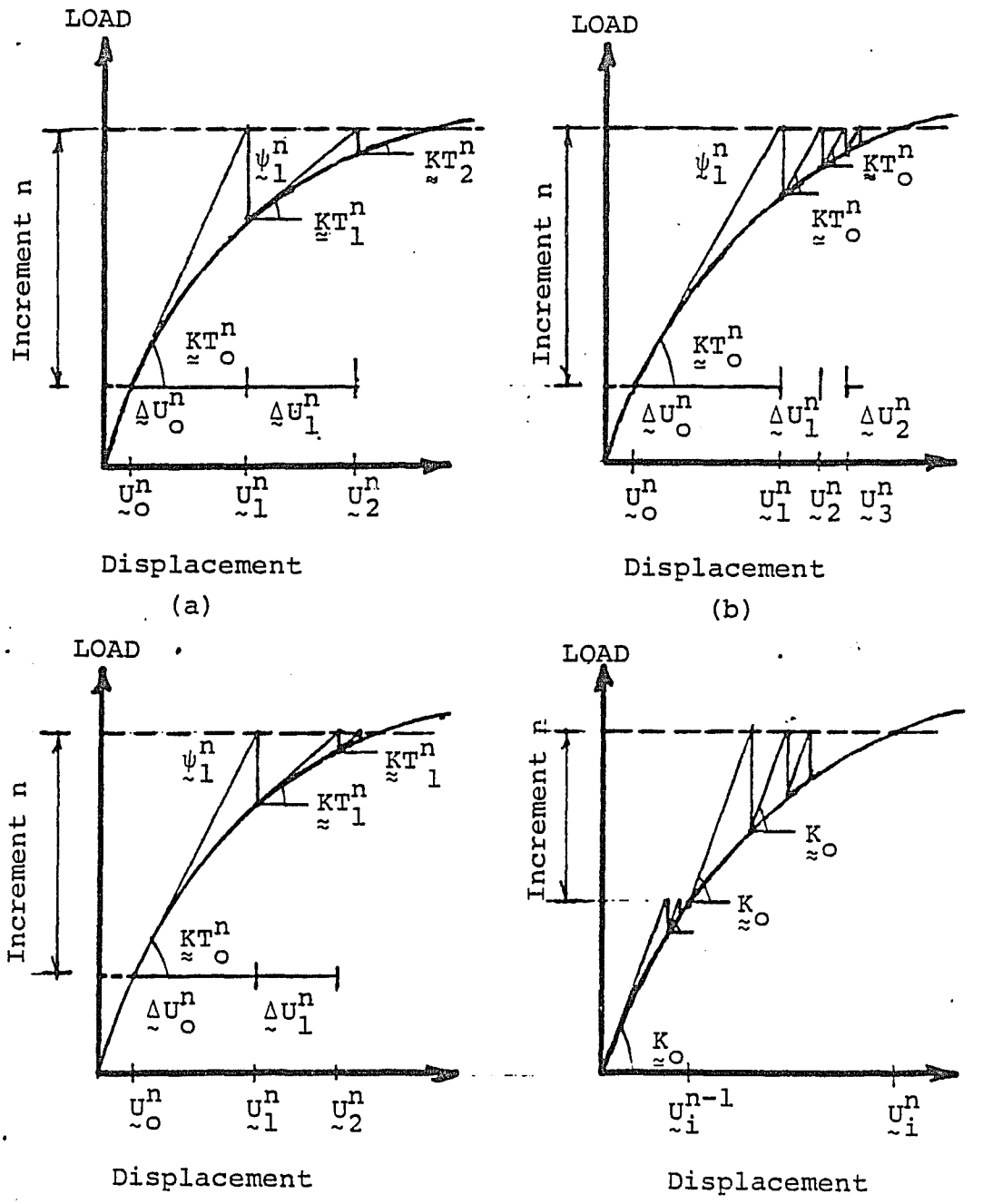

Figure 4. Newton-Raphson methods (one degree-of-freedom).

5.2 Modified Newton-Raphson Methods

It is evident that in the case of a full N-R method, the tangent stiffness matrix $[K_T]$ is to be updated in each load increment and iteration and a completely new set of equations has to be solved. This process can be highly expensive, particularly if relatively small load increments have to be used. To overcome this difficulty, some modifications of the full N-R algorithm is made by updating the stiffness matrix only when desired. For example, $[K_T]$ can be updated only at each load increment and is kept constant for all iterations within the load increment.

If Eq. (5.8) for full N-R is written as

$$\{\Delta U\}_i^n = -[K_{T_i}^n]^{-1} \{\psi\}_i^n \tag{5.10}$$

the modified algorithm will be

$$\{\Delta U\}_i^n = -[K_{T_o}^n]^{-1} \{\psi\}_i^n \qquad i \geq 0 \tag{5.11}$$

This modified algorithm is designated as KT1 method and is shown in Figure 4b. The tangent stiffness can also be updated at the beginning of the first iteration and kept constant for other iterations within the load increment. Thus, the algorithm for a load increment n can be written as

$$\{\Delta U\}_i^n = -[K_{T_1}^n]^{-1} \{\psi\}_i^n \qquad i \geq 1 \tag{5.12}$$

This algorithm is designated as KT2 and is shown in Figure 4c.

In another algorithm, the initial linear elastic stiffness matrix $[K_T]_0$, which is designated as $[K_0]$, is maintained during the entire analysis, as shown in Figure 4d. This algorithm is known as the "Initial Stress" method and was first advocated by Zienkiewicz et al.[88] for the solution of elasto-plastic problems. Though the initial stress method renders a practical solution to problems of elastic unloading and ill-conditioning, the convergence rate is extremely slow, particularly for highly nonlinear problems.

In the modified N-R methods described above, convergence is slower and large numbers of iterations may be required. It is, therefore, desirable to employ these techniques in conjunction with acceleration schemes.[89]

5.3 A Brief Review of Other Techniques

The methods described above give solutions only when the load-displacement path is monotonic. However, shells experience snap-through, or bifurcation buckling, when the applied load reaches a critical value. Under such situations, the N-R methods fail to give satisfactory solutions because of the singularity at the limit point or the existence of multiple stable equilibrium paths for a single value of the load. To trace the post limit response, the load parameter was incremented up to the limit point and thereafter a characteristic displacement was incremented and solved for the load parameter.[90-92] Sharifi and Popov introduced a fictitious spring at the limit point to overcome the singularity problem.[93]

The method of incrementing the displacement is described below:[34]

Figure 5a shows the snap through behavior of an arch or a shell. The N-R techniques can be employed to get solutions in the regions of O A B and C D E by incrementing the load parameter. To get a solution in the domain B C, the displacement component U_k of the vector $\{U\}$ is chosen. The load parameter λ is now unknown. Between B and C, there corresponds only one value of $\lambda\{R\}$ for a given U_k. We can write

$$[K_T]\ \{\Delta U\} = \{\psi\} + \Delta\lambda\{R\} \tag{5.13}$$

Moving $\Delta\lambda$ to the left-hand side in the vector of unknowns and imposing $\Delta U_k = 0$,

$$\begin{bmatrix} K_{T_{11}} & \cdots & & \cdots & K_{T_{n1}} \\ \vdots & & & & \vdots \\ & & -R & & \\ \vdots & & & & \vdots \\ K_{T_{n1}} & \cdots & & \cdots & K_{T_{nn}} \end{bmatrix} \begin{Bmatrix} \Delta U_1 \\ \Delta \dot{U}_{k-1} \\ \Delta\dot{\lambda} \\ \Delta \dot{U}_{k+1} \\ \Delta \dot{U}_n \end{Bmatrix} = \{\psi\} \tag{5.14}$$

Replacing column k of $[K_T]$ by $\{R\}$ destroys its symmetry and changes its band width. To avoid such an inconvenience, Eq. (5.13) can be solved twice with different load vectors but using the same $[K_T]$.

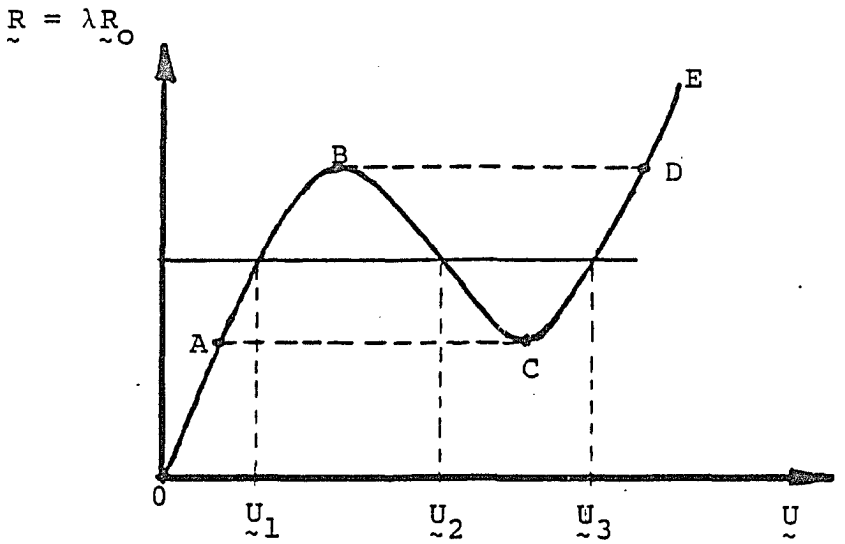

Figure 5a. Displacement increment method.

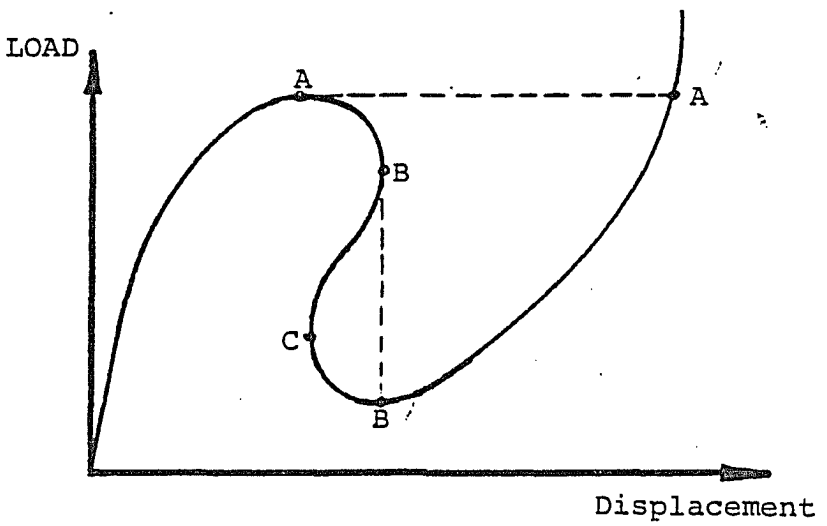

Figure 5b. Difficulties encountered in some geometrically non-linear problems when load or displacement incrementation is used.

$$[K_T]\ \{\Delta U\}^R = \{R\} \tag{5.15}$$

$$[K_T]\ \{\Delta U\}^\psi = \{\psi\} \tag{5.16}$$

The solution of Eq. (5.13) is then

$$\{\Delta U\} = \{\Delta U\}^\psi + \Delta\lambda\{\Delta U\}^R \tag{5.17}$$

The unknown $\Delta\lambda$ is solved as

$$\Delta U_k = 0 = \Delta U_k^\psi + \Delta\lambda\Delta U_k^R \tag{5.18}$$

$$\Delta\lambda = -\frac{\Delta U_k^\psi}{\Delta U_k^R} \tag{5.19}$$

The algorithm may be written as

(i) Choice of load increment j

(ii) Modify component k of U^j

(iii) Start iteration i

(iv) Compute residual $\{\psi\}$

(v) Compute $[K_T]$

(vi) Solve $[K_T]\ \{\Delta U\}^\psi = \{\psi\}$

$[K_T]\ \{\Delta U\}^R = \{R\}$

(vii) Compute $\Delta\lambda = -\frac{\Delta U_k^\psi}{\Delta U_k^R}$

$$\{U\}_{i+1} = \{U\}_i + \{\Delta U\}_i^\psi + \Delta\lambda_i\ \{\Delta U\}_i^R$$

$$\lambda_{i+1} = \lambda_i + \Delta\lambda_i$$

(viii) Check for convergence

(ix) Go to Step (i) if converged and step (iii) if not.

While it is not only difficult to decide the critical displacement component to be incremented, the algorithm fails to predict the response completely as in the case of snap back behavior. Figure 5b highlights some of the difficulties encountered in a post buckling analysis under such a situation. If the loads are incremented, at a point A the solution jumps suddenly to A' thereby missing a large portion of the equilibrium path. On the other hand, if the displacements are incremented, at a point B the solution jumps to point B'.

These difficulties led to the development of more sophisticated solution algorithms for post buckling analysis of shells involving snap through or snap back behavior. The earliest solution technique to deal with such problems was developed by Riks[94] and is known as the "Normal Plane" method. The basic idea is to modify the load level at each iteration, rather than holding the applied load level constant, so that the solution follows some specified path until convergence is reached. This path may lie in a plane normal to the tangent at the beginning of the load step (Figure 6a). Ramm[95] has presented a modified Rick's method by updating the normal plane in each iteration rather than iterating on a constant normal plane (Figure 6b). Crisfield[96,97] modified this technique by making the path normal to an arc instead of a plane (Figure 6c). This more popular technique is called "Arc-Length" method. Bergan[98,99] introduced a current stiffness parameter for varying the load level during an iteration to minimize

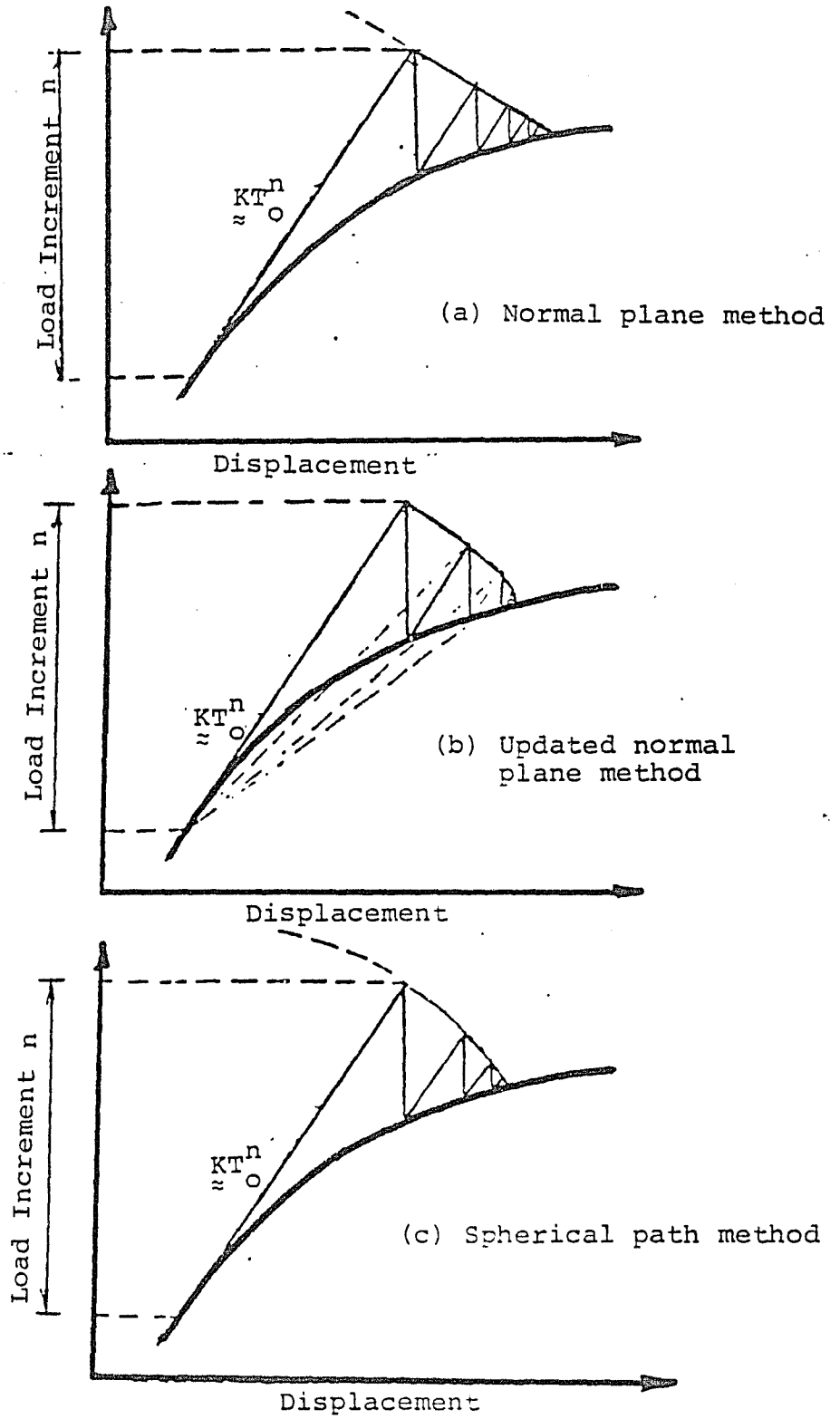

Figure 6. Arc length methods.

the residual force. An excellent presentation of numerous solution algorithms for nonlinear problems has been given by Rahman.[100] Detailed investigation of these techniques and efficient solution algorithms based on Crisfield's "Arc-Length" methods have been presented in a recent study by Kolar.[101]

5.4 Convergence Criteria

A critical problem associated with iterative solution scheme is the selection of a suitable criterion for determining when to stop iterations, so that equilibrium is nearly achieved. In an incremental-iterative solution strategy, the solution obtained at the end of each iteration is checked to see whether it has converged within an acceptable tolerance. If the convergence tolerance is too loose, inaccurate results are obtained, and if it is too tight, much effort is spent for needless accuracy. The convergence tolerance must, therefore, be realistic. The convergence tolerance, used for nonlinear structural analysis, is usually based on (i) displacements, (ii) out of balance (residual) forces, and (iii) internal energy.

5.4.1 Displacement Criterion

The iterative displacements $\{U\}_i$ at iteration i are used to monitor convergence of nonlinear solution. Although several possible criteria can be used, directional or total norm of the displacements is usually used.

Directional Norm. The directional norm can be specified as

$$\frac{\| \{\Delta U\}_i^j \|}{\| \{U\}_i^j \|} \times 100 \leq C_{T_j} \tag{5.20}$$

where $\| \{\Delta U\}_i^j \|$ = Euclidean norm of incremental displacement for the jth degree-of-freedom at the end of an iteration i, $\| \{\Delta U\}_i^j \|$ = Norm of total displacement for the jth degree-of-freedom at the end of ith iteration, C_{T_j} = Percentage value of the allowable convergence for jth degree-of-freedom.

Total Norm. Unlike the directional norm where convergence is checked for each degree-of-freedom, which can be expensive, Total Norm is used for all degrees-of-freedom. This is stated as

$$\frac{\| \{\Delta U\}_i \|}{\| \{U\}_i \|} \times 100 \leq C_T \tag{5.21}$$

where the norm is evaluated for all degrees-of-freedom.

5.4.2 Residual Force Criterion

If the residual forces in the structure are nearly equal to zero, then equilibrium is nearly achieved. Hence residual forces can be taken as a measure of checking convergence. Here again, the two commonly used criteria are

Directional Norm. This can be stated as

$$\frac{\| \{\psi\}_i^j \|}{\| \{R\}_i^j \|} = 100 \leq C_{T_j} \tag{5.22}$$

where $\{\psi\}_i^j$ = residual forces for the jth degree-of-freedom at the end of the ith iteration, $\{R\}_i^j$ = applied forces for the Jth degree-of-freedom at the end of the ith iteration.

This criterion is used for each degree-of-freedom to check for convergence.

Total Norm. This can be stated as

$$\frac{\| \{\psi\}_i \|}{\| \{R\}_i \|} \times 100 \leq C_T \tag{5.23}$$

where the norms are evaluated for all degrees-of-freedom.

5.4.3 Energy Convergence Criterion

In order to provide some indication of when both the displacements and forces are near their equilibrium value, Bathe and Cimento[102] introduced the use of energy convergence criterion. In this criterion, the amount of work done at iteration i by the out of balance forces on the iterative displacements can be compared with the initial value. Thus, convergence is deemed to have been reached when,

$$\frac{\{\psi\}_i^T \{\Delta U\}_i}{\{\psi\}_1^T \{\Delta U\}_1} \times 100 \leq C_T \tag{5.24}$$

Again, the choice and relative merits of various convergence criteria are discussed in detail in reference 100.

In the present work, options to choose both the displacement criterion and residual force criterion have been provided in the computer program, described in the next section.

5.5 Computer Program

A computer program GNATS was developed for Geometrically Nonlinear Analysis of Thin Shells using DKCT elements. Some of the subroutines developed for the linear analysis[80] have been used in developing this computer program. The program consists of one main routine and nineteen subroutines, with a total of approximately 2700 lines. The program has been implemented on the CDC CYBER 175 system, a 60-bit word machine, using the FORTRAN V language. The program requires eight temporary tape/disc drives for writing and reading some of the intermediate values and approximately 110 blocks of storage on the DEC-10 machine.

5.5.1 Capabilities and Limitation of the Program

GNATS has the following capabilities and limitations:

(a)	Element	: DKCT elements only	
(b)	Geometry of Shell	: Arbitrary	
(c)	Boundary Conditions	: (i)	Curvilinear displacements
		(ii)	Cartesian displacements
(d)	Loading	: (i)	Pressure loads
		(ii)	Gravity loads
		(iii)	Point loads

(e)	Numerical Integration	:	(i)	7-point integration
			(ii)	13-point integration
(f)	Tangent Stiffness	:	(i)	With respect to curvilinear frame
			(ii)	With respect to cartesian frame
(g)	Solution of Equations	:	(i)	Band solution
			(ii)	Frontal solution
(h)	Nonlinear Solution Algorithm	:	(i)	KT1 method
			(ii)	KT2 method
			(iii)	KT method

(Can trace load-displacement response up to limit point only)

(J)	Output Option	:	(i)	Displacements at nodes
			(ii)	Stresses at Gauss points
			(iii)	Reaction at nodes

5.5.2 Program Structure

As mentioned earlier, the program consists of one main routine and nineteen subroutines, some of which will be described below briefly.

(1) Main Program: This is a Master routine that reads all control variables, pre- and re-sets disc/tape units and initializes variables. It calls subroutines such as GDATA, STIFM, CONDEN, SOLVE, BSUB, TRAND, STRESS, CONVG and OUTPUT. It has one outer loop for load increments and one inner loop for iterations. It controls the formation of the tangent stiffness according to the algorithm desired and also the iteration loop by operating on the convergence requirements.

(2) GDATA: This subroutine reads geometric, material and boudnary data. It also reads the load data.

(3) STIFM: This is a large subroutine that computes the element tangent stiffness matrix and element consistent nodal loads (once only). This subroutine calls other subroutines such as SHAPE, GEMTRY, TCUBIC, BTADER, STRAIN and TRANS, the functions of which have already been explained in reference 80. This subroutine calculates separately the linear part of the element tangent stiffness matrix (once only) and the nonlinear part in global cartesian directions. The element tangent stiffness matrix and the element nodal load vector are then transformed into the curvilinear directions using the subroutine TRANS.

This subroutine uses tape 9 to read nonlinear part of the B matrix, tape 8 to write the transformation and linear part of the B matrices, tape 11 to write the element tangent stiffness matrix in curvilinear directions and tape 12 to write the transformed element nodal loads.

(4) CONDEN: This subroutine reads from tape 11 the element tangent stiffness matrix and tape 12 or tape 1 to read element nodal loads or residual nodal loads as the case may be and condenses them with respect to the central node. The coefficients that are condensed are written on tape 2 before condensation for later recovery of central nodal displacements. The condensed element nodal loads are then assembled to form a total structure nodal load vector. The condensed element tangent stiffness matrix is written on tape 3.

(5) SOLVE: This routine assembles and performs Gaussian elimination of the equilibrium equations including the right hand side load vector in ascending nodal order, inserting boundary conditions where necessary. This uses tape 3 to read element stiffness and stores the eliminated equations on tape 4 for later use in the resolution and back-substitution stages.

(6) BSUB: This accesses the eliminated equations in reverse order and carries out a back-substitution to find incremental displacements and reactions.

(7) TRAND: This subroutine transforms the incremental displacements in the curvilinear directions obtained from BSUB into global cartesian directions. It also recovers incremental displacements at the central node using the coefficients read from tape 2.

(8) STRESS: In this subroutine, the incremental displacements are added to obtain total displacements. It computes incremental and total stresses and residual nodal forces and transforms the residual nodal forces in local curvilinear components. This subroutine uses tape 8 to read linear part of B matrix and transformation matrix, tape 9 to write nonlinear part of B matrix and tape 1 to write the transformed residual nodal load vector.

(9) CONVG: This subroutine calculates Euclidean norms of (a) residual load vector, (b) applied load vector, (c) incremental displacement vector, and (d) total displacement vector and computes ratios of total and directional norms as explained in 5.4 and checks against the input tolerance limit for convergence according to the option desired.

(10) OUTPUT: This subroutine has the options to output (a) incremental and total nodal displacements, (b) incremental and total stresses at Gauss points and (c) total nodal reactions.

(11) FRONT: This subroutine is the well known Frontal solution technique due to Irons[103] and is taken from reference 35. It assembles the element stiffness matrix and element load vector and solves for the incremental nodal displacements and reactions.

A flow chart explaining the program structure is shown in Figure 7.

The program has several data check statements to avoid costly runs with data errors. The program has been tested with several numerical examples. The results and discussion of the numerical examples are reported in the next chapter.

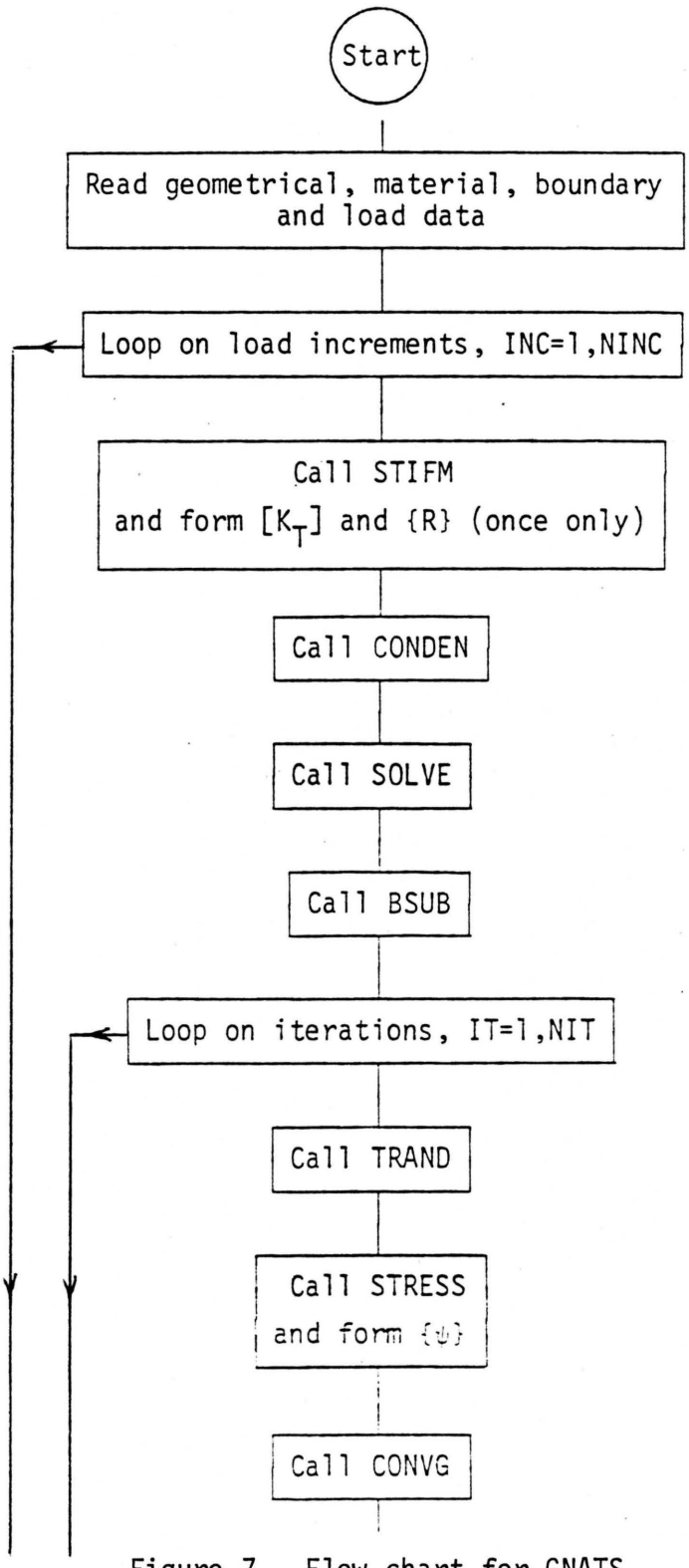

Figure 7. Flow chart for GNATS.

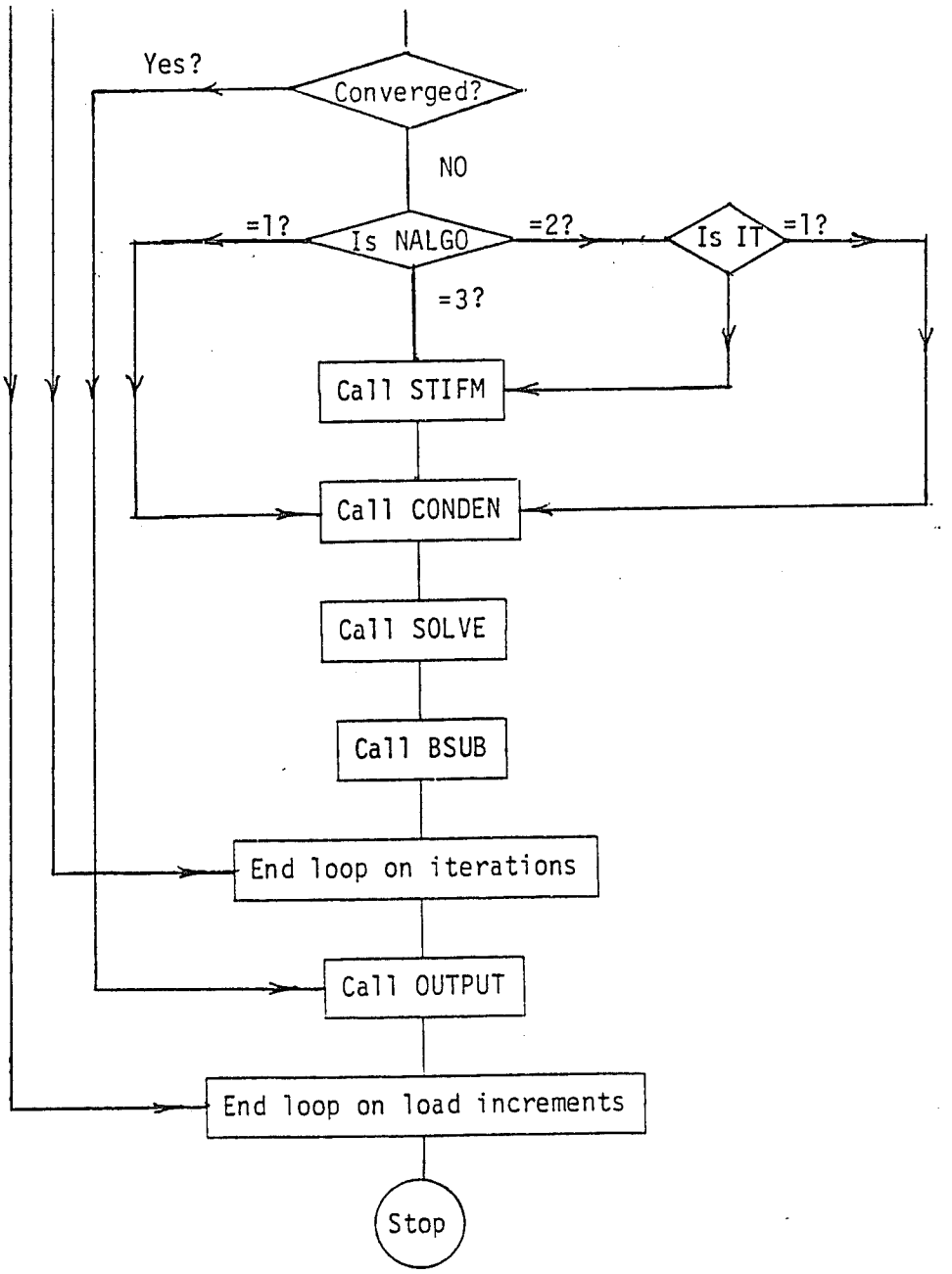

Figure 7. Flow chart for GNATS.

CHAPTER 6

EXAMPLES, RESULTS AND DISCUSSION

To assess the validity of the Geometrically Nonlinear (GNL) formulation of the DKCT element, several numerical examples were carried out and the results are discussed in this chapter. First, the examples relate to the linear buckling cases. Here, the examples include (i) columns, (ii) plates, (iii) ring, (iv) arches, and (v) shells. Second, examples of GNL analysis are presented. The examples include (i) plates, (ii) shallow arch and (iii) arbitrary shells. The results are compared with the available classical or numerical solutions. In the case of GNL analyses, the results are compared only up to the limit point. An attempt is also made to compare the economical aspect of the DKCT element with other elements. In a few examples of the linear analysis[80] the DKCT element was found to be more economical than the compared elements. Hence it is felt to compare the economical aspect of this element in the case of GNL analysis. Although it is very difficult to compare the economy in a strict sense, a rough comparison is made based on the total number of degrees-of-freedom. For this purpose, in the GNL analysis examples, the total number of degrees-of-freedom employed in the present work, as well as by others (wherever possible) is presented in the appropriate figures.

In the figures, where the comparison refers to the same example and authors, this presentation is made only once to avoid repetition. While a discussion on the other aspects of the solutions is presented in each example, the discussion on this economical aspect is presented at the end of this chapter.

The load-displacement paths were plotted on a CALCOMP plotter at the computer center of the University of Arizona. As mentioned earlier, computations were carried out in single precision on the CDC CYBER-175 computer, a 60 bit word machine. Discretization of the structure is done by m x n divisions in α and β directions with 2 mn number of elements. Unless and otherwise specified, the following techniques were adopted for the analyses.

(i) Numerical integration : 13-point integration

(ii) Nonlinear algorithm : KT2 solution algorithm

(iii) Solution of equations : Band solution

(iv) Convergence criterion : Displacement criterion

(v) Convergence tolerance : 0.0%

For the examples in this chapter, the following notations are used.

E = Young's modulus

ν = Poisson's ratio

h = Thickness of the structure

R = Radius of the structure

L = Length of the structure

b = Width of the structure

N, q = Uniformly distributed load

p = Point load

λ = Load factor

FEM = Finite Element Method of solution

psi = Pounds per square inch

6.1 Linear Buckling Examples

Linear instability analysis is an approach to the calculation of the intensity of the applied load for buckling of an elastic structure, where the effect of prebuckling deformations are neglected. Although the physical conditions associated with the collapse of structures involve the nonlinear aspects of instability as well as inelastic deformations, a linear instability analysis accurately describes the circumstances of failure that are important in design. Linear elastic instability theory therefore furnishes a basis for a large share of practical design formulations. Even where nonlinear phenomena must be taken into account to define accurately the magnitude of load to cause failure, the form of the solution is adequately given by linear instability analysis.[31]

When the effects of prebuckling deformations are neglected, the condition for stable equilibrium can be written as

$$[K_o] + \lambda [K_\sigma] \{U\} = \{0\} \tag{6.1}$$

where λ is the intensity of the applied load or the load factor.

This is a standard eigenvalue problem, the solution of which gives the eigenvalues λ and the associated eigenvectors $\{U\}$. Here the eigenvalues represent the buckling loads and the eigenvectors represent the mode shapes. However, the buckling load can also be obtained from the second variation of total potential energy that gives the condition for buckling as

$$|[K_o] + [K_\sigma]| = 0 \tag{6.2}$$

Eq. (6.2) represents the lowest load that causes the stiffness matrix to become indefinite from positive definite, which means that, the structure undergoes unstable equilibrium from the state of stable equilibrium. In the linear buckling examples below, the buckling loads have been evaluated by monitoring the sign of the determinant of the total stiffness matrix of the structure.

6.1.1 Columns

6.1.1.1 Column with Hinged Ends. Figure 8a shows a column with hinged ends, subjected to axial load of p, with the following properties.

L = 100 in. (2540 mm)

b = 1 in. (25.4 mm)

h = 1 in. (25.4 mm)

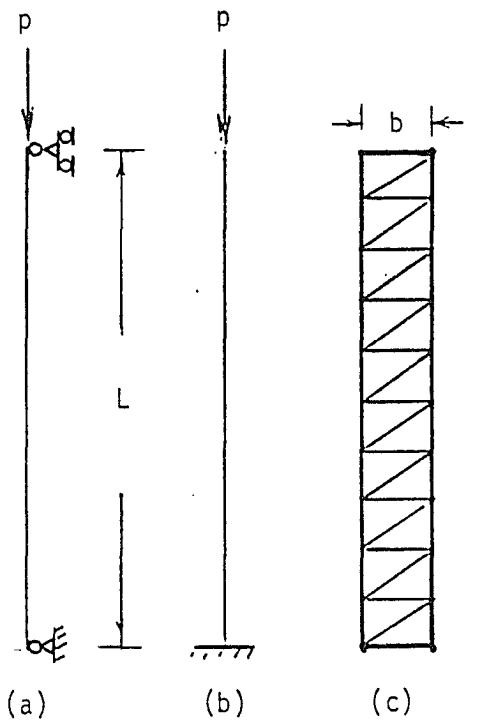

Figure 8. Euler columns and mesh for linear buckling analysis.

$E = 12 \times 10^5$ psi (82.74×10^5 kPa)

$\nu = 0$

The column is analyzed with a mesh of 10 x 1 (Figure 8c) (20 elements). The buckling load is compared with the well known Euler equation:

$$P_{cr} = \frac{\pi^2 E I}{l_e^2} \tag{6.3}$$

where

P_{cr} = buckling or critical load

l_e = effective length of the column

Table 1 presents the comparison of the results. The comparison shows excellent agreement with the analytical value.

6.1.1.2 Fixed-Free Column. This is again a Euler column with one end fixed and the other free and loaded axially at its free end as shown in Figure 8b. The properties of this column are the same as the previous column. The column is analyzed with the same mesh as above and the result is again compared with the Euler equation (6.3). The results are shown in Table 2. The comparison again shown excellent agreement with the theoretical value.

Table 1. Buckling Load for Hinged-Hinged Column

Type of Solution	Buckling load P_{cr}(pounds)
Euler equation (6.3)	98.696
This study	98.12 (0.58%)

Table 2. Buckling Load for Fixed-Free Column

Type of Solution	Buckling load P_{cr}(pounds)
Euler equation (6.3)	24.674
This study	24.50 (0.71%)

(Percentage error is shown in parentheses)

6.1.2 Plates

Here, simply supported rectangular plates of different aspect ratios (a/b), subjected to uniform compression on one side, as shown in Figure 9, have been analyzed. The buckling of plates, pressure loaded arches and rings have been extensively treated analytically by Timoshenko and Gere.[104]

The following properties are assumed.

$E = 10.92 \times 10^4$ psi (75.29×10^4 kPa)

$\nu = 0.3$

$h = 1$ in. (25.4 mm)

The plates are analyzed with a mesh of 4 x 2 (16 elements) and the results for the buckling load (N_{cr}) are compared with reference 104. Table 3 shows the results.

Although the results agree reasonably well with the theoretical values, the buckling loads predicted by the present numerical study are lower than the analytical values. This has been observed in the case of columns also. One reason for this is, when the local curvilinear axes are chosen to coincide with the global cartesian axes, the stiffness coefficients for the central nodal degrees-of-freedom become null. Hence, approximate displacements were introduced at the central node. This approximation causes the difference on the lower side of the theoretical values of the buckling loads.

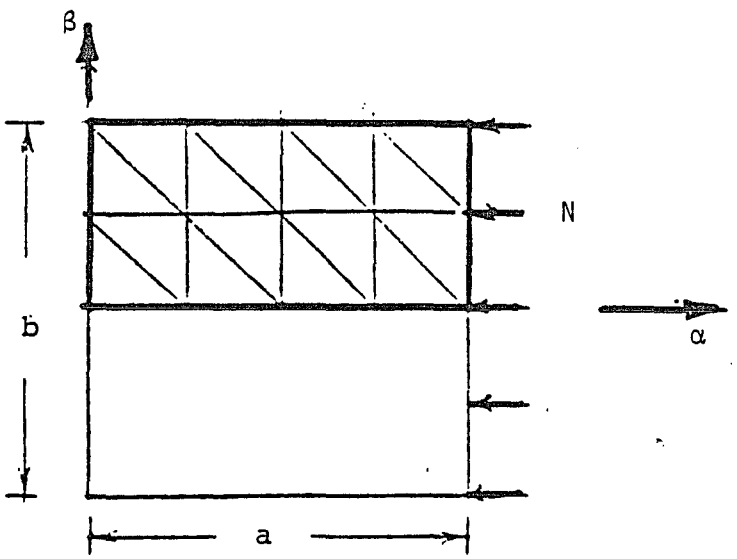

Figure 9. Simply supported rectangular plates for linear buckling analysis.

Table 3. Buckling Pressure of Simply Supported Plates

a/b	N_{cr} (psi)		
	Ref. 104	This study	error
0.2	266.48	264.2	0.86
0.4	79.94	78.5	1.80
0.6	50.73	50.5	0.45
0.8	41.45	40.5	2.29
1.0	39.48	39.2	0.71
1.2	40.76	40.5	0.64
1.414	44.31	42.5	2.73

6.1.3 Ring

A full circular ring under uniform normal pressure, as shown in Figure 10, has the following properties.

$b = 1$ in. (25.4 mm)

$h = 1$ in. (25.4 mm)

$R = 100$ in. (2540 mm)

$E = 12 \times 10^6$ psi (82.74×10^6 kPa)

$\nu = 0.0$

The ring is analyzed with a mesh of 10 x 1 for quarter symmetry. This problem has also been solved by Chang[105] using deep shell elements with 36 degrees-of-freedom per element. The buckling pressure can be given by the equation:

$$q_{cr} = \frac{k_{cr} E I}{R^3} \tag{6.4}$$

where

k_{cr} = buckling coefficient

I = moment of inertia

Table 4 presents a comparison of results.

The buckling pressure given by Timoshenko[104] is based on the assumption that the pressure acts always normal to the surface, while the value given by Chang[105] is based on the assumption that the pressure is conservative. (Chang has also presented results that include pressure stiffness effect for a number of linear buckling problems. However, for the purpose of comparison, values corresponding to

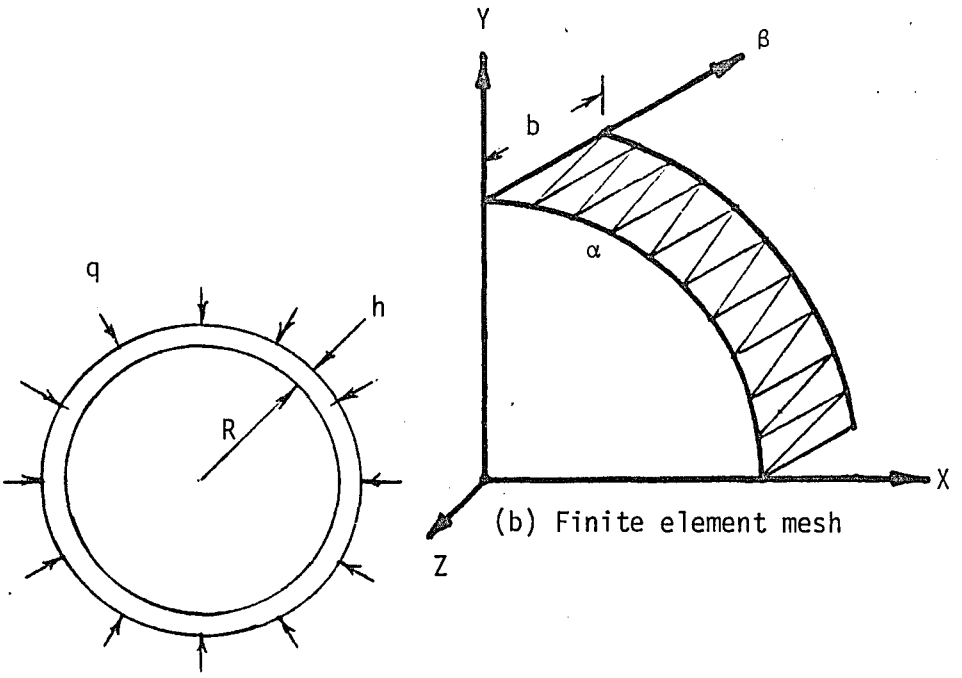

(a) Geometry

(b) Finite element mesh

Figure 10. Circular ring under uniform external normal pressure.

Table 4. Buckling Pressure Coefficient for a Circular Ring

Type of solution	k_{cr}
Analytical (ref. 104)	3.0
FEM (ref. 105)	4.0
This study	4.01

conservative loadings have been taken from reference 105). The result compares well with that of Chang. It is clear from the comparison with the result of Timoshenko that, neglect of nonconservative loading effects will produce buckling load on the unsafe side.

6.1.4 Arches

In this, examples of both shallow and deep circular arches will be studied and the results will be compared with the available standard solutions.

6.1.4.1 Hinged Semicircular Arch. This deep arch with hinged supports is subjected to uniform normal pressure (Figure 11a, 2α = 180 degrees). Solution to this problem has been given in reference 104 for nonconservative case and by Batoz[106] for conservative pressure using both shallow and deep shell theories, with D-K-T shell elements of 27 degrees-of-freedom.

The properties of the arch is taken to be the same as that of the ring. The arch is analyzed with three different meshes and the results for the buckling coefficient k_{cr} are compared with Timoshenko[104] and Batoz[106]. The buckling pressure is given by Timoshenko by the equation:

$$q_{cr} = \left(\frac{\pi^2}{\alpha^2} - 1\right) E\, I/R^3 \qquad (6.5)$$

$$= k_{cr}\, E\, I/R^3 \qquad (6.5a)$$

where α = half the subtended angle.

Table 5 shows the comparison of k_{cr}.

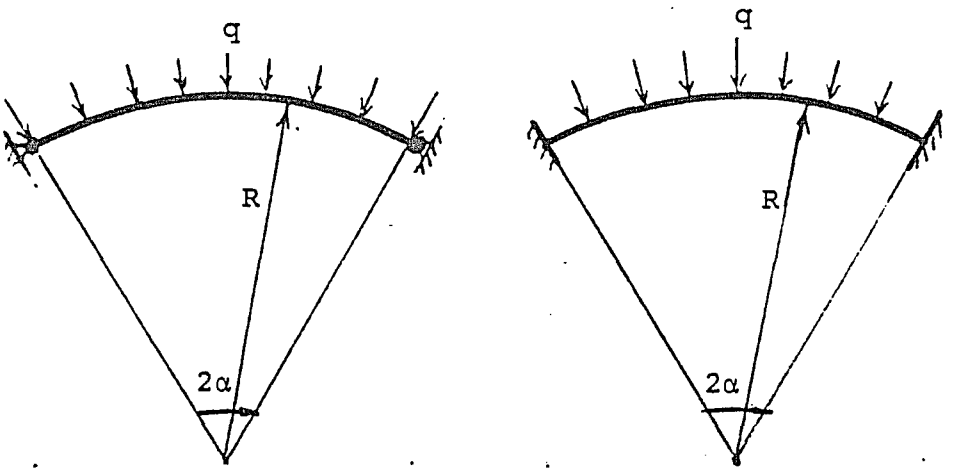

(a) Hinged arch (b) Clamped arch

Figure 11. Circular arches under uniform external normal pressure.

Table 5. Buckling Pressure Coefficient for Hinged Semi Circular Arch

Solution type		k_{cr}
Analytical (ref. 104)		3.0
Ref. (106) (FEM)	shallow shell theory	4.0
	Deep shell theory	3.273
Present study	12x1 mesh	3.315
	16x1 mesh	3.30
	20x1 mesh	3.295

The buckling coefficient has excellent agreement with the deep shell solution of Batoz, differing only by 0.67%.

6.1.4.2 Hinged Shallow Arch. A shallow circular arch, shown in Figure 11a, is under uniform normal pressure. The arch has the same properties as the ring and has been analyzed with different meshes. The angle 2α is taken as 1 radian for the arch. The buckling pressure is given by equation (6.5), when the pressure is nonconservative. Table 6 shows the results of references 104, 105 and the present study.

The result of the present study compares well with that of reference 105, with a difference of 3.66%.

6.1.4.3 Clamped Circular Arch. Figure 11b shows clamped circular arch subjected to uniform normal pressure. The buckling pressure for such an arch for nonconservative pressure is given by Timoshenko[104] by the equation:

$$q_{cr} = (k^2 - 1)\ E\ I/R^3 \tag{6.6}$$

$$= k_{cr}\ E\ I/R^3 \tag{6.7}$$

where k is the solution of the transcendal equation:

$$k \tan\alpha \cot(k\alpha) = 1 \tag{6.8}$$

The k values corresponding to α values are given in reference 104. The properties of the arch are again the same as the ring. Three such arches with $\alpha = 30°$, $60°$ and $90°$ were analyzed with meshes of 12 x 1, 16 x 1 and 22 x 1, respectively, and the results for k_{cr} are shown in Table 7.

Table 6. Buckling Pressure Coefficient for Shallow Hinged Circular Arch

Solution type		k_{cr}
Analytical (ref. 104)		38.478
Ref. (105) (FEM)		39.456
This Study	6x1 mesh	41.90
	8x1 mesh	41.0
	12x1 mesh	40.90

Table 7. Buckling Pressure Coefficient for Clamped Circular Arch

Type of solution	k_{cr}		
	$\alpha=30°$	$\alpha=60°$	$\alpha=90°$
Analytical (ref. 104)	73.322	18.141	8.0
Ref. (105) (FEM)	75.313 (2.72%)	19.598 (8.03%)	9.002 (9.0%)
This study	80.50 (9.79%)	23.40 (29.0%)	10.4 (30.0%)

(Precentage error is shown in parentheses)

Comparing the results of reference 104, this study gives appreciable increase in buckling pressure when the arch becomes deep from shallow but, no further appreciable increase with increase in deepness of the arch. This study shows that the effect of pressure stiffness is significant for deep arches.

6.1.5 Shells

External loads are usually carried by shells under the action of membrane compression. Shells are therefore susceptible to buckling since their thickness is very small. The study of buckling of this extensively used structure therefore becomes important.

6.1.5.1 Clamped Spherical Shell under a Central Point Load. Figure 12a shows a clamped sphereical shell under a central point load with the following properties.

R = 100 in. (2540 mm)

h = 0.7235 in. (18.38 mm)

$E = 2.816 \times 10^5$ psi (19.42×10^5 kPa)

$\nu = 1/3$

α = 30 deg.

The buckling problem of a clamped spherical cap under a central point load has been solved by Fitch[107], using Marguerre's nonlinear shallow shell theory. The critical load has been given by Fitch in a non-dimensional form as

$$k_{cr} = \frac{P_{cr} R}{2\pi D} \tag{6.9}$$

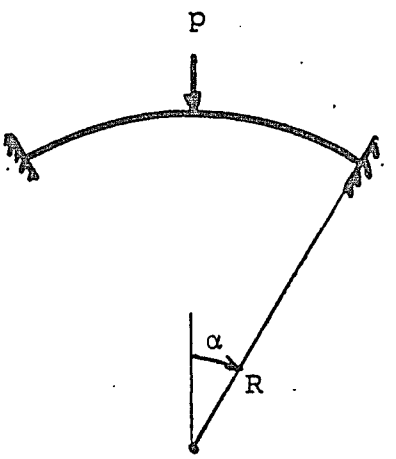

(a) Geometry

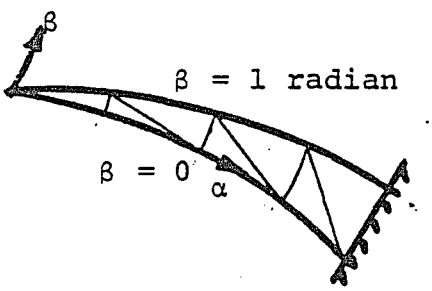

(b) Finite element mesh

Figure 12. Spherical cap under a central point load.

where

P_{cr} = critical applied point load

D = flexural rigidity

Fitch[107] has presented buckling loads for various shell parameters μ where,

$$\mu = 2[3(1-\nu^2)]^{1/4} (H/h)^{1/2} \qquad (6.10)$$

H = rise of the shell

The shell has been analyzed for symmetric buckling with 7 elements (Figure 12b). Table 8 shows the results for k_{cr}.

The buckling load coefficient agrees reasonably well with the shallow shell result of Fitch[107] with a difference of 5.31%.

6.1.5.2 Axially Loaded Cylindrical Panel. Figure 13 shows a cylindrical panel with its curved edges hinged and straight edges free. The panel is loaded axially with uniform compression (N). No analytical solution seems to be available to this problem. However, numerical solutions to this problem, using shell elements, have been given by Konig[108] and Chang[105]. The panel has the following properties.

$E = 10.2 \times 10^6$ psi (70.33×10^6 kPa)

$\nu = 0.333$

R = 18 in. (457.2 mm)

L = 27 in. (685.8 mm)

h = 0.063 in. (1.6 mm)

α = 81.9647 deg.

Table 8. Buckling Load for a Clamped Spherical Shell Under a Central Point Load

Solution type	k_{cr}
Analytical (ref. 107)	13.18
This study	12.48 (5.31%)

(Percentage error is shown in parenthesis)

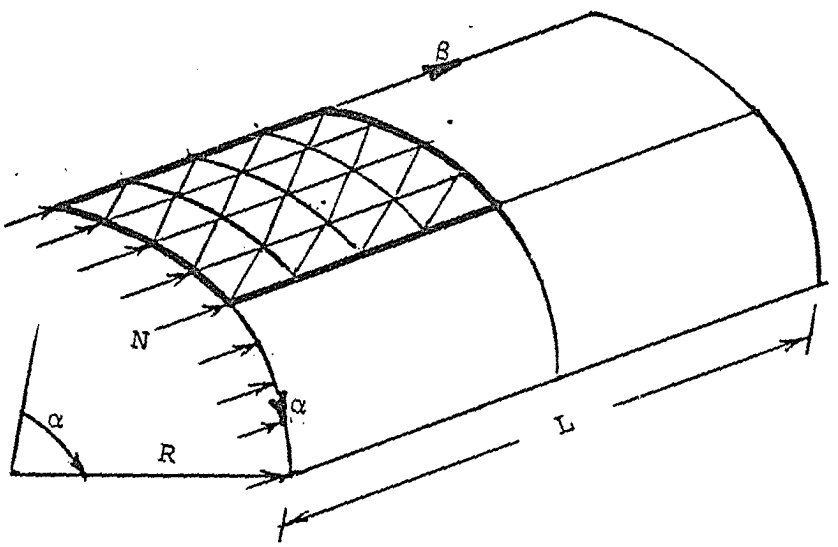

Figure 13. Axially loaded cylindrical panel.

The panel is analyzed for symmetric mode, using a mesh of 4 x 4 for one quarter area. Table 9 shows results of references 108, 105 and this study.

The comparison shows that the critical stress obtained by this study is 8.8% less than Konig's[108], while that of reference 105 is 5.32% more than the critical stress obtained by Konig.

6.1.5.3 Axially Loaded Cylinder. A full cylinder with hinged ends under axial compression is studied for buckling (Figure 14a). Only axisymmetric mode of buckling is considered. Hence, a segment of the cylinder with $\alpha = 10°$ and half length of the cylinder, as shown in Figure 14b, is discretized with a mesh of 5 x 1. The buckling load for such cylinders whose length is less than the critical length is given by Timoshenko[104].

$$L_{cr} = \frac{(R\ h/2)^{1/2}}{3(1-\nu^2)^{1/4}} \tag{6.11}$$

and

$$N_{cr} = \frac{E\ h^2}{R[3(1-\nu^2)]^{1/2}} \tag{6.12}$$

where N_{cr} is the critical axial membrane stress resultant.

The cylinder has the following properties.

$E = 10^6$ psi (6.895×10^6 kPa)

$\nu = 0.3$

$R = 100$ in. (2540 mm)

Table 9. Buckling Stress (σ_{cr}) for Axially Loaded Cylindrical Panel

Type of solution	σ_{cr}(psi)
Ref. (108) 3x6 mesh	2920.
Ref. (105) 7x7 mesh	3075.
This study 4x4 mesh	2663.

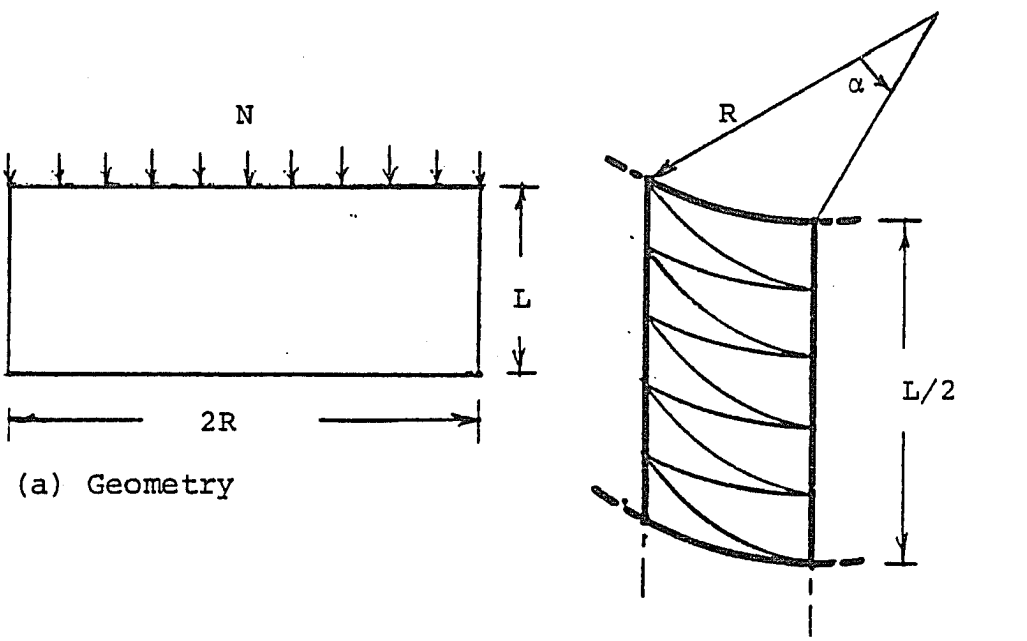

Figure 14. Axially loaded cylinder.

h = 1 in. (25.4 mm)

L = 17.282 in. (438.96 mm)

α = 10 deg.

Table 10 shows the results of references 104, 105 and the present study.

The comparison shows excellent agreement with the theoretical value with a difference of only 0.1%.

6.1.5.4 Hinged Cylinder under Normal Pressure. Figure 15a shows a cylinder with hinged ends subjected to uniform external pressure. For such a problem, Flügge[109] has derived buckling load expressions. Yamaki[110] and Almroth[111] have also given buckling pressure curves for different parameters of the cylinder. This problem has also been solved by Wang and Billington[112] using a semi-inextensional theory and also by Chang[105]. The following properties were assumed for the cylinder.

$E = 10^5$ psi (6.895×10^5 kPa)

$\nu = 0.3$

h = 0.01 in. (0.254 mm)

R = 1 in. (25.4 mm)

L = 5 in. (127 mm)

The cylinder is analyzed considering symmetric buckling with a mesh of 4 x 2, as shown in Figure 15b. The result of the present study is compared with that of references 112 and 105. Table 11 shows the comparison.

Table 10. Buckling Load for Axially Loaded Hinged Cylinder

Type of solution	N_{cr}(lbs/in)
Analytical (ref. 104)	6052.0
Ref. 105 (FEM)	6047.0
This study	6045.85 (0.10%)

(Percentage error is shown in parenthesis)

Table 11. Buckling Pressure for Hinged Cylinder

Solution type	q_{cr}(psi)
Analytical (ref. 112)	0.58
Ref. 105 (6x5 mesh)	0.56
This study (4x2 mesh)	0.62

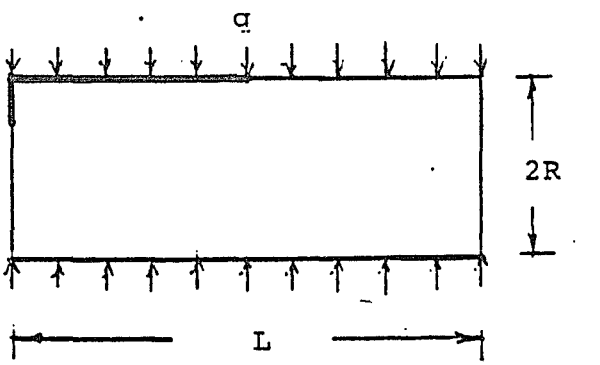

(a) Geometry

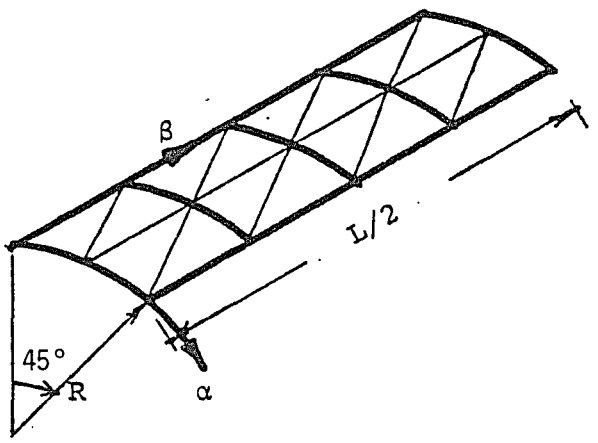

(b) Finite element mesh

Figure 15. Hinged cylinder under external normal pressure.

The comparison of the results shows that the buckling pressure given by reference 105 is lower than the analytical value. This is due to the inclusion of pressure stiffness effects in reference 105. The result of this study differs by 6.9% with the theoretical value and the difference could be lesser if a finer mesh had been used.

The above results for a number of numerical examples from a variety of problems, indicate good agreement with the available analytical and numerical values. This testifies to the accuracy of the DKCT element in linear buckling problems. It also checks the accuracy of the coefficients of $[K_\sigma]$, which will be used in the subsequent non-linear analysis. Solutions where non-conservative loadings are considered clearly indicate the importance of this effect on the buckling load; without this effect, the computed buckling load will be on the unsafe side.

Next, examples on full GNL analysis will be studied and the results will be compared and discussed with the available analytical and numerical values, to assess the behavior of the DKCT element and the accuracy of the nonlinear formulations.

6.2 Geometrically Nonlinear (GNL) Analysis Examples

6.2.1 Plates

The GNL analysis of the shells can be quite expensive and hence testing the element and the nonlinear formulation can be done in a relatively economical manner by starting with plate examples. Plates have very simple geometry and costly transformations to curvilinear

axes can be avoided by referring all variables to the global cartesian frames. Numerical results of plates with different geometry, boundary conditions and loadings will be discussed below.

6.2.1.1 Clamped Square Plate Under Uniformly Distributed Load. One of the standard test problems used in the GNL plate analysis is the large deflection behavior of a uniformly loaded square plate with all edges clamped. Classical solution to the nonlinear von Karman equations has been given by Levy[113]. Finite element solutions to this problem has also been given by a number of authors (references 60, 114-117) who have compared their solutions to the analytical solution of Levy.

Figure 16 shows the geometry and finite element discretizations of a square plate. The plate has the following properties.

$E = 10.92 \times 10^5$ psi (75.29×10^5 kPa)

$\nu = 0.3$ [508 mm]

a = 20 in. [2.54 mm]

h = 0.1 in. (2.54 mm)

A pressure of 0.3 psi was applied in six equal increments. Due to symmetry, a quarter of the plate was modelled with three different meshes. The mesh and the designated element are

(i) 2 x 2 mesh - 8 elements - DKCT8

(ii) 3 x 3 mesh - 18 elements - DKCT18

(iii) 4 x 4 mesh - 32 elements - DKCT32

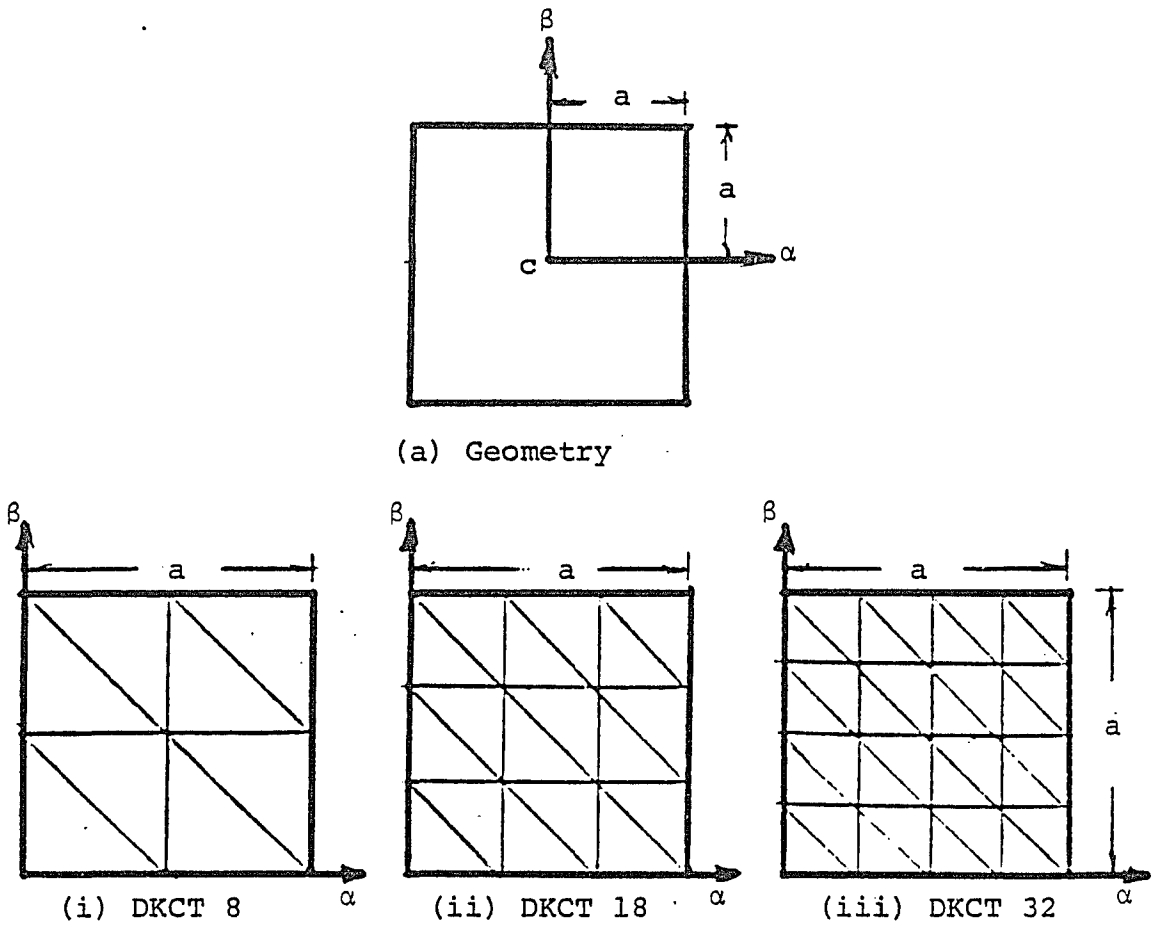

Figure 16. Square plates for GNL analysis.

Six analyses were carried out with the above three meshes and two integration orders (7- and 13-point integrations). For all these analyses a full N-R technique (KT) was employed with three iterations in each load increment. The central normalized transverse displacements and their corresponding normalized loads are given in Tables 12 and 13 for all the six cases. As the edge stresses obtained with DKCT8 elements were not satisfactory, the normalized extreme fiber stresses are given only for DKCT18 and DKCT32 elements in Tables 14 and 15. The results for the central deflections are compared with the analytical solution of Levy[113] and the numerical solution of Brebbia and Connor[114], who have used four noded shallow shell elements with 20 degrees-of-freedom per element. For extreme fiber stresses, comparison is made with Levy's solution and the numerical solution of Wood[60], who has employed three noded nonconforming plate bending elements with 15 degrees-of-freedom per element.

Figure 17 shows the normalized load-deflection curves of DKCT18 and DKCT32 elements, using 13-point integration. Figure 18 shows the same curve for 7-point integration. Figures 19 and 20 show the comparison of the two integration schemes for the DKCT32 and DKCT8 elements respectively. The analytical solution for displacements was measured from the plot of reference 32 and for stresses from reference 60. From Figures 17-20, it is seen that the results for the central deflections in all the six cases are in very good agreement with the analytical solution. In reference 114, the load deflection curve is

Table 12. Deflection of Clamped Square Plate Under Uniformly Distributed Load

(13-point integration)

Load increment	Load $p=qa^4/Dh$	$W = w_c / h$		
		DKCT8	DKCT18	DKCT32
1	50	0.840	0.840	0.830
2	100	1.227	1.234	1.215
3	150	1.516	1.540	1.518
4	200	1.744	1.780	1.756
5	250	1.932	1.980	1.196
6	300	2.093	2.150	2.125

Table 13. Deflection of Clamped Square Plate Under Uniformly Distributed Load

(7-point integration)

Load increment	Load $p=qa^4/Dh$	$W = w_c / h$		
		DKCT8	DKCT18	DKCT32
1	50	0.836	0.837	0.824
2	100	1.219	1.231	1.213
3	150	1.504	1.530	1.515
4	200	1.728	1.773	1.752
5	250	1.912	1.972	1.950
6	300	2.070	2.140	2.119

Table 14. Stresses at Center of Clamped Square Plate Under Uniformly Distributed Load

Load increment	Load $p=qa^4/Eh^4$	$S = \sigma a^2 / Eh^2$			
		Ngaus = 13		Ngaus = 7	
		DKCT18	DKCT32	DKCT18	DKCT32
1	4.579	2.62	2.530	2.58	2.500
2	9.158	4.09	3.988	4.04	3.939
3	13.736	5.23	5.118	5.17	5.050
4	18.315	6.14	6.033	6.07	5.946
5	22.894	6.93	6.822	6.85	6.716
6	27.473	7.63	7.520	7.54	7.400

Table 15. Stresses at the Mid Point of an Edge of a Clamped Square Plate Under Uniformly Distributed Load

Load increment	Load $p=qa^4/Eh^4$	$S = \sigma a^2 / Eh^2$			
		Ngaus = 13		Ngaus = 7	
		DKCT18	DKCT32	DKCT18	DKCT32
1	4.579	4.86	5.106	4.46	4.760
2	9.158	8.28	8.816	7.57	8.196
3	13.736	11.24	12.090	10.25	11.210
4	18.315	13.83	15.004	12.59	13.882
5	22.894	16.17	17.683	14.70	16.332
6	27.473	18.31	20.152	16.62	18.580

	DOF
Brebbia	125
DKCT32	225
DKCT18	144

DOF = total number of degrees-of-freedom

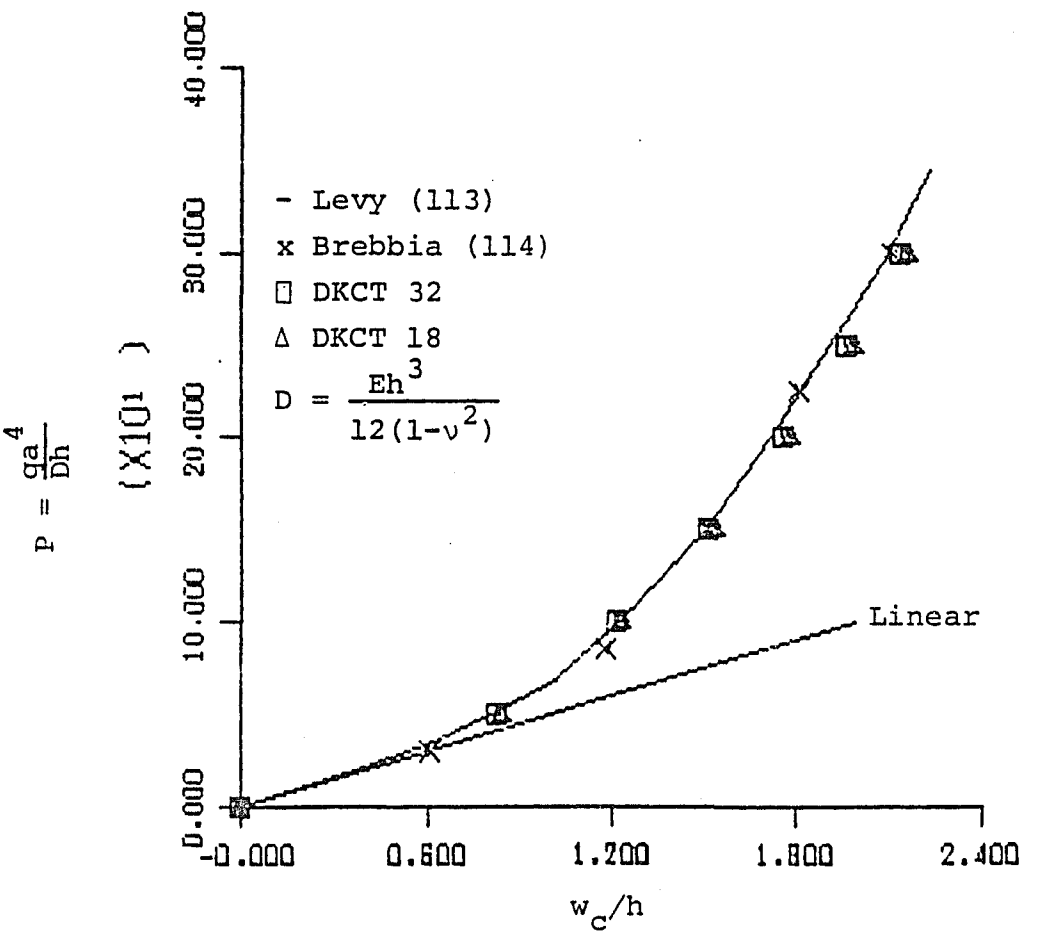

Figure 17. Load-central deflection curve for a clamped square plate under uniformly distributed load (13-point integration).

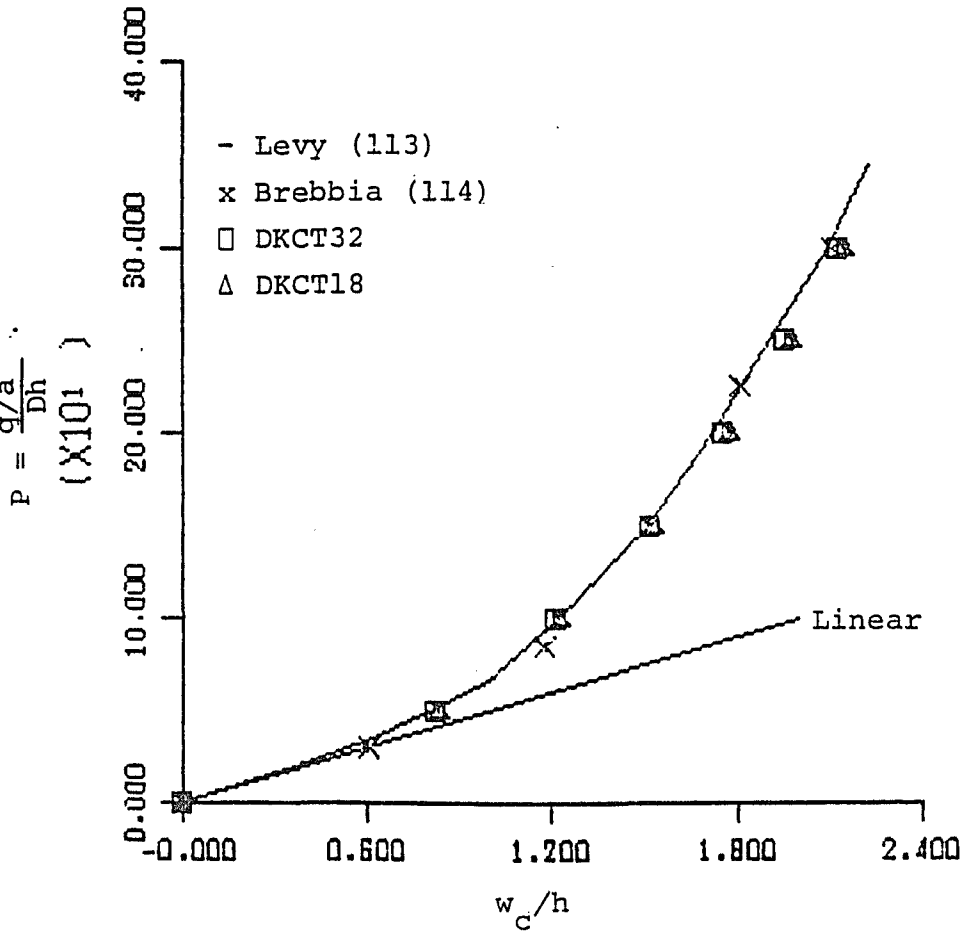

Figure 18. Load-central deflection curve for a clamped square plate under uniformly distributed load (7-point integration).

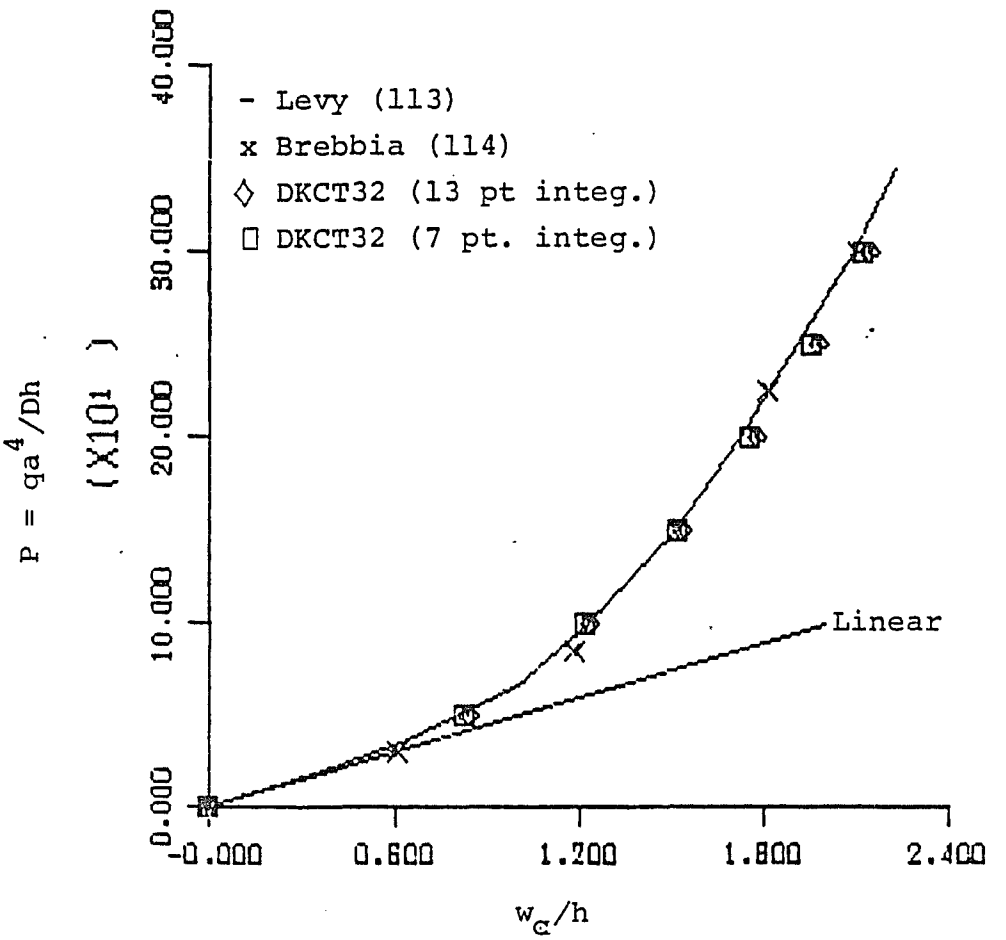

Figure 19. Load-central deflection curve for a clamped square plate under uniformly distributed load. (DKCT32)

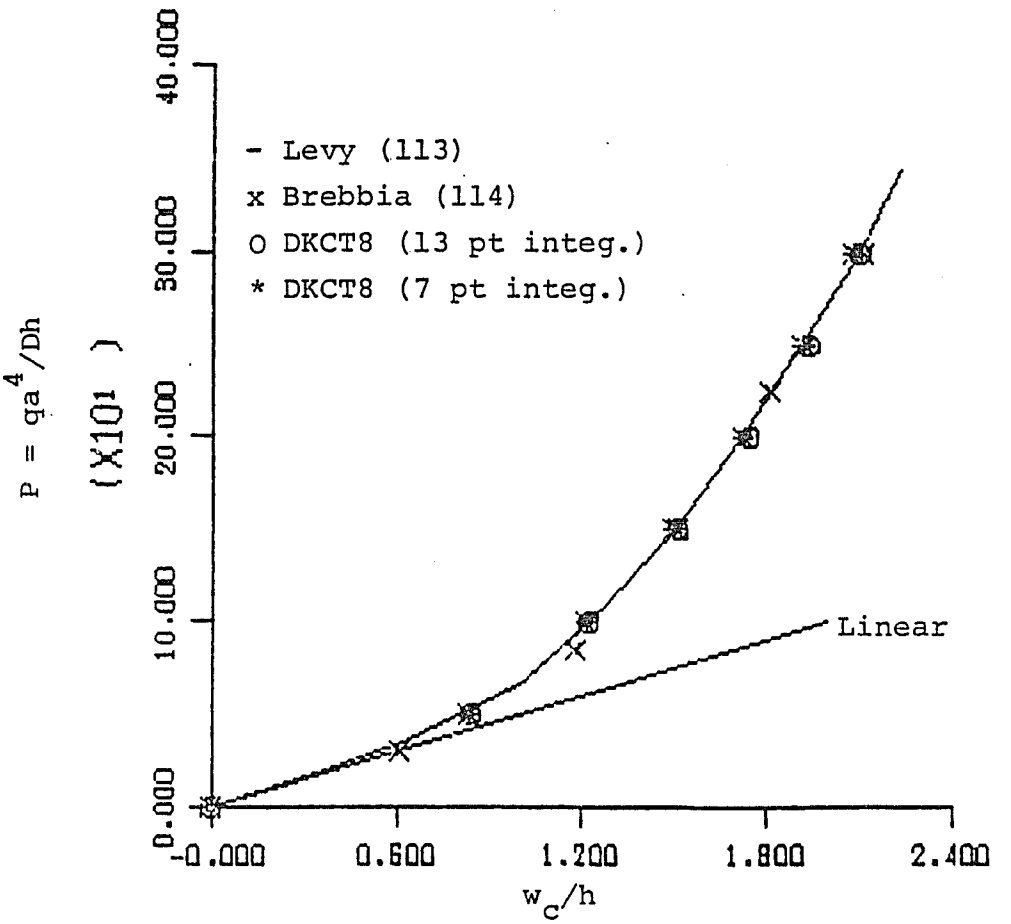

Figure 20. Load-central deflection curve for a clamped square plate under uniformly distributed load.(DKCT8)

shown to have slight difference with the analytical solution of Levy, but this difference is not found in reference 32.

The extreme fiber stresses at the mid point of an edge and at the center are next compared with the analytical solution of Levy[113] and the numerical solution of Wood[60]. Figure 21 shows comparison for stresses for DKCT18 and DKCT32 elements using 13-point integration and Figure 22 shows the same comparison for 7-point integration. Figure 23 shows the comparison of DKCT32 elements for the two integration schemes. From Figure 21, it is seen that the results of DKCT32 elements have excellent agreement for the edge stresses with the analytical values. At the center, the results agree more with the numerical solution of Wood. The edge stresses of DKCT18 elements are slightly smaller, but at the center they are higher than the analytical values, with a maximum difference of about 16%. From Figure 22, it is seen that for the 7-point integration, the edge stresses for the DKCT32 elements agree reasonably with the analytical values. The edge stresses of DKCT18 elements are much less. At the center, the order of integration does not have much effect and the stress distributions remain almost the same. The effect of order of integration is again shown in the case of DKCT32 elements. It is seen that, while the integration order affects the edge stresses, it has not much influence for the central stresses. As mentioned earlier, the edge stresses obtained with DKCT8 elements are in appreciable difference with the analytical solution and hence their values are not compared.

	DOF
Wood	180
DKCT32	225
DKCT18	144

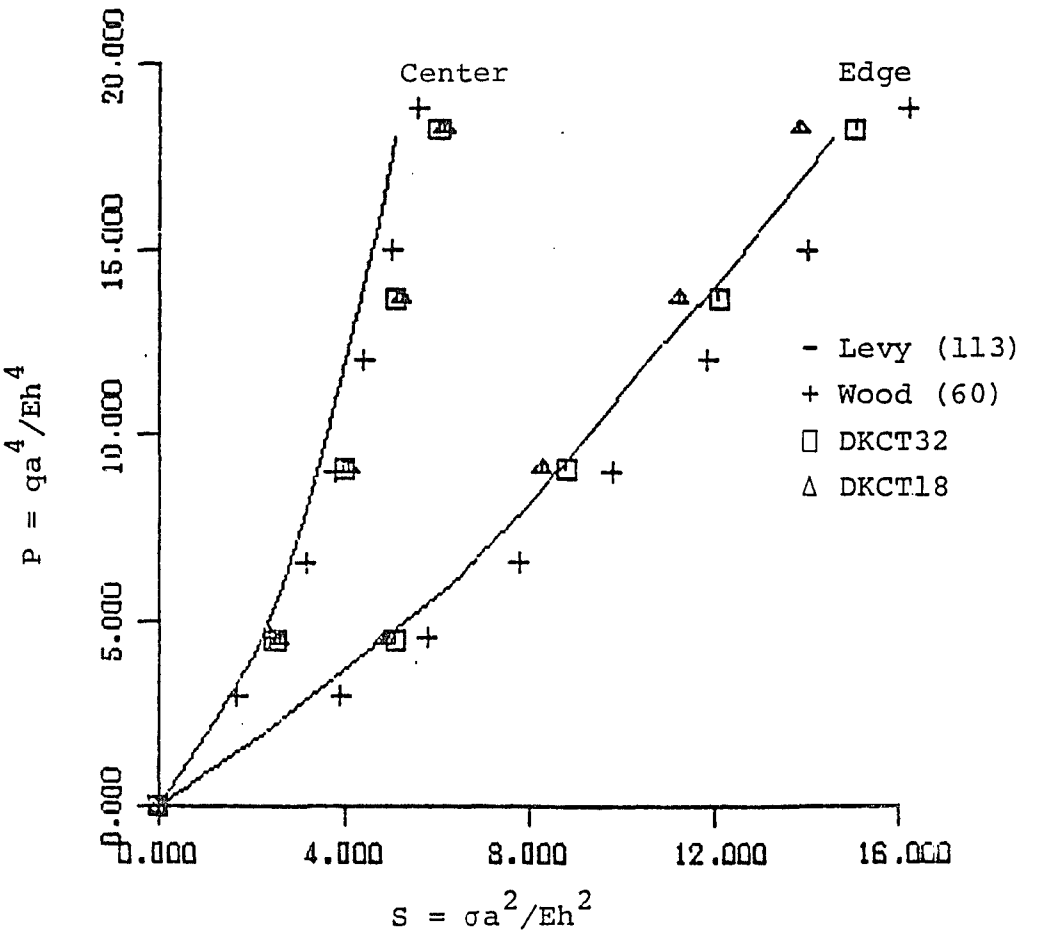

Figure 21. Load-stress curves for a clamped square plate under uniformly distributed load (13-point integration).

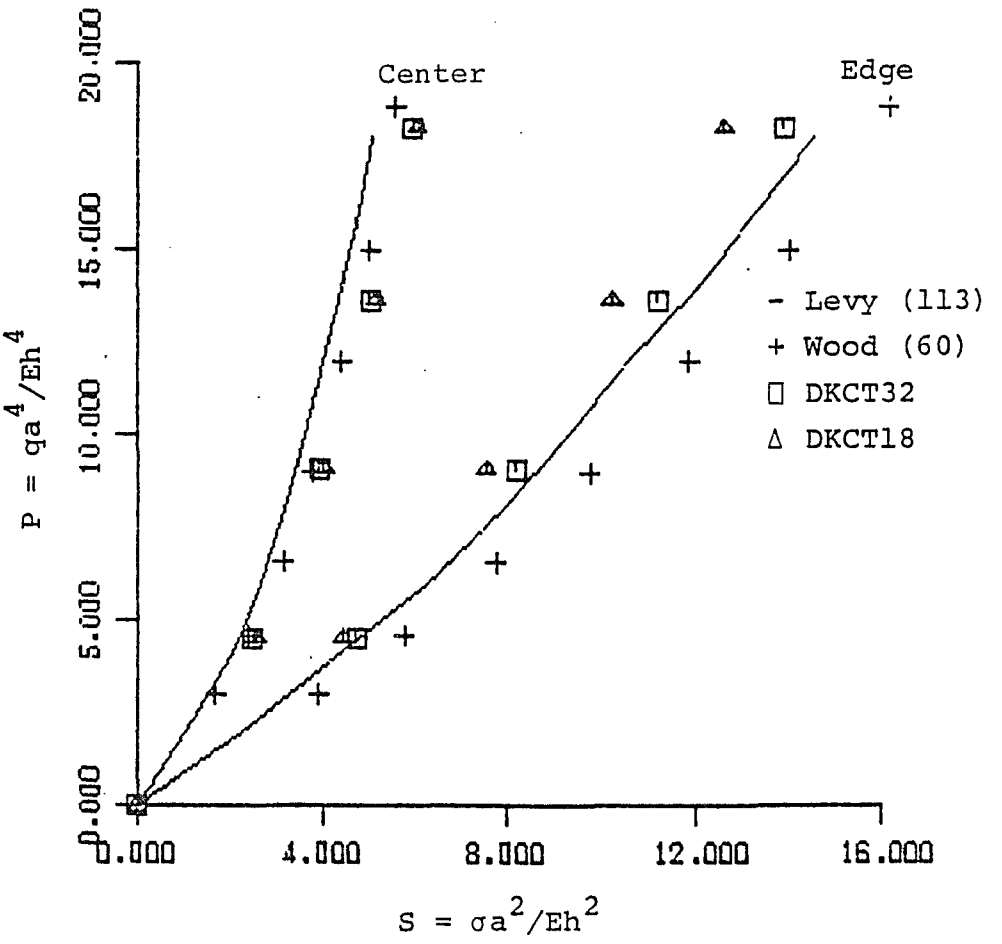

Figure 22. Load-stress curves for a clamped square plate under uniformly distributed load (7-point integration).

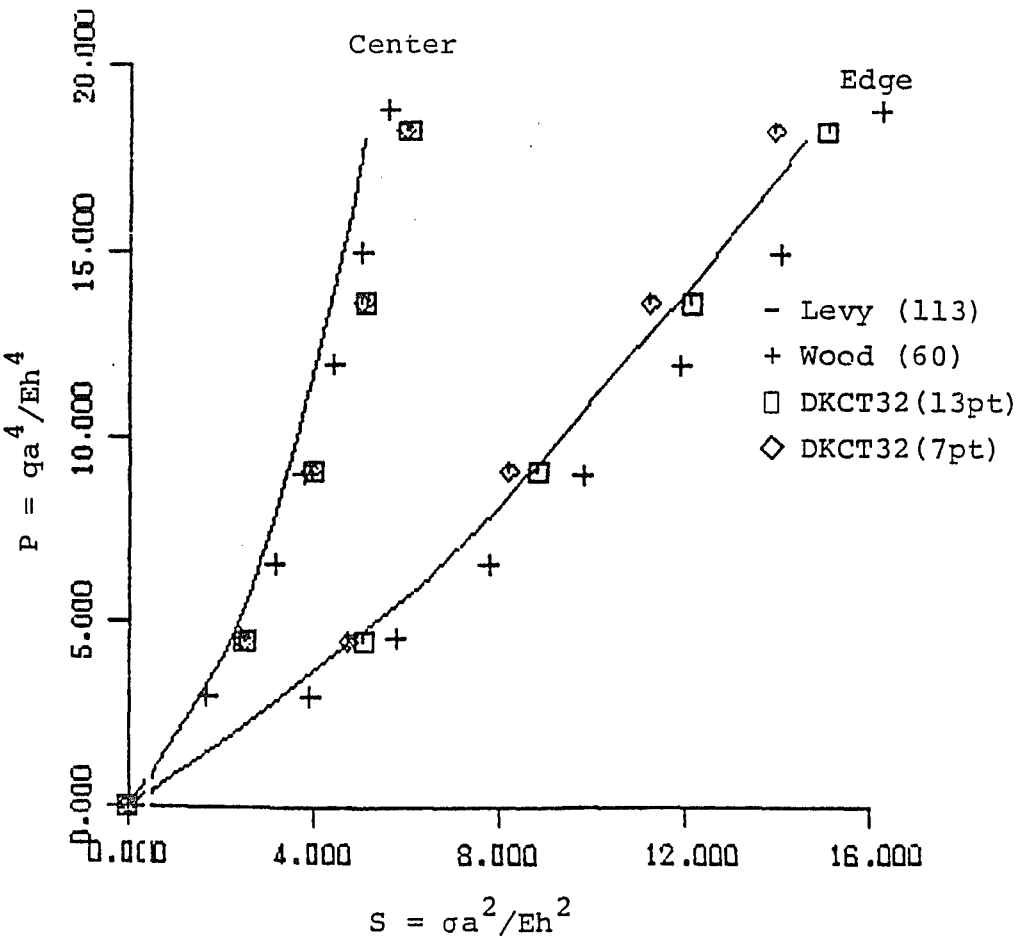

Figure 23. Load-stress curves for a clamped square plate under uniformly distributed load.

6.2.1.2 Simply Supported Square Plate under Uniformly Distributed Load. The analytical solution to this problem is again given by Levy[118], using a double Fourier series. The numerical solution is given among others by Wood[60] and Wilson[116]. The properties for this plate are same as the clamped plate. The plate is analyzed with (i) DKCT18 and (ii) DKCT32 elements, as shown in Figure 16 and a 13-point integration scheme. A pressure of 2.0964 psi was applied in six load increments with a load factor of 0.083 for the first two increments and 0.166 for the next four increments. The KT technique is again used with two to three iterations in each cycle. The normalized central displacements and stresses are shown in Table 16. Figure 24 shows the comparison of the load central displacement path with that of Levy[118] and Wood[60]. The comparison shows that the DKCT32 elements give satisfactory results up to the normalized load of 4.0, but thereafter the deflection increases with a maximum of 9.09%. The DKCT18 follows the trend of DKCT32 with larger increase than DKCT32. The maximum difference in the central normalized displacements for the DKCT18 elements is 11.88% with the analytical solution. Figure 25 shows the normalized load stress path at the center of the plate. The comparison here also is along the trend of the displacement path. The DKCT32 shows a maximum increase of 14.91%, while the DKCT18 shows 16.39%.

6.2.1.3 Clamped Circular Plate under Uniformly Distributed Load. Analytical solution to a clamped circular plate under uniformly distributed load, using Ritz energy method has been presented by Weil

Table 16. Deflections and Stresses for a Simply Supported Square Plate Under Uniformly Distributed Load

Load increment	Load $p=qa^4/Eh^4$	$W = w_c/h$		$S = \sigma a^2/Eh^2$	
		DKCT18	DKCT32	DKCT18	DKCT32
1	1.	0.54	0.526	1.10	1.08
2	2.	0.80	0.773	1.80	1.79
3	4.	1.10	1.081	2.78	2.74
4	6.	1.35	1.316	3.50	3.49
5	8.	1.53	1.495	4.10	4.09
6	10.	1.686	1.644	4.70	4.64

	DOF
Wood	125
DKCT32	225
DKCT18	144

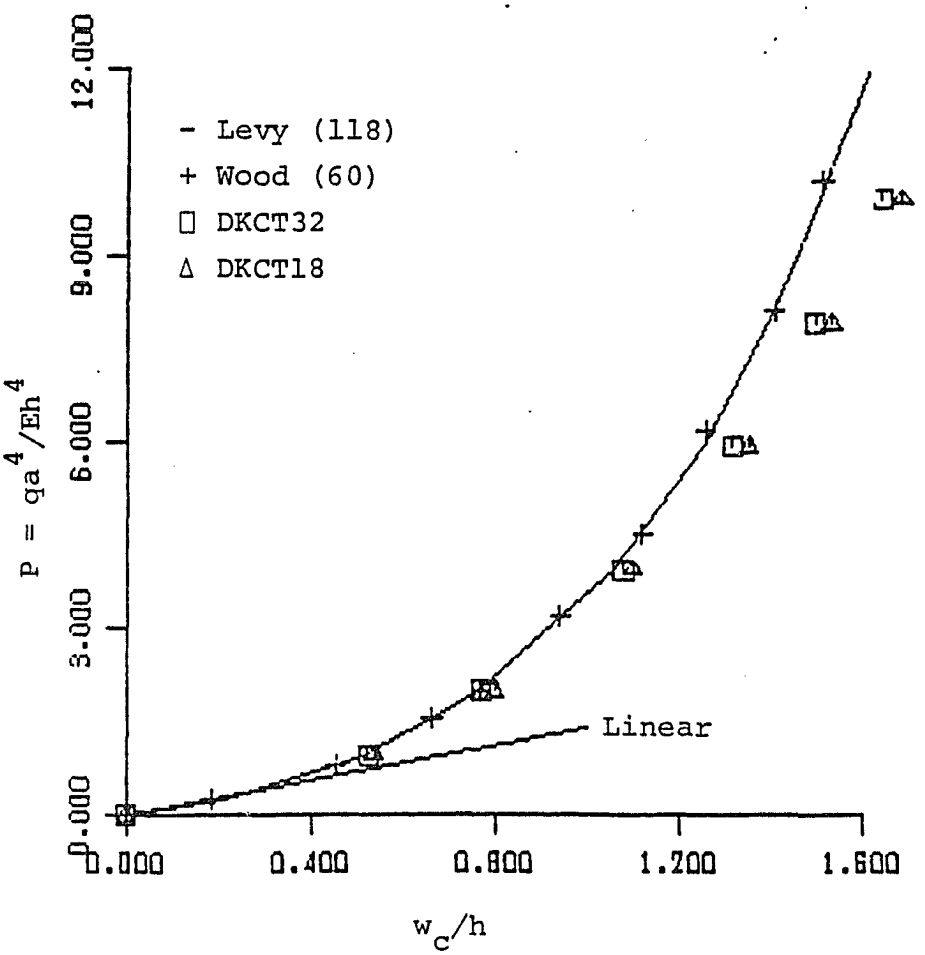

Figure 24. Load-central deflection curve for a simply supported plate under uniformly distributed load.

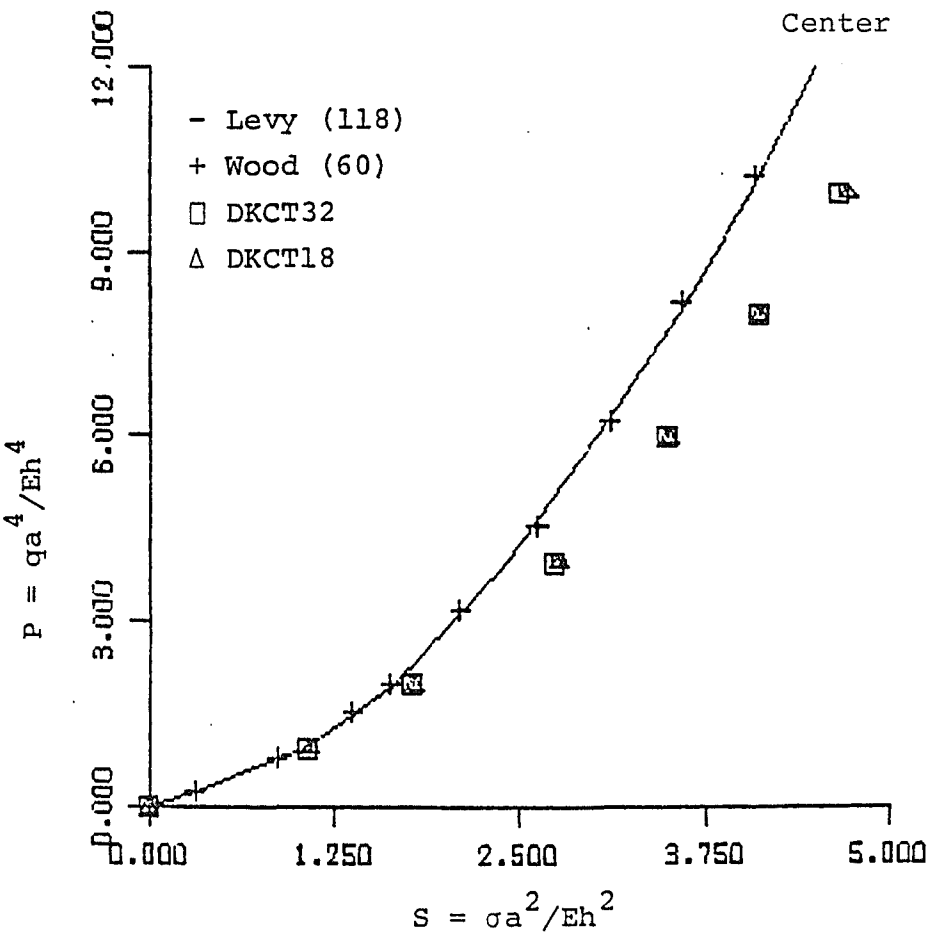

Figure 25. Load-stress curve for a simply supported square plate under uniformly distributed load.

and Newmark[119] as a special case of clamped elliptical plates. Finite element solution to this problem is again provided by Wood[60] using nonconforming plate bending elements.

Figure 26 shows the geometry and the mesh idealization for one quarter of the plate. The plate has the following data:

$R = 50$ in. (1270 mm)

$h = 1$ in. (25.4 mm)

$E = 10.92 \times 10^5$ psi (75.293×10^5 kPa)

$\nu = 0.3$

$q = 2.7952$ psi [8.0 kPa]

The pressure q is applied in seven increments with a load factor of 0.25 in the first increment and 0.125 in the next 6 increments. Again, a full N-R technique (KT) was employed requiring 3 iterations for most of the increments. The normalized central deflection and stress values for DKCT32 element mesh are shown in Table 17.

Figure 27 shows the normalized load-deflection path for the center of the plate, compared with Newmark[119] and Wood[60]. The results agree reasonably well up to the normalized load of 8.0 and thereafter the difference increases with a maximum of 7.99%. Figure 28 shows the comparison of normalized load-stress path at the center and at the boundary of the plate. Again, excellent agreement is seen for the edge stresses, while stresses at the center are higher than the analytical value by a maximum of 11.58%. Wood[60] reports a difference of

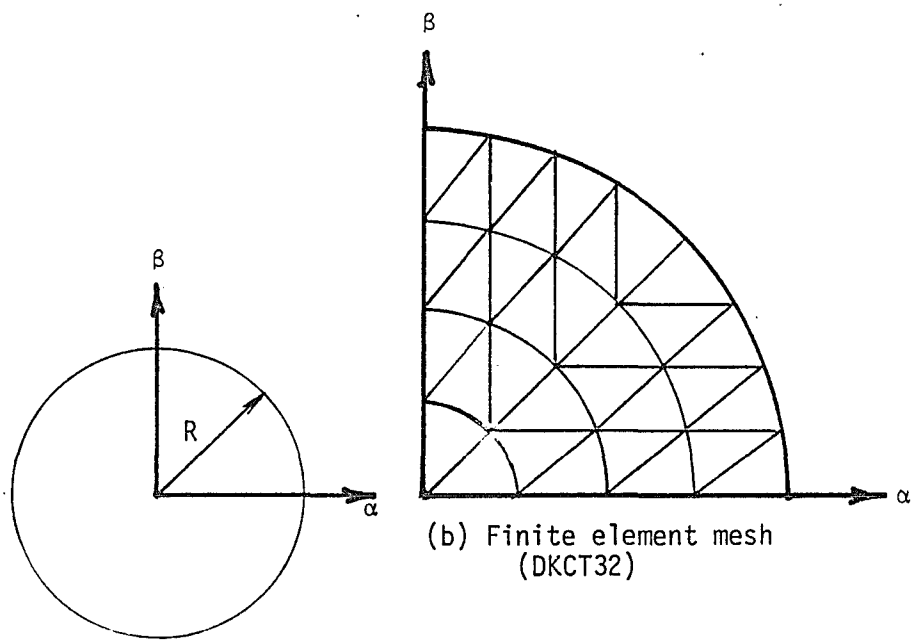

(a) Geometry

(b) Finite element mesh (DKCT32)

Figure 26. Clamped circular plate.

Table 17. Deflections and Stresses of a Clamped Circular Plate Under Uniformly Distributed Load

Load increment	Load $p=qa^4/Eh^4$	$W = w_c/h$	$S = \sigma a^2 / Eh^2$	
			Center	Edge
1	4.	0.608	1.90	2.96
2	6.	0.807	2.68	4.21
3	8.	0.969	3.30	5.33
4	10.	1.106	3.90	6.35
5	12.	1.223	4.40	7.31
6	14.	1.327	4.80	8.20
7	16.	1.419	5.30	9.05

	DOF
Wood	180
DKCT32	225

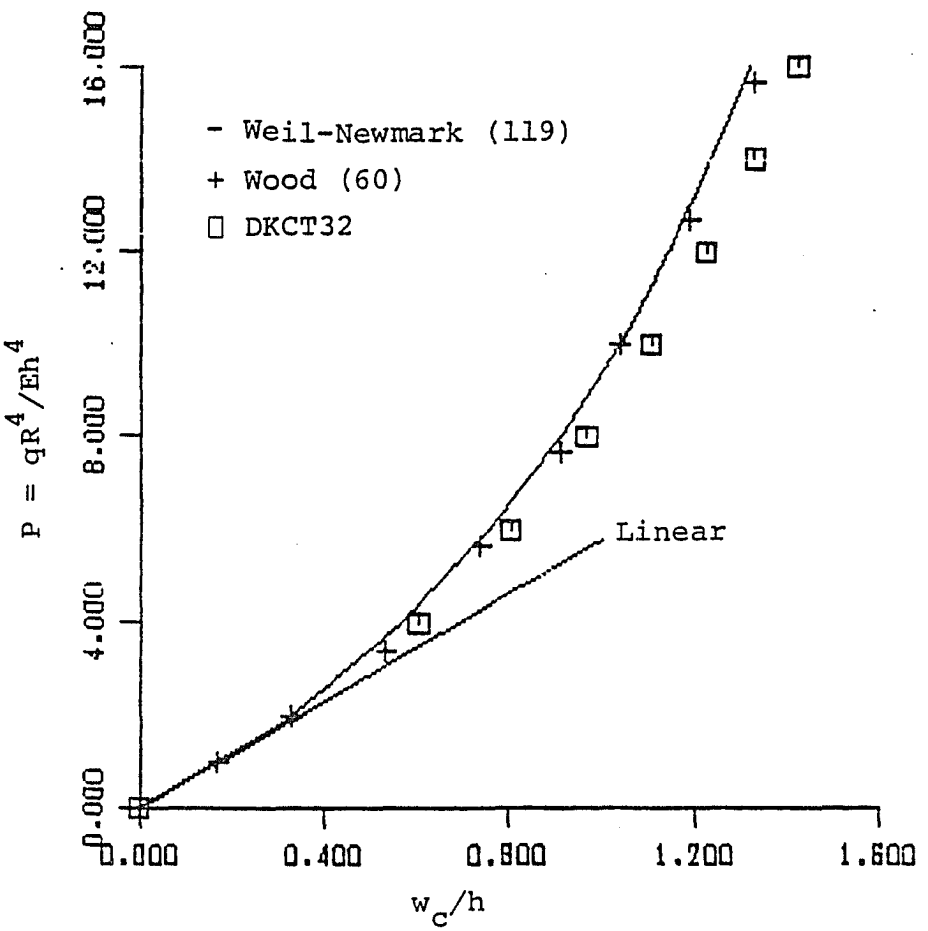

Figure 27. Load-central deflection curve for a clamped circular plate under uniformly distributed load.

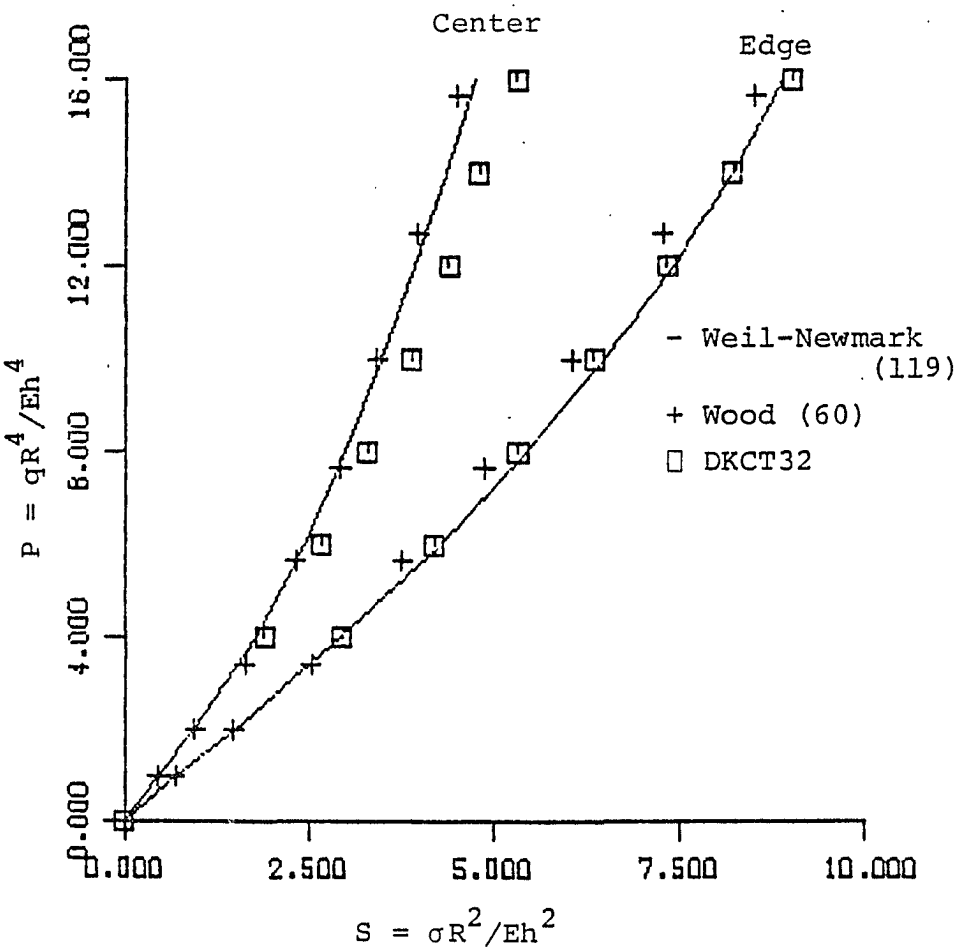

Figure 28. Load-stress curves for a clamped circular plate under uniformly distributed load.

8% for the central stresses and 15% for the edge stresses, when using 41 triangular hybrid elements.

6.2.1.4 Clamped Square Plate under a Central Point Load. The problem of a clamped square plate under a central point load has been solved analytically by Adotte[120] using finite difference technique. The finite element solution to this problem has been given by Brebbia and Connor[114]. Due to symmetry, one quarter of the plate is analyzed using DKCT32 mesh. The geometry and the discretization are as shown in Figure 16. The plate has the following properties:

$a = 100$ in. (2540 mm)

$h = 1$ in. (25.4 mm)

$E = 10.92 \times 10^5$ psi $(75.29 \times 10^5$ kPa)

$\nu = 0.3$

A total central point load of 3000 pounds was applied in 6 increments with load factors of 0.083 for the first two increments and 0.166 for the next four increments. The analysis was carried out using KT technique and 3 iterations per cycle. The normalized load-central deflection values are given in Table 18. Figure 29 shows the comparison of the load deflection paths with the analytical and numerical solutions plot from reference 114. The central deflections agree well up to the normalized load of 400, but thereafter increase with a maximum difference of 10.84% with the analytical solution and about 6.2% with the numerical solution of reference 114.

Table 18. Deflections of a Clamped Square Plate Under a Central Point Load

Load increment	Load $p=pa^2/Dh$	$W = w_c/h$
1	100.	1.354
2	200.	1.970
3	400.	2.720
4	600.	3.267
5	800.	3.700
6	1000.	4.050

	DOF
Brebbia	80
DKCT32	225

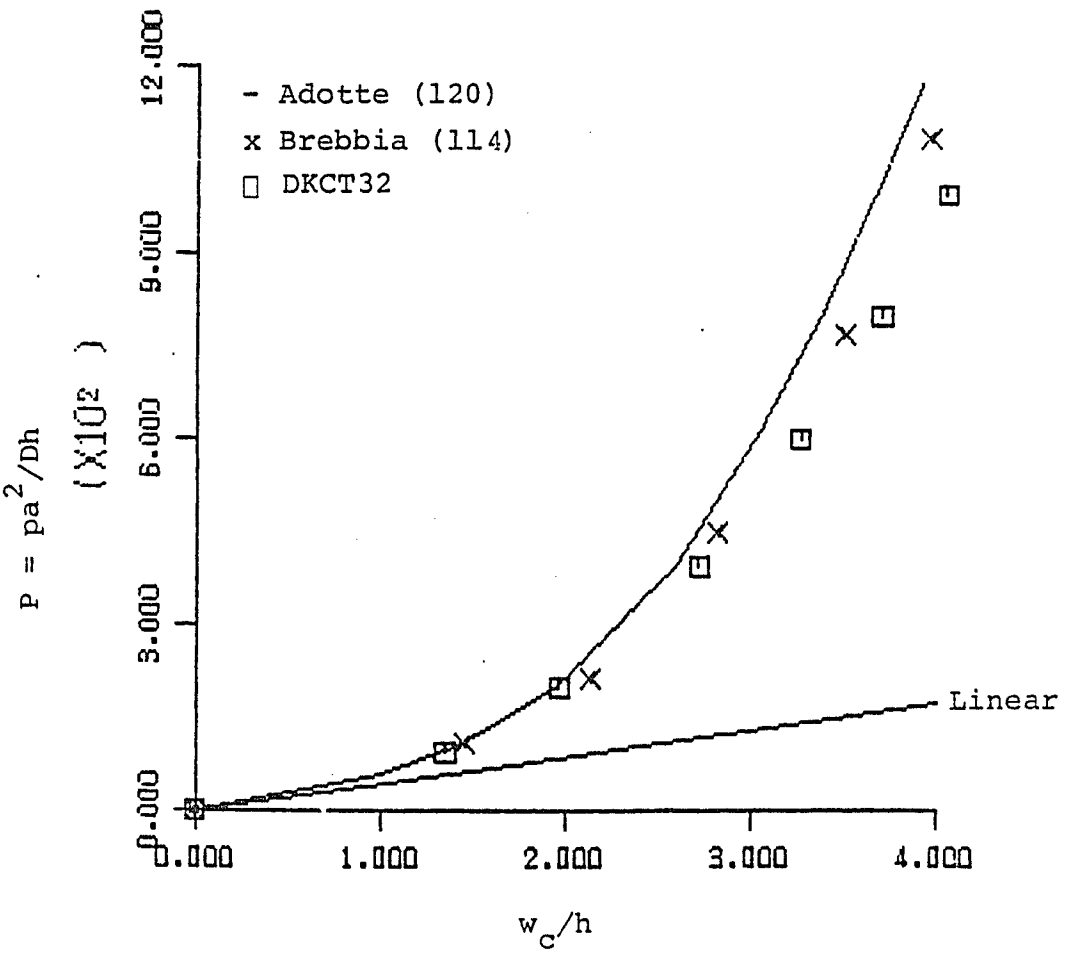

Figure 29. Load-central deflection curve for a clamped square plate under a central point load.

6.2.1.5 Clamped-Free Square Plate with Eccentric Concentrated Load. A square plate with two opposite edges clamped and the other two free is loaded by a concentrated load, as shown in Figure 30. No analytical solution to this problem seems to be available. Experimental and finite element solutions to this problem have been given by Kawai and Yoshimura[115] who have employed four noded conforming plate bending elements of 20 degrees-of-freedom per element for their numerical solution. The plate has the following properties:

$2a = 400.0$ mm

$h = 1.98$ mm

$E = 2.15 \times 10^4$ kg/mm^2

$\nu = 0.3$

A point load of 20 kg was applied in five equal increments and the analysis was carried out with about 3 iterations per cycle. Table 19 shows the load displacement values at the points A and B of the plate. Figure 31 shows the comparison of the load-deflection paths at points A and B of the plate with the numerical solutions of Kawai and Yoshimura who have used 50 elements, which are reported to have good agreement with their experimental results. The deflections of the present study agree reasonably well with the numerical solution of Kawai and Yoshimura with a difference of only 2.56% at A and 4.55% at B at their maximum values.

The results of the plate examples studied so far indicate that the deflections are in good agreement with the compared values in the

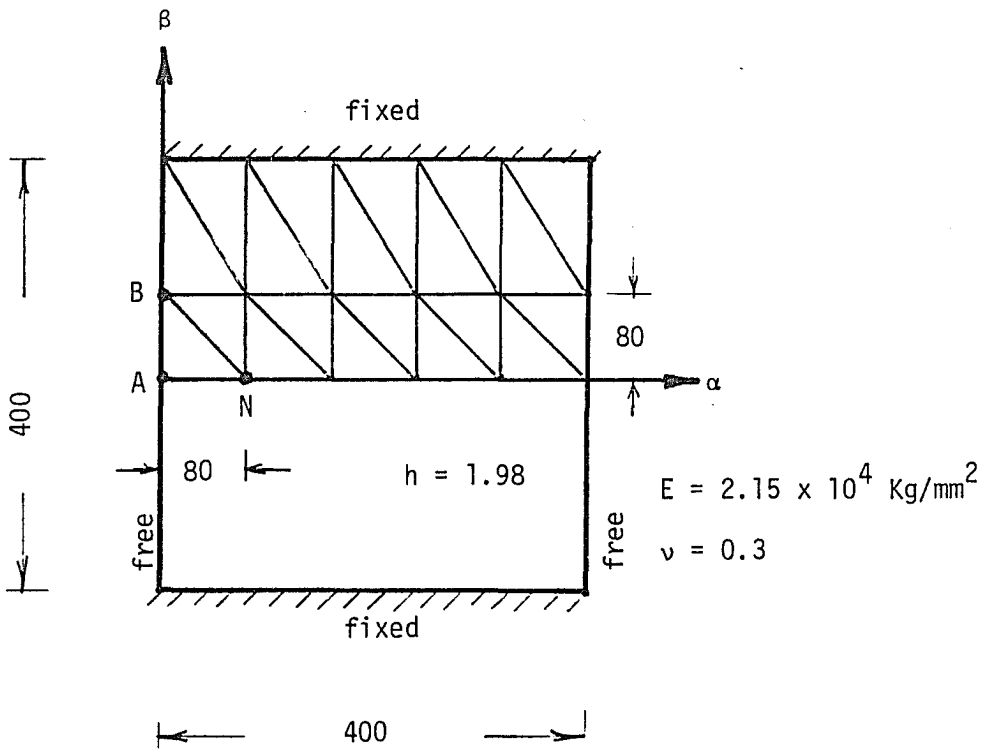

(All dimensions are in mm)

Figure 30. Fixed-free square plate under a point load at N.

Table 19. Deflections of a Fixed-Free Plate Under a Concentrated Load

Load increment	Load p(kg)	w(mm) At A	w(mm) At B
1	4.	0.47	0.356
2	6.	0.94	0.620
3	12.	1.29	0.860
4	16.	1.56	1.040
5	20.	1.72	1.150

	DOF
Kawai	330
This Study	162

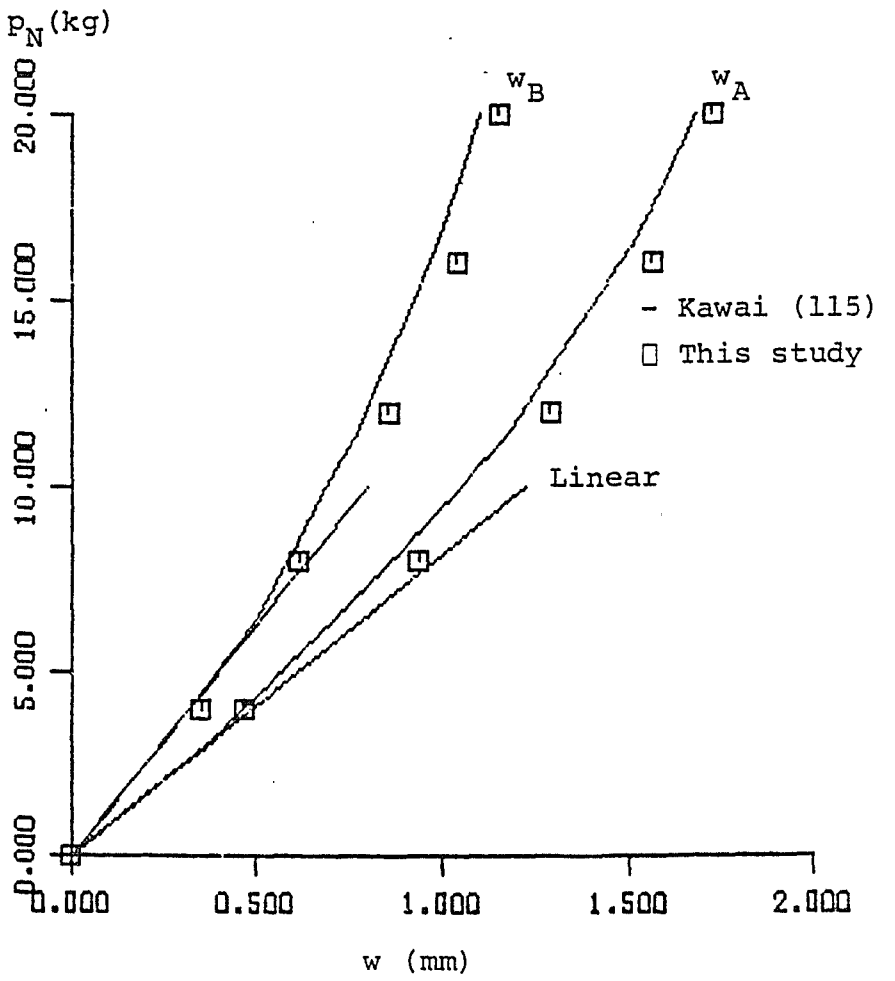

Figure 31. Load-deflection curves for a fixed-free square plate under a point load at N.

examples of 6.2.1.1 and 6.2.1.5 and do not agree quite well in the other examples. The stresses agree very well at the clamped edges in the examples of 6.2.1.1 and 6.2.1.3 and are higher at the center in the examples of 6.2.1.1 to 6.2.1.3. The reason for this can be recalled from the linear buckling examples of columns and plates. The condensed central node plays as important role as the other nodes. When the chosen curvilinear axes coincide with the glogal cartesian axes the stiffness coefficients of the central node become zero. Any approximation introduced for the central node disturbs the complex nonlinear solution. When the relative transverse displacements increase with increase in loads, as in the case of simply supported plates, the difference in the nonlinear solution increases. This is also evidenced from the results for the edge stresses in the clamped plates. Near the edges, the displacements are very small and hence approximate displacements introduced for the central node did not affect the solution near the edges. Otherwise, the nonlinear load displacement path is quite smooth and reasonably agreeable in the examples.

6.2.2 Arch and Shells

After testing series of plate examples, the GNL formulation and the behavior of the DKCT elements will be tested on a variety of examples of arch and shells. The results will be compared with the available published analytical and numerical solutions.

6.2.2.1 Clamped Shallow Circular Arch under a Central Point Load. Due to their simple geometry, circular arches are often cited examples in the literature. The GNL analysis of circular arches have

been performed by a number of authors using bar, beam or shell elements.

Figure 32 shows a shallow circular arch clamped at both ends and loaded by a central point load p. One half of the arch is analyzed considering symmetric buckling with a mesh of 5 x 1 and the following data:

$E = 1 \times 10^7$ psi (6.895×10^7 kPa)

$\nu = 0.0$

R = 133.114 in. (3381.1 mm)

h = 0.1875 in. (4.7625 mm)

$\alpha = 7.34$ deg.

Total load p = 40 lbs.

No. of increments = 7

Load factors = 0.25, 0.125, 0.125, 0.062, 0.063, 0.062, 0.063

The analysis was carried out with a full N-R technique (KT) with 2 to 3 iterations per cycle. This problem has also been solved by Brink and Kratzig[121], Dupuis[122] and Bathe[123]. The load-central normal deflection values of the present study are shown in Table 20. Figure 33 shows the load deflection paths compared with the numerical solution of Brink and Kratzig[121], who have used 2 curved bar elements and Dupuis et al., who have used 32 beam elements.

The structure deforms continuously into a symmetric stable configuration undergoing small rotations. The result of the study

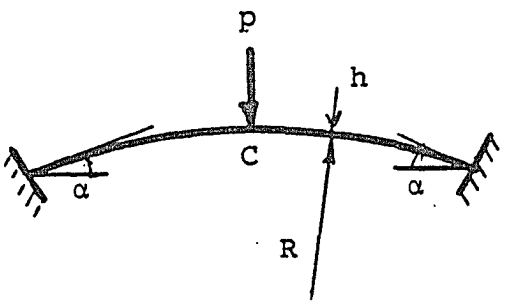

(a) Geometry

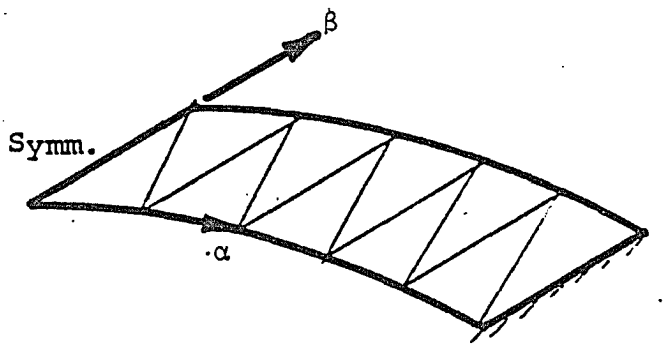

(b) Finite element mesh

Figure 32. Clamped shallow arch under a central point load.

Table 20. Deflections of Shallow Circular Arch Under a Central Point Load

Load increment	Load P (lbs)	w c (ins)	Load increment	Load P (lbs)	w c (ins)
1	10.0	0.038	6	27.5	0.149
2	15.0	0.060	7	30.0	0.181
3	20.0	0.084			
4	22.5	0.100			
5	25.0	0.122			

	DOF
Brink and Kratzig	21
This Study	108

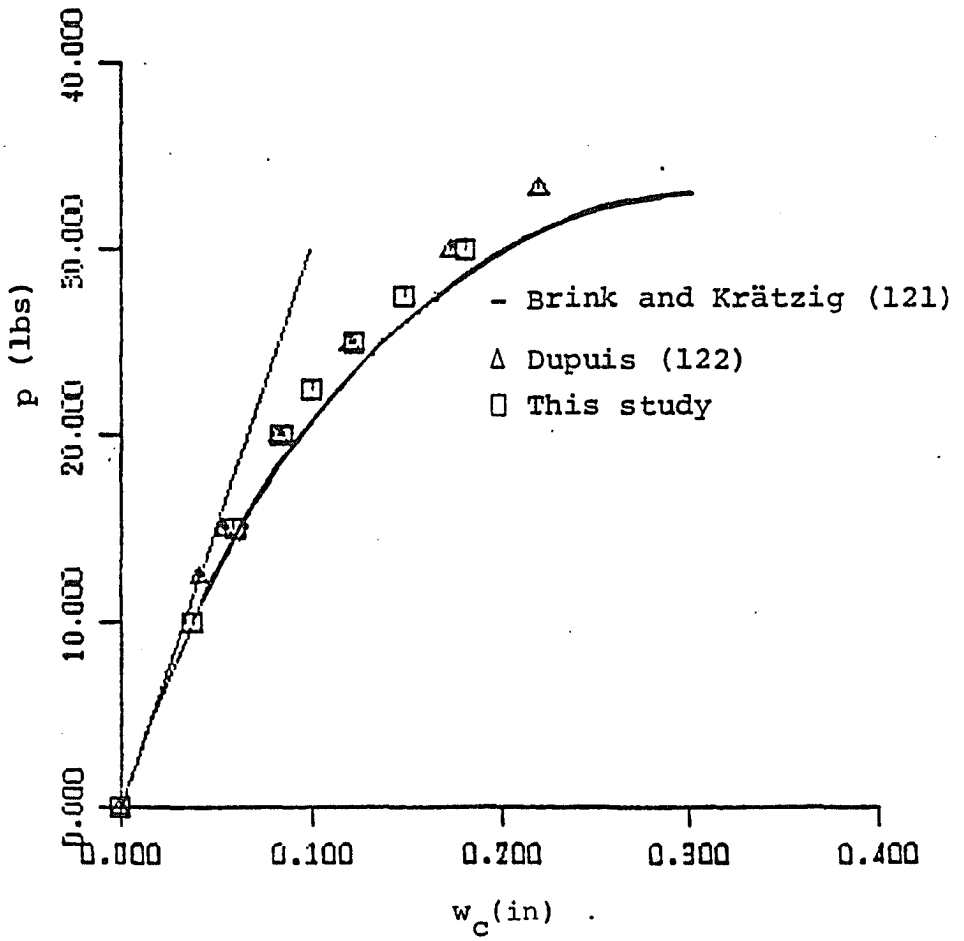

Figure 33. Load-central deflection curve for a clamped shallow arch under a central point load.

agrees well with that of Brink and Kratzig[121] who have used exact non-linear formulations considering large rotations. The maximum central normal deflection of this study is lesser than Brink's by 9.5% and more than Dupuis by 4.93%.

6.2.2.2 Clamped Cylindrical Panel under Uniform External Normal Pressure. An often cited example in the literature for the GNL analysis of shells is a shallow cylindrical panel clamped on all edges and subjected to external normal pressure, as shown in Figure 34. Finite element solution to this problem has been given by a number of authors (references 50, 76, 96, 114, 117, 124-128).

Due to symmetry, a quarter of the panel is modelled with a 2 x 2 mesh and analyzed with the following data:

$L = 20$ in. (508 mm)

$R = 100$ in. (2540 mm)

$h = 0.125$ in. (3.175 mm)

$\alpha = 0.1$ radian

$E = 450{,}000$ psi (31.03×10^5 kPa)

$\nu = 0.3$

A pressure of 0.3 psi was applied in 9 unequal increments and the analysis was carried out with KT2 technique and Frontal solution with 2 to 6 interations per cycle. The cylindrical panel softens up to about 0.24 psi and begins to stiffen thereafter due to membrane tensile stress in the longitudinal direction. The solution at this pressure oscillated, requiring more iterations to stabilize. The shell

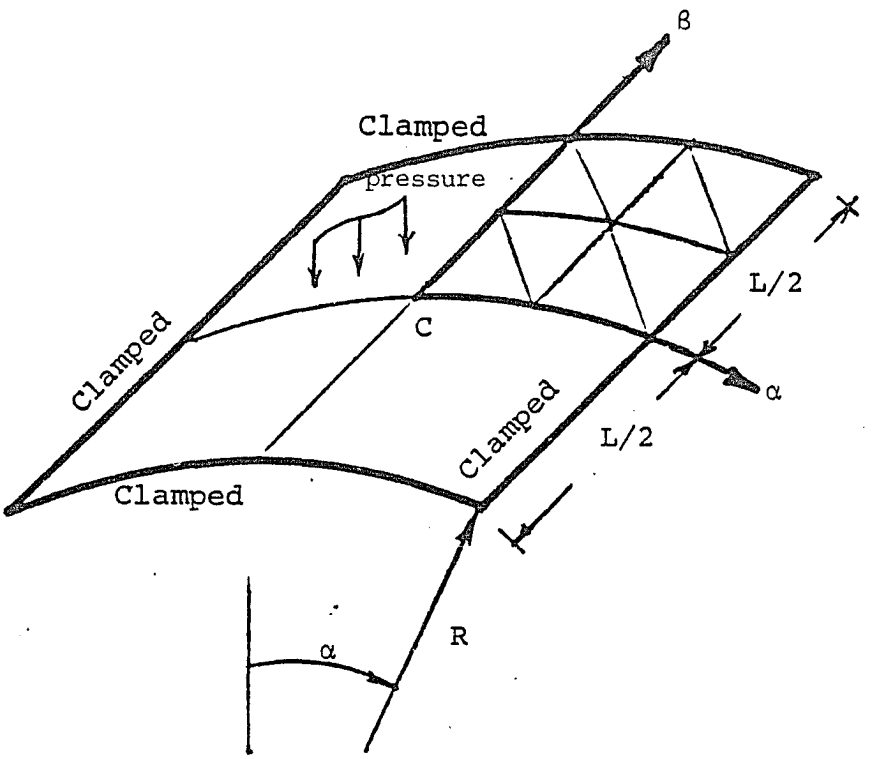

Figure 34. Clamped cylindrical panel under external normal pressure.

does not experience snap through situation due to this stiffening effect. The pressure-central normal displacement values of this study are given in Table 21. The load-deflection path is compared up to the point of inflection with Dhatt[76], who has used D-K theory, Gallagher's[117] deep shell triangular elements (27 degrees-of-freedom per element) and Horrigmoe's[50] hybrid flat triangular elements (5 displacements and 6 stresses degrees-of-freedom per node) and shown in Figure 35a. Figure 35a indicates that the deflection compares very well with Dhatt[76] and is less only by 4.6% at its maximum value. Comparison is also made slightly beyond this point with Horrigmoe's[50] solution and shown in Figure 35b. Figure 35b shows good comparison with Horrigmoe's solution. Horrigmoe[50] has also produced a number of results for the central deflections using both triangular and quadrilateral elements with finer meshes, which are softer than the curve taken for the comparison.

6.2.2.3 Hinged-Free Cylindrical Panel under a Central Point Load. Another often cited example in the literautre is a cylindrical panel with curved edges hinged and straight edges free, loaded at the center by a concentrated load, as shown in Figure 36. Finite element solution to this problem is given by a number of authors (references 50, 62, 64, 96, 128-130. Due to symmetry, a quarter of the shell is modelled with a mesh of 3 x 3 and analyzed with the following data:

$$R = 2540 \text{ mm}$$

$$L/2 = 254 \text{ mm}$$

$$h = 12.7 \text{ mm}$$

Table 21. Deflections of Clamped Cylindrical Shell Under Uniform External Pressure

Load increment	Load q (psi)	w c (ins)	Load increment	Load q (psi)	w c (ins)
1	0.04	0.010	6	0.22	0.123
2	0.08	0.024	7	0.24	0.156
3	0.12	0.041	8	0.27	0.210
4	0.16	0.061	9	0.30	0.263
5	0.20	0.100			

	DOF
Harrigmoe	176
Gallagher	144
This Study	81

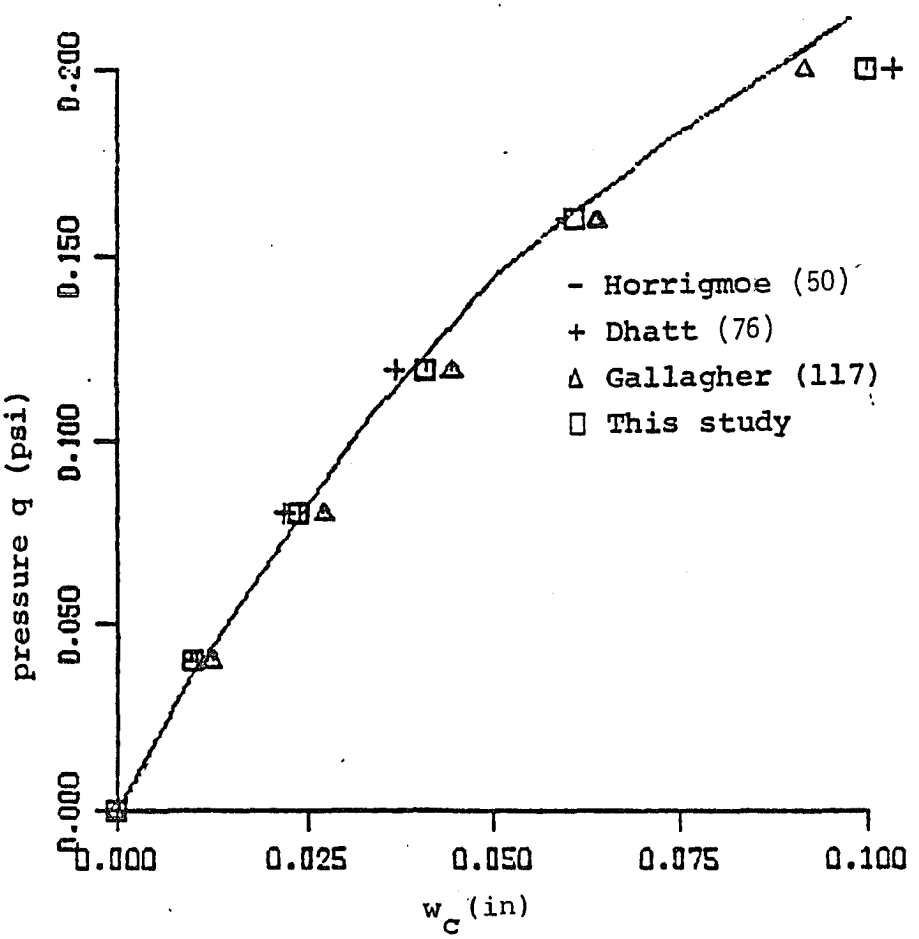

Figure 35a. Load-central deflection curve -1 for a clamped cylindrical panel under uniform normal pressure.

	DOF
Horrigmoe	176
This Study	81

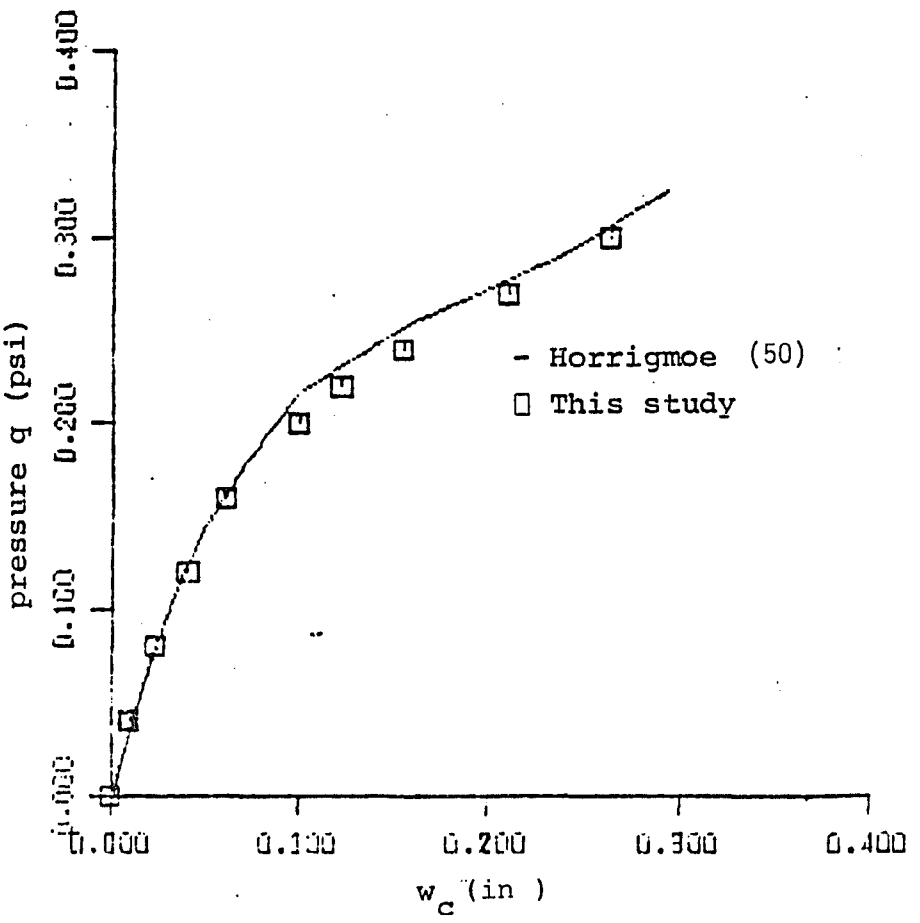

Figure 35b. Load-central deflection curve -2 for a clamped cylindrical panel under uniform normal pressure.

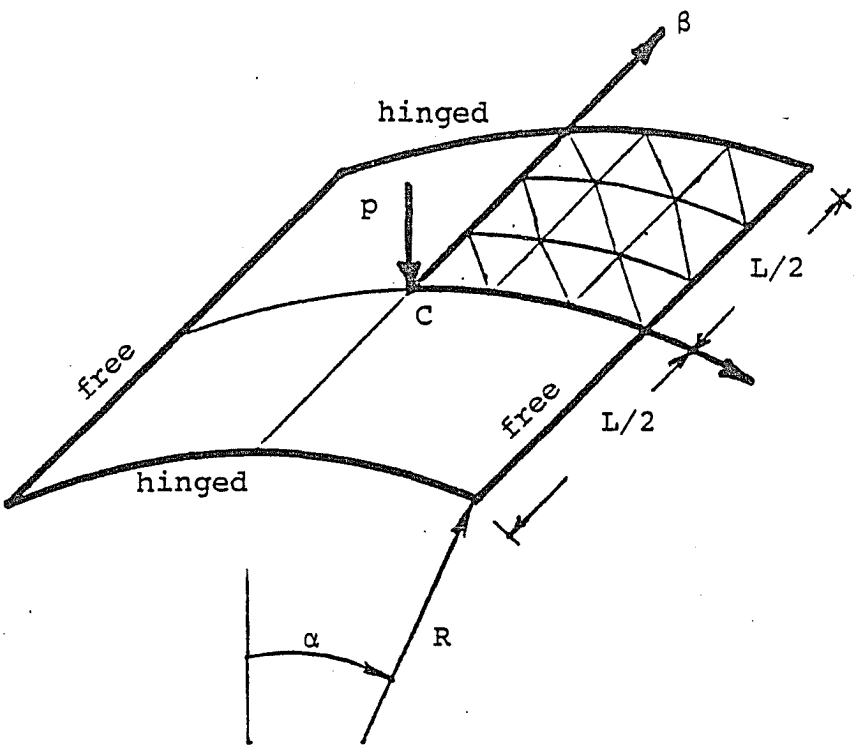

R = 2540. mm
L = 508. mm
h = 12.7 mm
E = 3.10 275 KN/mm^2
ν = 0.3
α = 0.1 radian

Figure 36. Hinged-free cylindrical panel under a central point load.

α = 0.1 radian

E = 3.10275 kN/mm^2

ν = 0.3

A load of 2.2 kN was applied at the center of the shell in ten unequal increments and the analysis was carried out with KT2 technique and band solution with 3 to 4 iterations per cycle. The solution kept oscillating with increasing deflections at the load of 2.2 kN, indicating the reach of limit point and hence was stopped after 4 iterations at this load. The shell undergoes shap through behavior beyond this load.

The load-central normal deflection values of this study are shown in Table 22. Figure 37 shows the load deflection paths of Horrigmoe's [50] 3 x 3 quadrilateral elements, Surana's [129] 2 x 2 degenerated isoparametric elements (40 degrees-of-freedom per element), Sabir and Lock's [130] cylindrical shell elements and the present study. The present study gives a very flexible result. While there is good agreement in the solution near the limit point as well as in the limit load, where there is only 2.28% difference in the deflection, there is considerable difference from the beginning up to a load of 1.5 kN. The deflection of this study is higher by about 28% on an average up to a load of 2.0 kN. This large difference in the deflection can be attributed to the Kirchhoff's effect, as there is as much as 20 to 30% more deflection in the linear solution itself compared with their solutions. There seems to be no clear indication that the shear deformation is neglected for this very thin shell in their studies.

Table 22. Deflections of Hinged-Free Cylindrical Panel Under a Central Concentrated Load

Load increment	Load P (kN)	w c (mm)	Load increment	Load P (kN)	w c (mm)
1	0.50	1.91	6	1.75	7.27
2	0.75	2.94	7	1.90	8.07
3	1.0	3.92	8	2.0	8.54
4	1.25	4.95	9	2.10	9.44
5	1.50	6.06	10	2.20	11.21

	DOF
Horrigmoe	176
Surana	105
Sabir & Lock	125
This Study	144

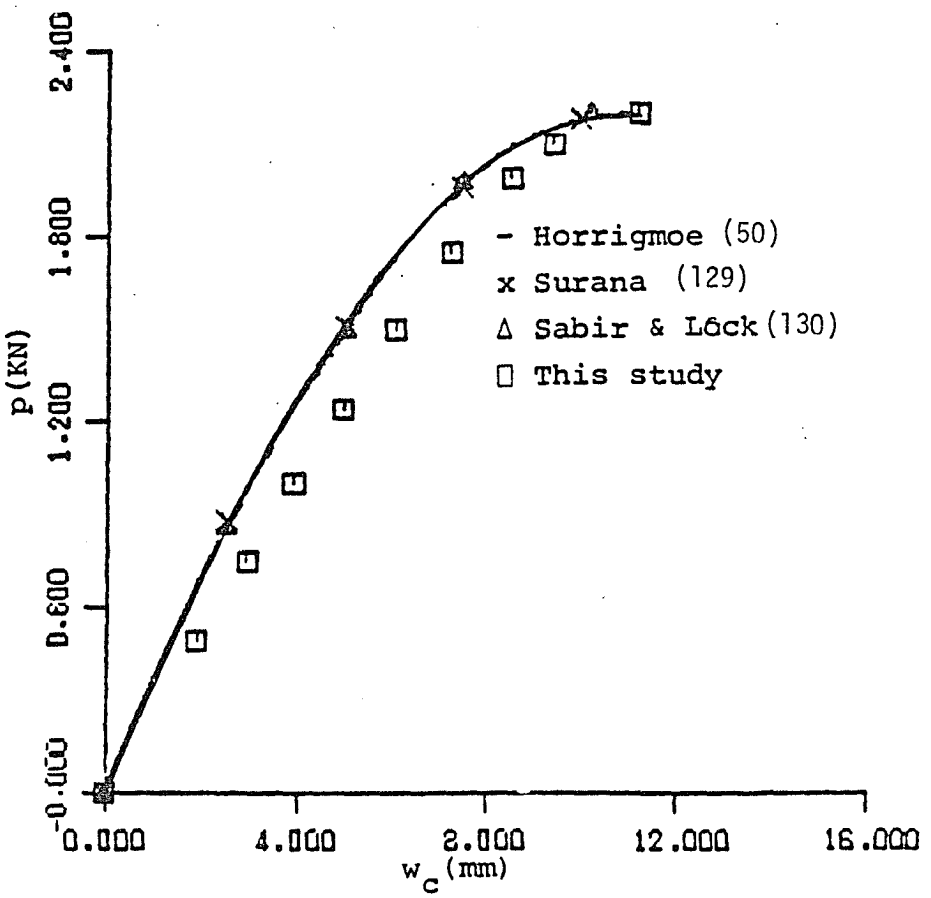

Figure 37. Load-central deflection curve for a hinged-free cylindrical panel under a central point load.

The thin shell that includes the transverse shear strain energy is expected to be stiffer than the shell that excludes it as in the present case. This reasoning seems to be strengthened from the next example of a spherical shell with similar loading and hinged boundaries.

6.2.2.4 Hinged Shallow Spherical Shell under a Central Point Load. A shallow spherical shell, square in plan and hinged along its edges is subjected to a central concentrated load, as shown in Figure 38. This is, again, a standard testing example, cited in the literature often. Analytical series solution to this problem has been given by Leicester[131], whose solution is taken as the reference solution for comparison. Finite element solution to this problem has been given by a number of authors (references 50, 62, 64, 76, 117, 124, 127, 129, 132, 133). Due to symmetry, a quarter of the shell has been modelled with a mesh of 2 x 2 and the analysis was carried out with the following data:

Radius of sphere R_o=104.554 in. (2658.50 mm), R = 100 in. (2540 mm)

h = 3.9154 in. (99.45 mm)

E = 10,000.0 psi (6.895×10^4 kPa)

ν = 0.3

a = 30.9017 in. (784.9 mm)

A central concentrated load of 2 kips was applied in the first increment and 1 kip in the next 8 increments. KT2 technique and Band solution was used with 3 to 4 iterations per cycle for the analysis. The normalized load-central normal deflection values are given in

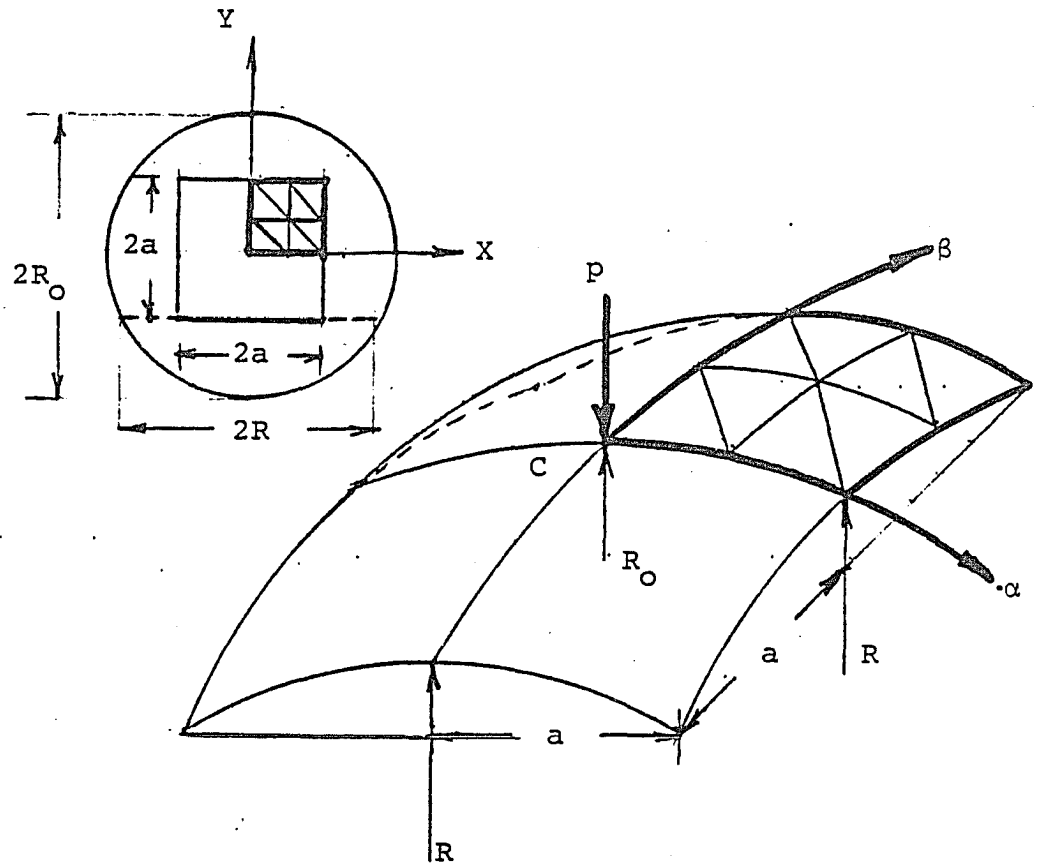

Figure 38. Hinged spherical shell under a central point load.

Table 23. At a load of 10 kips, the solution oscillated with increasing deflections, indicating the reach of limit point. Wood[62] reports a limit point load of 10.292 kips and mentions that the limit point loads obtained by Matsui[124] is 11.15 kips, by Bathe[64] is 10.157 and by Frey[132] is 10.0 kips. The solution plot of Gallagher[117] seems to give a limit point load of 11.026 kips. The shell exhibits snap through behavior beyond the limit point and the solution was stopped. Figure 39 shows the comparison of the normalized load deflection paths of Leicester[131] (analytical), Gallagher[117] (3 x 3 deep shell triangular elements), Wood[62] (4 x 4 9-noded Lagrangian elements with 43 degrees-of-freedom per element) and the present study. Here again, the deflection of the present study is much larger than the analytical solution. It is observed that there is about 30 to 35% difference in the linear solution itself. However, the present solution agrees very well with that of Pica and Wood[62], who have used a Mindlin formulation, where constraints on shear deformation have been imposed with selective integration for shear energy terms. It is, however, well known that the reduced or selective integration introduces spurious zero energy modes and sometimes fails to give converged solution.

6.2.2.5 Pinched Cylinder. Figure 40 shows a cylinder pinched by a tensile pull by two opposite point loads at the center of the cylinder and the finite element idealization adopted for the analysis. The cylinder has the following properties:

$$E = 10.5 \times 10^6 \text{ psi } (72.4 \times 10^6 \text{ kPa})$$

$$\nu = 0.3125$$

Table 23. Deflections of Hinged Spherical Shell Under a Central Point Load

Load increment	Load P (kips)	$w_{c/h}$	Load increment	Load P (kips)	$w_{c/h}$
1	2.0	0.182	6	7.0	0.73
2	3.0	0.278	7	8.0	0.88
3	4.0	0.380	8	9.0	1.09
4	5.0	0.490	9	10.0	1.42
5	6.0	0.60			

	DOF
Gallagher	144
Wood	325
This Study	81

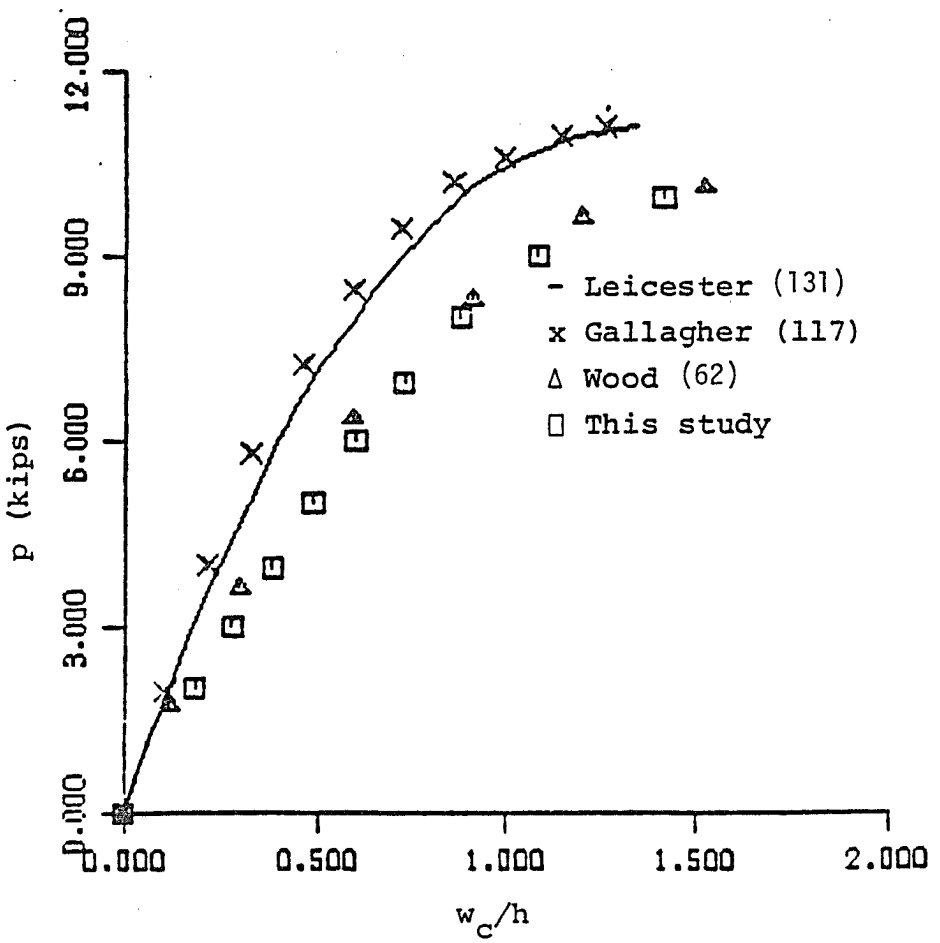

Figure 39. Load-central deflection curve for a spherical shell under a central point load.

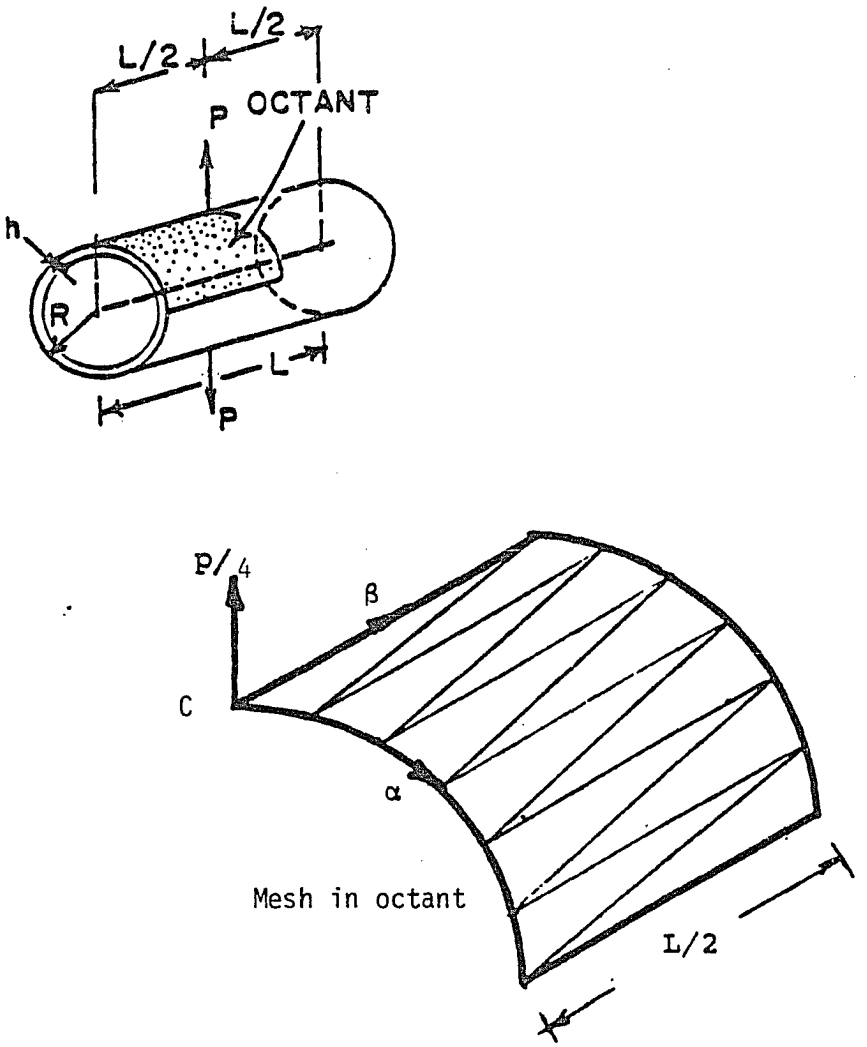

Figure 40. Pinched cylinder and a typical mesh.

L = 10.35 in. (262.89 mm)

R = 4.953 in. (125.81 mm)

h = 0.093 in. (2.36 mm), H = 0.0859 in. (2.18 mm)

There seems to be no analytical solution to this problem. Finite element solution to this problem has been given by Chang[105] using deep shell triangular elements (36 degrees-of-freedom per element) with a mesh of 4 x 1 for 1/8th of the cylinder. There is a discrepancy in the length of the cylinder mentioned by Chang[105]. While he mentions a length of 10.5 on page 146, he shows a length of 10.35 on page 205. For this study, a length of 10.35 was assumed. Due to symmetry, one octant of the cylinder was modelled with 6 x 1 mesh. Incremental loads of 100 lbs was applied in each of the six increments and the analysis was carried out with KT2 technique and Band solution and 2 to 3 iterations in each cycle. The normal displacement values under the load are shown in Table 24. Figure 41 shows the plot of load-central normal deflection path compared with Chang[105]. The shell stiffens with increase in the pull. The result compares well with Chang up to a load of 300 lbs but thereafter this study shows more stiffening with a maximum difference of about 11%. Chang has reported zero energy modes in his element. This and the discrepancy in length could be the reason for the difference. However, the trend of the load displacement path agrees well.

6.2.2.6 Clamped Spherical Cap under a Central Point Load. Another often cited example in the literature is a clamped spherical cap under a central point load (Figure 42a). Finite difference

Table 24. Deflections of a Pinched Cylinder

Load increment	Load P (lbs)	w_c (ins)
1	100.	0.1097
2	200.	0.1940
3	300.	0.2770
4	400.	0.3427
5	500.	0.4070
6	600.	0.4677

	DOF
Chang	162
This Study	126

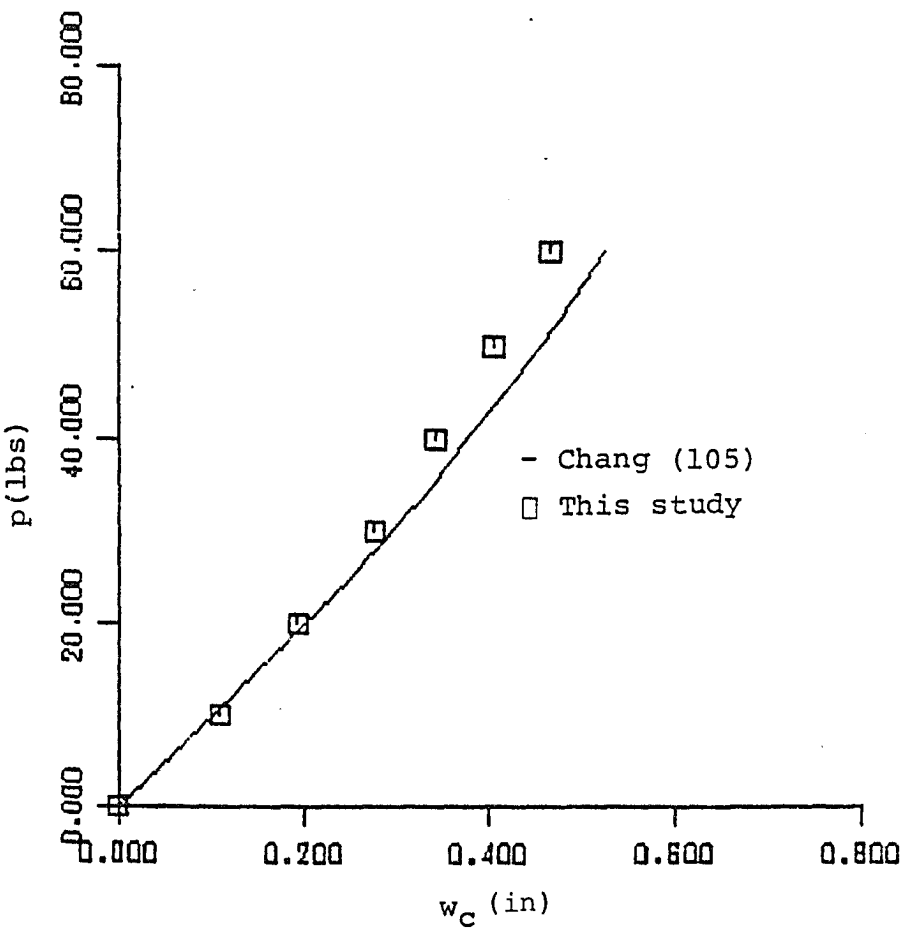

Figure 41. Load-deflection curve of a pinched cylinder.

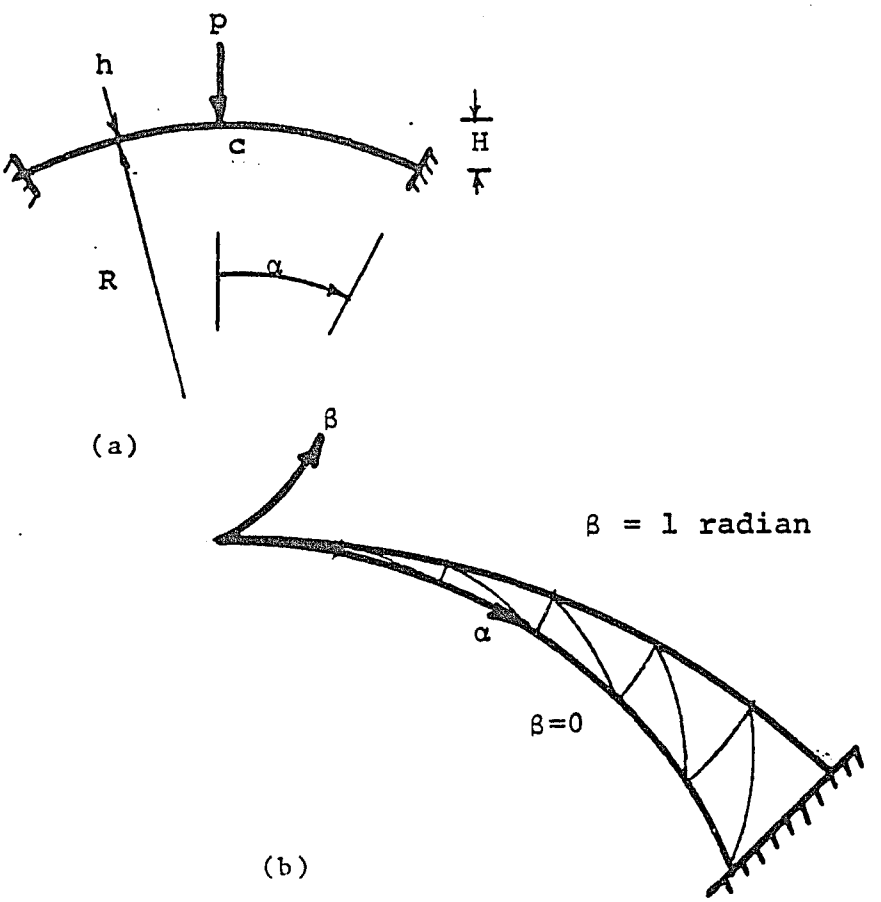

Figure 42. Spherical cap under a central point load.

solution to this problem has been given by Mescall[134] and finite element solution has been given by a number of authors (references 60, 87, 135, 136). Due to symmetry, a slice of the shell is modelled by 11 elements (Figure 42b) and analyzed with the following data:

$R = 4.76$ in. (120.9 mm)

$h = 0.01576$ in. (4 mm)

$\alpha = 10.9$ deg.

$E = 10 \times 10^6$ psi (6.9×10^7 kPa)

$\nu = 0.3$

A total load of 43.98 lbs. was applied at the apex in 7 increments and the analysis was carried out with KT2 technique and Band solution with 3 iterations in each cycle. The load-central normal deflection values are given in Table 25. Figure 43 shows the comparison of the load-deflection paths of Wood[60] who used 6 paralinear axisymmetric elements and Bathe[87] who used 10 quadratic axisymmetric elements with no equilibrium iterations and the present study. The result of the present study compares well with Bathe up to a load of 12.566 lbs and with Wood up to a load of 18.84 lbs but thereafter gives very stiff solution. This is due to the shell undergoing large rotations with increase in loads. As the present formulation accounts only for small rotations, the elements get stiffer in the region of large rotations.

Table 25. Deflections of Clamped Spherical Cap Under a Central Point Load

Load increment	Load P (lbs)	w c (ins)
1	6.283	0.0073
2	12.566	0.0158
3	18.84	0.0269
4	25.12	0.0390
5	31.415	0.0505
6	37.698	0.0614
7	43.98	0.0713

	DOF
Bathe	106
Wood	52
This Study	117

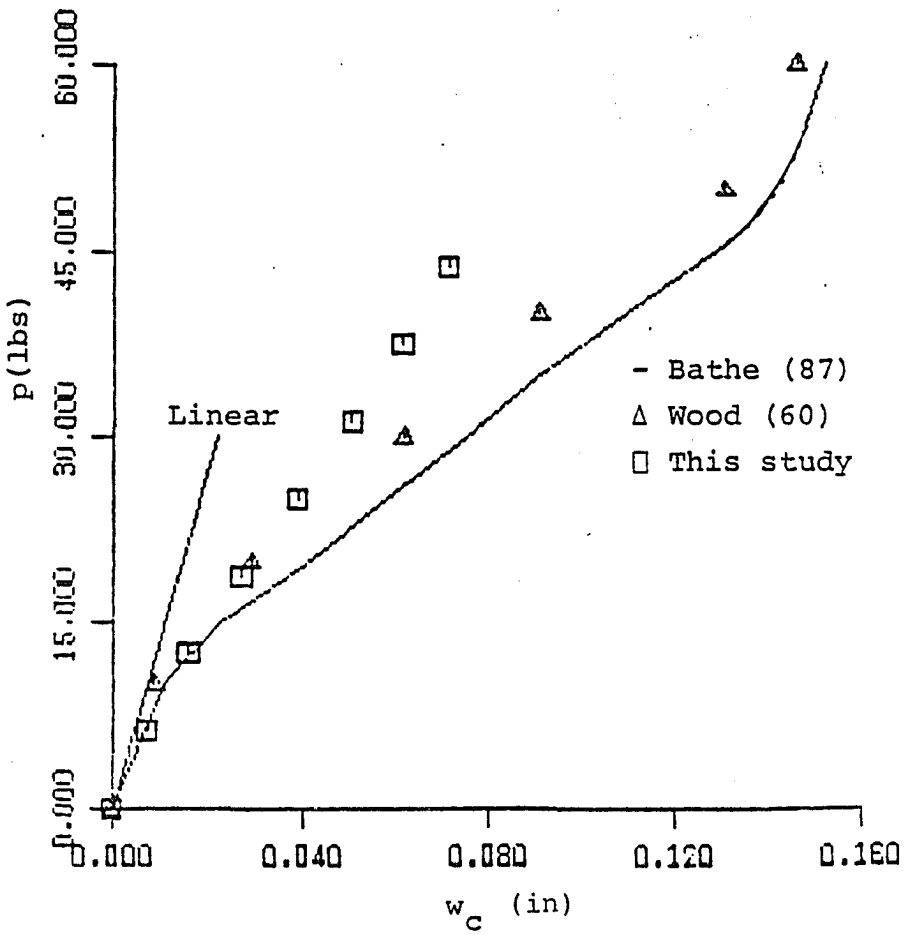

Figure 43. Load-apex deflection curve of a spherical cap under a central point load.

6.2.2.7 Clamped Parabolic Shell under a Central Point Load. The last example in the GNL analysis of shells is a parabolic shell square in plan, clamped at its edges and loaded at the apex with a concentrated load (Figure 44). The equation of the lower surface of the shell is given by:

$$Z = H\left(1 - \frac{X^2}{a^2}\right)\left(1 - \frac{Y^2}{b^2}\right) \tag{6.13}$$

where H = central rise of the lower surface of shell

a,b = sides of the shell.

No analytical solution seems to be available for this problem. Finite element solution to this problem has been given by Wood[137] and Oliver[136] using degenerate isoparametric elements (40 degrees-of-freedom per element). Due to symmetry, a quarter of the shell is analyzed with 3 x 3 mesh and the following data:

a = 300 in. (7620 mm)

H = 50 in. (1270 mm)

h = 6 in. (152.4 mm)

$E = 30 \times 10^6$ psi (20.69×10^7 kPa)

$\nu = 0.0$

A load of 4000 lbs was applied in the first increment and in each of the subsequent 8 increments an increment of 2000 lbs was added. The analysis was carried out with KT2 technique and Band solution with 3 iterations in each cycle. The normalized load-central normal

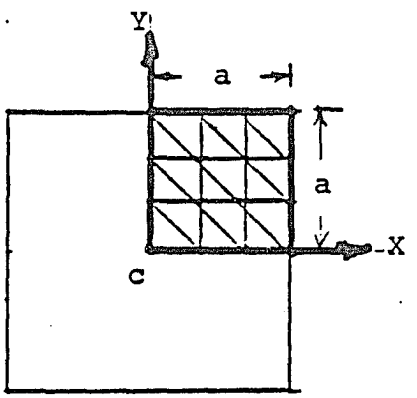

$$Z = H\left(1 - \frac{X^2}{a^2}\right)\left(1 - \frac{Y^2}{a^2}\right)$$

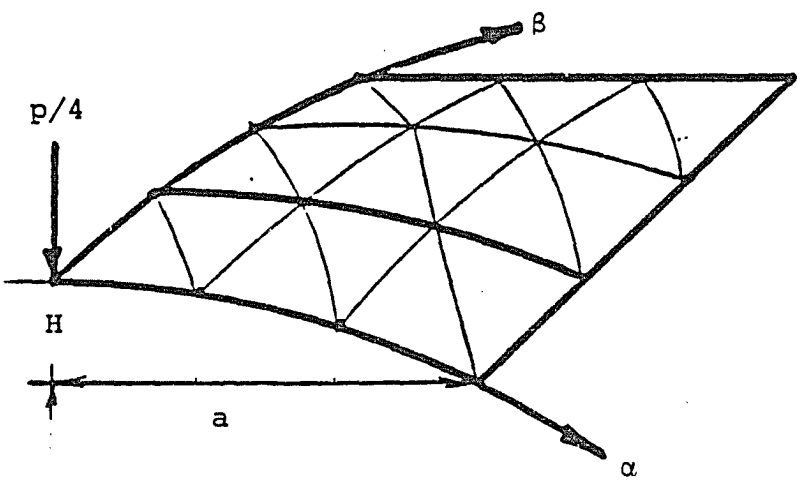

Figure 44. Clamped parabolic shell under a central point load.

deflection values are shown in Table 26. Figure 45 shows the comparison of normalized load-central normal deflection paths of Wood[137] Oliver and Onate[136] and the present study. Up to the first six load steps, there is excellent agreement with the solution of Wood[137] and in the 7th increment it agrees very well with Onate[136], but thereafter stiffer solution is obtained. This again, as in the previous example, is due to the effect of large rotations in the shell with increasing loads.

From the examples on the GNL analysis of shells, the results of the present study indicate good agreement with the compared solutions, in the region of small rotations. From the variety of examples in this chapter studied so far, the applicability of the nonlinear formulations has been clearly demonstrated. The DKCT element gives accurate solutions in the linear buckling problems. The accuracy of solutions is affected in some cases of GNL analysis of plates. In the GNL analysis of shells, the DKCT element is accurate in the region of small rotations. However, in the region of large rotations, the element fails to give accurate solutions.

Regarding the economical aspect of the DKCT element, it can be seen from the plate examples of the GNL analysis that it is not in general economical. This is understandable as the DKCT element is a shell element, while most of the elements compared are plate bending elements. In the case of arch example, the comparison is made with the beam elements and naturally the DKCT element is more expensive. In the shell examples, it can be seen that the DKCT element is in

Table 26. Deflections of a Clamped Parabolic Shell Under a Central Point Load

Load increment	Load $p=pa^2/Eh^4$	w_c/h
1	9.2	0.3922
2	13.8	0.639
3	18.4	0.925
4	23.0	1.247
5	27.6	1.567
6	32.2	1.875
7	36.8	2.173
8	41.4	2.452
9	46.0	2.675

	DOF
Wood	200
Oliver & Onate	200
This Study	144

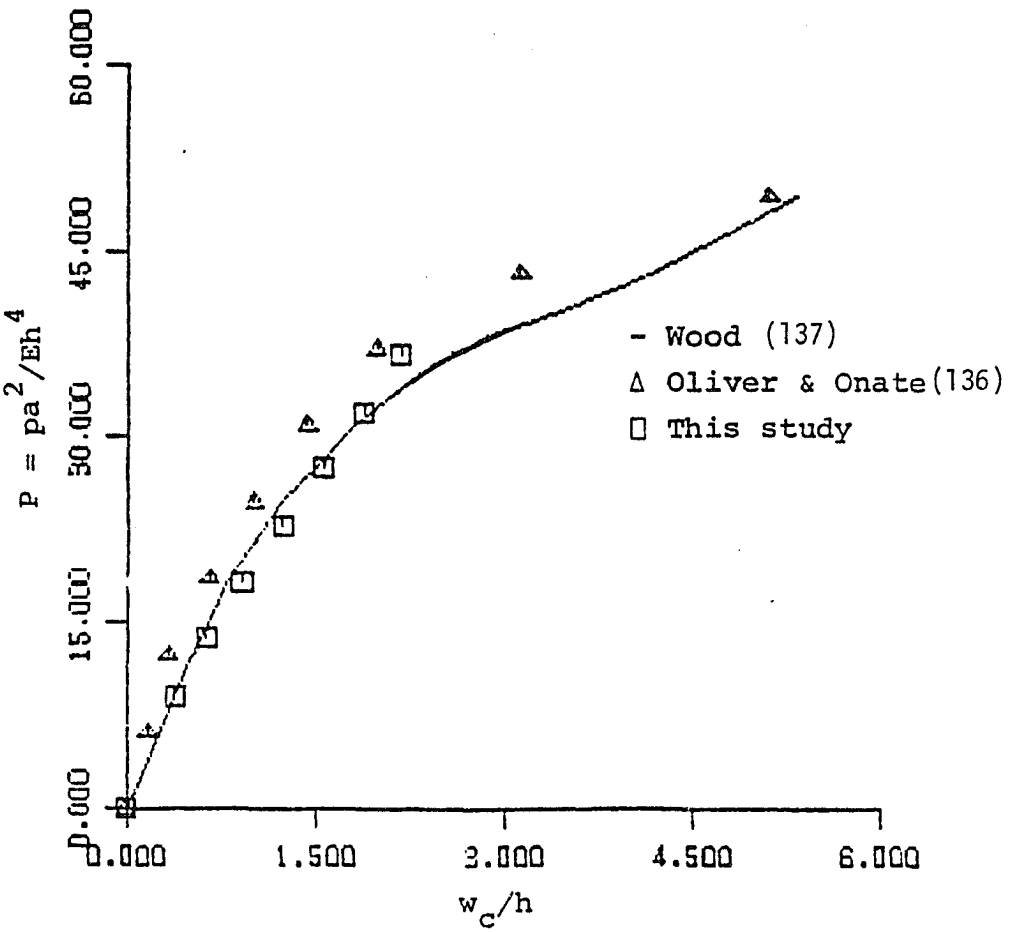

Figure 45. Load-central deflection curve of a clamped parabolic shell under a central point load.

general more economical than the compared shell elements. Again, in the spherical cap example (6.2.2.6), the DKCT element is compared with the axisymmetric elements and is therefore understandably less economical. In order to establish the economy of the DKCT element, a proper comparison of this element with arbitrary deep shell elements should be made. At present the DKCT element with 27 degrees-of-freedom seems to be more economical than the alternate degenerated isoparametric element, of 40 degrees-of-freedom. However, this needs to be further established with more study.

A summary of the formulation, conclusion and suggestions are presented in the next chapter.

In Chapter 2, the basic tensor equations of kinematics of deformation of an arbitrary thin shell have been presented. The linear and nonlinear strain equations have been derived in tensor notation.

In Chapter 3, the linear DKCT element has been reviewed briefly. The element linear equations for strains and stresses have been derived. Expressions for linear element stiffness, consistent nodal loads and their transformations to local curvilinear coordinates have also been reviewed.

In Chapter 4, geometrically nonlinear formulation of the DKCT element, for large displacement and small rotations, in a total Lagrangian approach, has been derived in detail, from the principles of continuum mechanics. This includes the nonlinear strain-displacement relation, element tangent stiffness matrix, the incremental and total equilibrium equations.

In Chapter 5, solution techniques of the nonlinear equilibrium equations have been elaborated. Various modifications to the Newton-Raphson techniques in conjunction with various convergence criteria have been derived in detail. A computer program developed for the Geometrically Nonlinear Analysis of Thin Shells (GNATS) has been explained. The important subroutines of the program structure have been explained. The capabilities and limitations of the program have been mentioned. A schematic explanation of the program structure has been presented with a simple flow chart.

In Chapter 6, the applicability of the GNL formulation has been demonstrated through numerous examples. These are standard examples,

solved analytically or numerically by others. Section 6.1 covers linear buckling cases of a variety of structures such as columns, plates, ring, arches and shells. Section 6.2 covers GNL analysis of a variety of plates, shallow arch and arbitrary shells. The result of each example has been compared with the published analytical and or numerical values, followed by discussion on the comparison. The results of the examples have been presented in the form of tables and computer plots.

7.2 Conclusions

A geometrically nonlinear formulation for a doubly curved triangular thin shell element based on the discrete Kirchhoff theory has been presented. The element has 3 nodes and 27 degrees-of-freedom of displacements and their derivatives. The formulation of the element is with respect to the local curvilinear axes. The shell displacements, strains and stresses are computed in the natural curvilinear frames of the shell. This element with its nonlinear capabilities has been tested on a wide variety of problems.

First, the element is tested for linear buckling problems. From the number of examples tested, it is shown to have a very good agreement on the computed buckling loads with the compared solutions. Next, the element is tested on a full GNL analysis of plates, arch and arbitrary shells. In the case of plates, the solutions of the present study in general are reasonably satisfactory. In the case of shells, where large rotations were encountered, the solutions are

very stiff and did not match with the compared solutions. However, in the region of small rotations, excellent agreement has been found with the compared solutions. In the examples of hinged-free cylindrical panel (6.2.2.3) and hinged spherical shell (6.2.2.4), the solutions of the present work are more flexible. In the later case, it agrees very well with a numerical solution based on Mindlin formulation, where shear locking was avoided. As nonlinear analysis of shells is very expensive any reduction in the number of element equations is highly desirable. Hence this DKCT element with only 27 degrees-of-freedom was compared for its computational economy. From the comparison, it seems that this element is more economical than the alternate degenerated isoparametric elements, but this needs to be established with more study. However, this element is less economical than the beam, plate bending, shallow shell or axisymmetric elements. From the number of examples tested, the GNL formulation and the DKCT element have been found to be in general accurate. However, there are some setbacks in the formulation.

When the local curvilinear axes coincide with the global cartesian axes, the stiffness coefficients of the centroidal degrees-of-freedom become null. Therefore, introduction of any approximation for the central node highly disturbs the nonlinear solution. This was evidenced from the examples of columns and plates. While the error is insignificant in the linear buckling examples, the accuracy of the solution was not quite satisfactory in the examples of GNL analysis. This is due to the accumulation of error in load steps

and iterations. The central node also causes minor difficulties. The stiffness coefficients of the centroidal degrees-of-freedom have to be written on a tape before condensation, for later use in the recovery of central nodal displacements. Writing on or reading from a tape device is time consuming and increases the cost of the analysis. Also the process of condensing and recovering the centroidal degrees-of-freedom is cumbersome to program.

The second setback is the restriction to small rotations. Any GNL analysis will not be realistic without including large rotations, as slender structures such as rods, plates and thin shells can undergo large rotations under certain boundary and loading conditions. The complete load-displacement path, including snap through and snap back behavior of some arches and shells could not be carried out due to the restriction on rotations. The restriction to small rotations came as a result of tensor formulation with rotational degrees-of-freedom as nodal variables. The rotations are not tensorial variables and therefore cannot be summed up in an arbitrary manner in an incremental procedure[138]. Since finite rotation cannot be represented by a vector, its coordinate transformation often required a complex and unorthodox treatment[126]. The element formulation ends up with highly complicated expressions involving products of trigonometric functions[139].

The third setback is the nonlinear solution algorithms. Although various modified N-R techniques using Band or Frontal solutions have been developed, giving a wider choice in the solution algorithms,

these are incapable of tracing the equilibrium path near the limit point and to points beyond. This means a complete equilibrium path, which is essential for a thorough understanding of the behavior of arches and shells cannot be achieved.

Barring a few such setbacks, there are definite advantages. Among the shell elements available today, there are only two acceptable choices (i) the D-K shell elements and (ii) the degenerated isoparametric elements. Of these two, the DKCT element of the former class, has the following advantages. (i) It is formulated in the natural curvilinear coordinates. (ii) It is based on arbitrary deep shell theory. (iii) It represents rigid body modes exactly. (iv) It totally avoids the problems of element locking (both membrane and shear locking) and therefore does not need the determination and use of numerical factors "to made the element work". (v) It preserves the full rank of the stiffness matrix. (iv) The element is simple, economical, efficient and accurate. Due to these advantages, the present DKCT element is a strong candidate for the GNL analysis of thin shells.

7.3 Suggestions

As discussed earlier, the inclusion of large rotations is very important for a realistic GNL analysis of thin shells. Alternate method of formulation using nodal variables other than the rotational degrees-of-freedom should be thought of to circumvent the difficulties of including finite rotations. A further reduction in the element

variables can be considered, dropping the independent membrane displacement gradients such as $u_{,\alpha}$, $u_{,\beta}$, $c_{,\alpha}$ and $v_{,\beta}$ as nodal degrees-of-freedom. It is extremely important to associate the GNL analysis with powerful solution algorithms such as Crisfield's "arc length methods" to trace the complete equilibrium path. As shell structures are predominantly used in automobile, aircraft and spacecraft structures with great efficiency using composite materials, the GNL formulation should be extended to accommodate anisotropic material behavior. Also these structures are often subjected to dynamic loads and the formulation should therefore include dynamic effects. It is also important to extend the formulation to nonlinear material behavior and possibly to include fracture phenomenon that arise from the high thermal and fatigue loads.

7.4 Some General Remarks

Thin shell structures are able to sustain heavy loads by virtue of their curvature. The curved middle surface produces a large variety of different response phenomena, especially in the geometrically nonlinear range. Stretching and bending modes interact in a considerably more unpredictable manner than in linear problems. Often the strain tensors change their participation during certain loading process, giving rise to surprising response phenomena. The investigation of thin shell structures particularly with unknown response behavior thus requires:

(i) a precise description of their basic kinematic and dynamic equations.

(ii) a discretization, modelling the undeformed and deformed geometry with great care.

(iii) numerical algorithms, stable, convergent and adequately sensible to the intended phenomena.

The nonlinear problems of shells are much more complicated than structures of other geometric forms and the increasing importance of shell buckling is evidenced by numerous research works and books that are still being published (references 110, 111, 139, 140). With the finite element technique as a powerful tool, research works are still being carried out on an appropriate nonlinear finite element shell theory[141]. As of today, the D-K shell elements and the degenerated isoparametric elements represent the state-of-the-art for nonlinear analysis of shells, but further improvements are clearly desirable. These improvements should address the problems of nonlinear static and dynamic analysis.

REFERENCES

1. Kirchhoff, G., "Vorlesungen uber Mathematische Physik," Mechanik, Vol. 1, 1976.

2. Love, A. E. H., "On the small vibration and deformation of thin elastic shells," Phil. Trans Royal. Sci., Vol. 179, 1888.

3. Meissner, E., "Das Elastizitatsproblem dunner schalen von Ringflachen-Kugel-order Kegelform," Physik.Z., Vol. 14, pp. 343-349, 1913.

4. Vlasov, V. Z., "The basic differential equations in the general theory of elastic shell," NACA, TM 1241, 1951.

5. Nagdi, P. M., "On the theory of thin elastic shells," Quart. J. Applied Math., Vol, No. 4, pp. 369-380, 1957.

6. Sanders, J. L., "An improved first approximation theory for thin shells." NASA Report 24, 1959.

7. Koiter, W. T., "A consistent first approximation in the general theory of thin elastic shells," First IUTAM symposium on Theory of thin elastic shells (Ed. W. T. Koiter) North Holland, 1960.

8. Goldenveizer, A. L., Theory of Elastic Thin Shells, Pergamon, Oxford, 1961.

9. Novozhilov, V. V., The Theory of Thin Shells, Noordhoff Groningen, Netherlands, 1964.

10. Budiansky, B. and Sanders, J. L., "On the best first order linear shell theory," Progress in Applied Mechanics, The Prager Anniversary Vol. Macmillan pp. 129-140, 1963.

11. Reissner, E., "On the foundation of the theory of elastic shells," Proc. 11th. Int. Cong. on Applied Mechanics, Munich, pp. 20-30, 1964.

12. Sechler, E. E., "The historical development of shell research and design," in: Thin Shell Structures (Ed. Y. C. Fung and E. E. Sechler) Prentice Hall Inc., New Jersey, pp. 3-25, 1974.

13. Marguerre, K., "Zur theorie der gekrummten Plate grosser Formanderung," Proc. 5th. Int. Cong. on Applied Mechanics, Wiley and Sons, pp. 93-101, 1938.

14. Donnell, L. H., "Stability of thin walled tubes under torsion," NACA TR 479, 1934.

15. Mushtari, Kh. M. and Galimov, K. Z., "Non-linear theory of thin elastic shells," NASA TT-F62, 1962.

16. Novozhilov, V. V., Foundations of the Nonlinear Theory of Elasticity, Graylock Press, Baltimore, 1953.

17. Synge, J. L. and Chien, W. Z., "The intrinsic theory of elastic shells and plates," Von Karman Anniversary Vol., Cal Tech., p. 103, 1941.

18. Chien, W. C., "The intrinsic theory of thin shells and plates," Part I-General theory, Quart. App. Math, Vol. 1, pp. 297-327, 1944.

19. Chien, W. C., "The intrinsic theory of thin shells and plates," Part III-Application to thin shells, Quart. App. Math., Vol. 2, pp. 120-135, 1944.

20. Erickson, J. L. and Truesdell, C., "Exact theory of stress and strain in rods and shells," Archive for Rational Mechanics and Analysis, Vol. 1, pp. 295-323, 1959.

21. Sanders, J. L., "Nonlinear theories for thin shells," Quart. App. Math., Vol. 21, pp. 21-36, 1963.

22. Leonard, R. W., "Nonlinear first approximation thin shell and membrane theory," Ph.D Thesis, Virginia Polytech. Inst., Virginia, 1961.

23. Koiter, W. T., "General equations of elastic stability for thin shells." Proc. Symp. on the Theory of Thin Shells, Univ. of Houston, Texas, 1967.

24. Budiansky, B., "Notes on nonlinear shell theory," J. Appl. Mech., pp. 393-401, June 1968.

25. Reissner, E., "Linear and nonlinear theory of shells," in: Thin Shell Structures- Theory, Experiment and Design. (Ed. Y. C. Fung and E. E. Sechler), Prentice Hall, New Jersey, pp. 29-44, 1974.

26. Pietraszkiewicz, W., "Introduction to the nonlinear theory of shells," Ruhr Univ., Bochum, Mitt. Inst. fur Mech. No. 10, 1977.

27. Pietraszkiewicz, W., Thin Shell Theory - New Trends and Applications, Springer-verlag, Berlin, pp.153-208, 1980.

28. Pietraszkiewicz, W., Theory of shells, North Holland, New York, 1980.

29. Pietraszkiewicz, W. and Szwabowicz, M. L., "Entirely Lagrangian nonlinear theory of thin shells." Archive of Mech., Vol. 33, pp. 273-288, 1981.

30. Schmidt, R., "On geometrically nonlinear theories for thin elastic shells," in: Flexible Shells (Ed. E. Axelrad and F. A. Emmerling), Springer-Verlag, Berlin, pp. 76-90, 1984.

31. Gallagher, R. H., Finite Element Analysis - Fundamentals, Prentice Hall Inc., New Jersey, 1975.

32. Zienkiewicz, O. C., The Finite Element Method, 3rd. Edition, McGraw-Hill, London, 1977.

33. Bathe, K. J., Finite Element Procedures in Engineering Analysis, Prentice Hall Inc., New Jersey, 1982.

34. Dhatt, G. and Tarzot, G., Finite Element Method Displated , John Wiley and Sons, New York, 1984.

35. Hinton, E. and Owen, D. R. J., Finite Element Programming, Academic Press, London, 1977.

36. Adini, A., "Analysis of shell structures by the finite element method." Ph.D thesis, U. Calif., Berkley, 1961.

37. Gallagher, R. H., "Analysis of plate and shell structures," Proc. Symp on application of finite element methods in Civil engg., Vanderbilt Univ., Nashville, Tenn., 1969.

38. Gallagher, R. H., "Application of finite element analysis," Proc. 2nd. US-Japan seminar on matrix methods of structural analysis and design, Univ. of Alabama Press, Huntsville, Alabama, pp. 641-678, 1972.

39. Gallagher, R. H., "Shell elements," Proc. of first world conf. on finite elements, Bournemouth, England, 1975.

40. Gallagher, R. H., "Problems and progress in thin shell finite element analysis," in: Finite Elements for Thin Shells and Curved Members, (Ed. D. G. Ashwell and R. H. Gallagher), John Wiley and Sons, New York, 1976.

41. Stricklin, J. A., Heisler, W. E., McDougell, H. R. and Stebbins, F. J., "Nonlinear analysis of shells of revolution by the matrix displacement method," AIAA J., Vol. 6, pp. 2306-2312, 1966.

42. Yaghmai, S., "Incremental and large deformations in mechanics of solids with application to axisymmetric shells," Ph.D thesis, Dept. of Civil Engg., U. Calif., Berkley, 1968.

43. Schmidt, L. A., Bogner, F. K. and Fox, R. L., "Finite deflection structural analysis using plate and shell discrete elements," AIAA J., pp. 781-791, 1968.

44. Prato, C. A., "A mixed finite element method for thin shell analysis," Research report R. 68-33, Dept. of Civil Engg., M.I.T., 1968.

45. Connor, J. J. and Will, G. T., "A mixed finite element shallow shell formulation," in: Recent Advances in Matrix Methods of Analysis and Design, (Ed. R. H. Gallagher, Y. Yamada and J. T. Oden) Univ. of Alabama Press, Huntsville, Alabama, pp. 105-137, 1971.

46. Tahiani, C. and Lachance, L., "Linear and nonlinear analysis of thin shallow shells by mixed finite elements," J. Comp, and Struct., Vol. 5, pp. 167-177, 1975.

47. Noor, A. K. and Hartley, S. J., "Nonlinear shell analysis via mixed isoparametric elements," J. Comp. and Struct., Vol. 7, pp. 615-626, 1977.

48. Horrigmoe, G. and Bergan, P. G., "Incremental variational prinsiples and finite element models for nonlinear problems," J. Comp. and Struct., Vol. 7, pp. 201-217, 1976.

49. Horrigmoe, G. and Bergan, P. G., "Nonlinear analysis of free form shells by finite elements," J. Comp. Meth. in Appl. Mech. and Engg., Vol. 16, pp. 11-35, 1978.

50. Horrigmoe, G., "Hybrid stress finite element model for nonlinear shell problems," Int. J. for Num. Meth. in Engg., Vol. 12, pp. 1819-1839, 1978.

51. Boland, P. L. and Pian, T. H. H., "Large deflection analysis of thin elastic structures by the assumed stress hybrid finite element model," J. Comp. and Struct., Vol. 7, pp. 1-12, 1977.

52. Parisch, H., "Geometrical nonlinear analysis of shells," J. Comp, Meth. in Appl. Mech. and Engg., Vol. 14, pp. 159-178, 1978.

53. Gallagher, R. H., "Geometrically nonlinear finite element analysis," Proc. of Spec. Conf. on the Finite element method in Civil Engg., McGill Univ., 1972.

54. Gallagher, R. H., "The finite element method in shell stability analysis," J. Comp. and Struct., Vol. 3, pp. 543-557, 1973.

55. Gallagher, R. H., "Finite element analysis of geometrically nonlinear problems," in: Theory and Practice in Finite Element Structural Analysis (Ed. Y. Yamada and R. H. Gallagher) Univ. of Tokyo, 1973.

56. Gallagher, R. H., "Finite element representations for thin shell instability analysis," in: Buckling of Structures (Ed. B. Budiansky), Springer-Verlag, New York, pp. 40-51, 1976.

57. Gallagher, R. H., "Geometrically nonlinear shell analysis," in: Finite Elements in Nonlinear Mechanics (Ed. P. Bergen et al.), Tapir Publishers, Norway, Vol. 1, pp. 243-264, 1977.

58. Idelsohn, S., "On the use of deep, shallow or flat shell finite elements for the analysis of thin shell structures," J. Comp. Meth. in Appl. Mech. and Engg., Vol. 26, pp. 321-330, 1981.

59. Ahmad, S., Irons, B. M. and Zienkiewicz, O. C., "Analysis of thick and thin shell structures by curved finite elements," Int. J. for Num. Meth. in Engg., Vol. 2, pp. 419-451, 1970.

60. Wood, R. D., "The application of finite element method to geometrically nonlinear structural analysis," Ph.D Thesis, Univ. of Wales, Swansea, 1973.

61. Wood, R. D. and Zienkiewicz, O. C., "Geometrically nonlinear finite element analysis of beams, frames, arches and axisymmetric shells," J. Comp. and Struct., Vol. 7, pp. 725-735, 1977.

62. Pica, A. and Wood, R. D., "Post buckling behaviour of plates and shells using a Mindlin shallow shell formulation," J. Comp. and Struct., Vol. 12, pp. 759-768, 1980.

63. Ramm, E., "A plate/shell element for large deflections and rotations," in: Formulation and Computation Algorithms in Finite Element Analysis (Ed, K. J. Bathe, J. T. Oden and W. Wunderlich), M. I. T. Press, 1977.

64. Bathe, K. J. and Bolourchi, S., "A geometric and meterial nonlinear plate and shell element," J. Comp. and Struct., Vol. 11, pp. 23-48, 1980.

65. Bathe, K. H. and Ho, L. W., "Some results in the analysis of thin shell structures," in: Nonlinear Finite Element Analysis in Structural Mechanics (Ed. W. Wunderlich, E. Stein, and K. J. Bathe), Springer-Verlag, New York, pp. 122-150, 1981.

66. Krakelend, B., "Nonlinear analysis of shells using degenerated isoparametric elements," in: Finite Elements in Nonlinear Mechanics (Ed. P. Bergen et al.), Tapir Publishers, Norway, Vol. 1, pp. 265-284, 1977.

67. Zienkiewicz, O. C., Taylor, R. L. and Too, J. M., "Reduced integration technique in general analyasis of plates and shells," Int. J. for Num. Meth. in Engg., Vol. 3, pp. 575-586, 1971.

68. Hughes, T. J. R., Taylor, R. L. and Knoknukulchi, K., "A simple and efficient finite element for plate bending," Int. J. for Num. Meth. in Engg., Vol. 11, pp. 1529-1543, 1977.

69. Wempner, G. A., Oden, J. T. and Kross, D. A., "Finite element analysis of thin shells," Jl. ASCE, EM6, pp. 1273-1294, 1968.

70. Dhatt, G., "Numerical analysis of thin shells by curved triangular elements based on Discrete-Kirchhoff hypothesis," Proc. Symp. on Application of finite element method in Civil Engg. Nashville, Tenn., pp. 255-278, 1969.

71. Stricklin, J. A. Haisler, W. E., Tisdale, P. and Gunderson, R., "A rapidly convergin triangular plate element," AIAA J., Vol. 7, No. 1, pp. 180-181, 1969.

72. Batoz, J. L., Bathe, K. J. and Ho, L. W., "A study of the three-node triangular plate bending elements," Int. J. for Num. Meth. in Engg., Vol. 15, pp. 1771-1812, 1980.

73. Batoz, J. L. and Dhatt, G., "An evaluation of two simple and effective triangular and quadrilateral plate bending elements," Proc. New and future developments in commercial finite element methods, Los Angeles, pp. 352-368, 1981.

74. Batoz, J. L., "An explicit formulation for an efficient triangular plate bending element," Int. J. for Num. Meth. in Engg., Vol. 18, pp. 1077-1089, 1982.

75. Wempner, G., "Finite elements, finite rotations and small strains of flexible shells," Int. J. Solids and Struct., Vol. 5, pp. 117-153, 1969.

76. Dhatt, G., "Instability of thin shells by finite element method," IASS Symp. for folded plates and prismatic structures, Vienna, 1970.

77. Batoz, J. L., Cattopadhyay, A. and Dhatt, G., "Finite element large deflection analysis of shallow shells," Int. J. for Num. Meth. in Engg., Vol. 10, pp. 39-58, 1976.

78. Bathe, K. J. and Dvorkin, E., "Our Discrete-Kirchhoff and isoparametric shell elements for nonlinear analysis - an assessment," J. Comp. and Struct., Vol. 16, pp. 89-98, 1983.

79. Batoz, J. L., "Analyse non Lineaire des Coques Minces Elastiques De Formes Arbitraires par Elements Triangulaires Coubes," D.Sc Dissertation, Univ. of Laval, Quebec, Canaga, 1977.

80. Sridhara Murthy, S., "A triangular anisotropic thin shell element based on Discrete-Kirchhoff theory," Ph.D thesis, U. Arizona, Tucson, Oct. 1983.

81. Cowper, G. R., "Gaussian quadrature formulas for triangles," Int. J. for Num. Meth. in Engg., Vol. 3, pp. 405-407, 1971.

82. Bathe, K. J., "An assessment of current finite element analysis of nonlinear problems in solid mechanics," in: Numerical Solution of Partial Differential Equations-III (Ed. B. Hubbard), Academic Press, London, pp. 117-164, 1976.

83. Malvern, L. E., Introduction to the Mechanics of a Continuous Medium, Prentice-Hall Inc., New Jersey, 1969.

84. Eringen, C. A., Mechanics of Continua, John Wiley and Sons, New York, 1967.

85. Fung, Y. C., A First Course in Continuum Mechanics, 2nd. Edition, Prentice-Hall Inc., New Jersey, 1977.

86. Oden, J. T., Finite Elements of Nonlinear Continua, McGraw-Hill Co., New York, 1972.

87. Bathe, K. J., Ramm, E. and Wilson, E. L., "Finite element formulations for large deformation dynamic analysis," Int. J. for Num. Meth. in Engg., Vol. 9, pp. 353-386, 1975.

88. Zienkiewicz, O. C., Valliappan, S. and King, I. P., "Elasto-plastic solutions of engineering proglems- Initial stress-Finite element approach," Int. J. for Num. Meth. in Engg., Vol. 1, pp. 75-100, 1969.

89. Nayak, G. C. and Zienkiewicz, O. C., "Note on the Alpha constant stiffness method for the analysis of nonlinear problems," Int. J. for Num. Meth. in Engg., Vol. 4, pp. 579-582, 1972.

90. Zienkiewicz, O. C., "Incremental displacement in nonlinear analysis," Int. J. for Num. Meth. in Engg., Vol. 3, pp. 587-592, 1971.

91. Haisler, W. E. and Stricklin, J. A., "Displacement incrementation in nonlinear structural analysis by the self correcting method," Int. J. for Num. Meth. in Engg., Vol. 11, pp. 3-10, 1977.

92. Batoz, J. L. and Dhatt, G., "Incremental displacement algorithms for nonlinear problems," Int. J. for Num. Meth. in Engg., Vol. 14, pp. 1262-1267, 1979.

93. Sharifi, P. and Popov, E. P., "Nonlinear finite element analysis of sandwich shells of revolution," A.I.A.A. J. pp. 715-722, 1973.

94. Riks, E., "An incremental approach to the solution of snapping and buckling problems," Int. J. of Solids and Struct., Vol. 15, pp. 529-551, 1979.

95. Ramm, E., "Strategies for tracing nonlinear response near limit points," in: Nonlinear Finite Element Analysis in Structural Mechanics (Ed: W. Wunderlich, E. Stein and K. J. Bathe), Springer-Verlag, Berlin, pp. 63-89, 1981.

96. Crisfield, M. A., "A fast incremental/iterative solution procedures that handles snap through," J. Comp. and Struct., Vol. 13, pp. 55-62, 1981.

97. Crisfield, M. A., "An arc length method including line searches and accelerations," Int. J., for Num. Meth. in Engg., Vol. 19, pp. 1269-1289, 1983.

98. Bergan, P. G., Horrigmoe, G., Krakeland, B. and Soreide, T. H., "Solution techniques for nonlinear finite element problems," Int. Jl. for Num. Meth. in Engg., Vol. 12, pp. 1677-1696, 1978.

99. Bergan, P. G., "Automated incremental-iterative solution schemes," in: First Int. Conf. on Num. Meth. for nonlinear problems, Swansea, UK, pp. 291-305, 1980.

100. Abdel, Rahman, H. H., "Computational models for the nonlinear analysis of reinforced concrete flexural slab systems," Ph.D Thesis, Dept. of Civil Engg., Univ. of Wales, Swansea, 1982.

101. Kolar, R., "Efficient solution methods for nonlinear finite element analysis," Ph.D thesis, Dept. of Civil Engg., and Engg. Mechanics, Univ. of Arizona, 1984.

102. Bathe, K. J. and Cimento, A. P., "Some practical procedures for the solution of nonlinear finite element equations," Comp. Meth. in Appl. Mech. and Engg., Vol. 22, pp. 59-85, 1980.

103. Irons, B. M., "A frontal solution program for finite element analysis," Int. Jl. for Num. Meth. in Engg., Vol. 2, pp. 5-32, 1970.

104. Timoshenko, S. P. and Gere, J. M., "Theory of elastic stability," second edition, McGraw-Hill Book Co., New York, 1961.

105. Chang, S. C., "An integrated finite element nonlinear shell analysis system with interactive computer graphics," Report no. 81-4, Dept. of Structural Engg., Cornell University, New York, Feb. 1981.

106. Batoz, J. L., "Curved finite elements and shell theories with particular reference to the buckling of a circular arch," Int. Jl. for Num. Meth. in Engg., Vol. 14, No. 5, pp. 774-779, 1979.

107. Fitch, J. R., "The buckling and post buckling behaviour of spherical caps under concentrated loads," Int. Jl. Solids and Struct. Vol. 4, pp. 421-446, 1968.

108. Konig, M., Nagy, D. and Striner, P., "Buckling analysis with ASKA program system," Computer Meth. in Appl. Mech. and Engg., Vol. 16, pp. 185-212, 1978.

109. Flugge, W., "Stresses in Shells," Second edition, Springer-Verlag, New York, 1973.

110. Yamaki, N., "Elastic stability of circular cylindrical shells," North-Holland, Amsterdam, 1984.

111. Brush, D. O., and Almroth, B. O., "Buckling of bars, plates and shells," McGraw-Hill Book Co., New York, 1975.

112. Wang, Y. S. and Billington, D. P., "Buckling of cylindrical shells by wind pressure," Jl. ASCE, EM5, pp. 1005-1024, Oct. 1974.

113. Levy, S., "Square plate with clamped edges under normal pressure producing large deflections," N.A.C.A. Technical Note 847, May, 1942.

114. Brebbia, C. and Connor, J., "Geometrically nonlinear analysis," Jl. ASCE, EM2, pp. 462-483, 1969.

115. Kawai, T. and Yoshimura, N., "Analysis of large deflection of plates by the finite element method," Int. Jl. Num. Meth. in Engg., Vol. 1, pp. 123-133, 1969.

116. Murray, D. and Wilson, E. L., "Finite element large deflection analysis of plates," Jl. ASCE, EM1, pp. 143-165, 1969.

117. Thomas, G. R. and Gallagher, R. H., "A triangular thin shell finite element - Nonlinear analysis," NASA report no. CR-2483, July 1975.

118. Levy, S., "Bending of rectangular plates with large deflections," NACA Tech. Note 846, 1942.

119. Weil, N. A. and Newmark, N. M., "Large deflection of elliptical plates," Jl. Appl. Mech., Vol. 23, pp. 21, 1956.

120. Adotte, G., "Second order theory in orthotropic plates," Proc. A.S.C.E., J. Struct. Div. Vol. 93, No. ST 5, Oct. 1967.

121. Brink, K. and Kratzig, W. B., "Geometrically correct formulations for curved finite bar elements under large deformations," in: Non-linear finite element analysis in structural mechanics, (Ed: W. Wunderlich, E. Stein and K. J. Bathe), Springer-Verlag, Berlin, pp. 236-256, 1981.

122. Dupuis, G. A. et al., "Nonlinear material and geometric behaviour of shell structures," Comp. and Struct., Vol. 1, pp. 223-239, 1971.

123. Bathe, K. J., Odezeimer, H. and Wilson, E. L., "Static and dynamic geometric and material nonlinear analysis," UC-SESM Report No. 74-4, UC-Berkley, 1974.

124. Matsui, T. and Matsouka, O., "A new finite element scheme for instability analysis of thin shells," Int. J. for Num. Meth. in Engg., Vol. 10, pp. 145-176, 1976.

125. Wennerstrom, H., "Nonlinear shell analysis performed with flat elements," in: Finite elements in nonlinear mechanics (Ed: P.G. Bergan et al.), Tapir Publishers, Trondheim, Norway, Vol. 1, pp. 285-301, 1977.

126. Kanok-Nukulchai, W., Taylor, R. L. and Hughes, T. J. R., "A large deformation formulation for shell analysis by the finite element method," Comp. and Struct., Vol. 13, pp. 19-27, 1981.

127. Chang, T. Y. and Sawamiphakdi, K., "Large deformation analysis of laminated shells by the finite element method," Comp. and Struct., Vol. 13, pp. 331-340, 1981.

128. Stein, E., Berg, A. and Wagner, W., "Different levels of nonlinear shell theory in finite element stability analysis," in: Buckling of shells (Ed: E. Ramm), Springer-Verlag, Berlin, pp. 91-136, 1982.

129. Surana, K., "Geometrically nonlinear formulation for the curved shell elements," Int. Jl. for Num. Meth. in Engg., Vol. 19, pp. 581-615, 1983.

130. Sabir, A. B. and Lock, A. C., "The application of finite elements to the large deflection geometrically nonlinear behavior of cylindrical shells," in: Variational methods in engineering, (Ed: C. A. Brebbia and H. Tottenham), Southhampton University press, 7, pp. 66-75, 1973.

131. Leicester, R. H., "Large elastic deformation and snap through of shallow doubly curved shells," Ph.D Thesis, Dept. of Civil Engg., Univ. of Illinois, Urbana, 1966.

132. Frey, F., "L'analyse nonlineaire des structures par la methode des elements finis et son application a la construction metallique," These de Doctorat, Univ. de Liege, 1977-78.

133. Stein, E., Wagner, W. and Lambertz, K. H., "Geometrically nonlinear theory and incremental analysis of thin shells," in: Flexible shells - Theory and applications (Ed. E. L. Axlerad and F. A. Emmerling), Springer-Verlag, Berlin, p. 22, 1984.

134. Mescall, J. F., "Large deflection of spherical shells under concentrated loads," Jl. Appl. Mech., Vol. 32, pp. 936-938, 1965.

135. Haisler, W. L., Stricklin, J. A. and Stebbins, F. J., "Development and evaluation of solution procedure for geometrically nonlinear analysis," A.I.A.A. J., Vol. 10, pp. 264-272, 1972.

136. Oliver, J. and Onate, E., "A total Lagrangian finite element formulation for geometrically nonlinear analysis of shells," in: Flexible shells - Theory and applications (Ed: E. L. Axelrad and F. A. Emmerling), Springer-Verlag, pp. 241-256, 1984.

137. Wood, R. D., "The application of finite element methods to geometrically nonlinear structural analysis," Report no. C/Ph/20/73, Univ. of Wales, Swansea, 1973.

138. Argyris, J. H., Dunne, P. C., Malejannakis, G. A. and Schelkle, E., "A simple triangular facet shell element with application to linear and nonlinear equilibrium and elastic stability problems," Comp. Meth. in Appl. Mech. and Engg., Vol. 10, pp. 371-403 and Vol. 11, pp. 96-131, 1977.

139. Ramm, E., "Buckling of Shells," (Ed. E. Ramm), Springer-Verlag, Berlin, 1982.

140. Kollar, L. and Dulacska, E., "Buckling of shells for engineers," John Wiley & Sons, New York, 1984.

141. Ernst, L. J., "A geometrically nonlinear finite element shell theory," Doctoral Thesis, Univ. of Technology, Delft, May, 1981.